ABSTRACT

INFORMATION RETRIEVAL AND MINING IN HIGH DIMENSIONAL DATABASES

by
Xiong Wang

This dissertation is composed of two parts. In the first part, we present a framework for finding information (more precisely, active patterns) in three dimensional (3D) graphs. Each node in a graph is an undecomposable or atomic unit and has a label. Edges are links between the atomic units. Patterns are rigid substructures that may occur in a graph after allowing for an arbitrary number of whole-structure rotations and translations as well as a small number (specified by the user) of edit operations in the patterns or in the graph. (When a pattern appears in a graph only after the graph has been modified, we call that appearance "approximate occurrence.") The edit operations include relabeling a node, deleting a node and inserting a node. The proposed method is based on the geometric hashing technique, which hashes node-triplets of the graphs into a 3D table and compresses the label-triplets in the table. To demonstrate the utility of our algorithms, we discuss two applications of them in scientific data mining. First, we apply the method to locating frequently occurring motifs in two families of proteins pertaining to RNA-directed DNA Polymerase and Thymidylate Synthase, and use the motifs to classify the proteins. Then we apply the method to clustering chemical compounds pertaining to aromatic, bicyclicalkanes and photosynthesis. Experimental results indicate the good performance of our algorithms and high recall and precision rates for both classification and clustering. We also extend our algorithms for processing a class of similarity queries in databases of 3D graphs.

In the second part of the dissertation, we present an index structure, called *MetricMap*, that takes a set of objects and a distance metric and then maps those

objects to a k-dimensional pseudo-Euclidean space in such a way that the distances among objects are approximately preserved. Our approach employs sampling and the calculation of eigenvalues and eigenvectors. The index structure is a useful tool for clustering and visualization in data intensive applications, because it replaces expensive distance calculations by sum-of-square calculations. This can make clustering in large databases with expensive distance metrics practical.

We compare the index structure with another data mining index structure, *FastMap*, proposed by Faloutsos and Lin, according to two criteria: relative error and clustering accuracy. For relative error, we show that (i) *FastMap* gives a lower relative error than *MetricMap* for Euclidean distances, (ii) *MetricMap* gives a lower relative error than *FastMap* for non-Euclidean distances (i.e., general distance metrics), and (iii) combining the two reduces the error yet further. A similar result is obtained when comparing the accuracy of clustering. These results hold for different data sizes. The main qualitative conclusion is that these two index structures capture complementary information about distance metrics and therefore can be used together to great benefit. The net effect is that multi-day computations can be done in minutes.

We have implemented the proposed algorithms and the *MetricMap* index structure into a toolkit. This toolkit will be useful for data mining, visualization, and approximate retrieval in scientific, multimedia and high dimensional databases.

INFORMATION RETRIEVAL AND MINING IN HIGH DIMENSIONAL DATABASES

by
Xiong Wang

A Dissertation
Submitted to the Faculty of
New Jersey Institute of Technology
in Partial Fulfillment of the Requirements for the Degree of
Doctor of Philosophy

Department of Computer and Information Science

October 2000

APPROVAL PAGE

INFORMATION RETRIEVAL AND MINING IN HIGH DIMENSIONAl DATABASES

Xiong Wang

Dr. Jason T. L. Wang, Dissertation Advisor — Date
Associate Professor of Computer Science, NJIT

Dr. James A. M. McHugh, Committee Member — Date
Professor of Computer Science, NJIT

Dr. David Nassimi, Committee Member — Date
Associate Professor of Computer Science, NJIT

Dr. Frank Y. Shih, Committee Member — Date
Professor of Computer Science, NJIT

Dr. Euthimios Panagos, Committee Member — Date
Member of Technical Staff, AT&T Labs Research, NJ

BIOGRAPHICAL SKETCH

Author:	Xiong Wang
Degree:	Doctor of Philosophy
Date:	October 2000

Undergraduate and Graduate Education:

- Doctor of Philosophy in Computer Science,
  New Jersey Institute of Technology, 2000
- Master of Science in Computer Science,
  Fudan University, Shanghai, China, 1989
- Bachelor of Science in Mathematics,
  Xiamen University, China, 1982

Major: Computer Science

Presentations and Publications:

Xiong Wang, Jason T.L. Wang, Dennis Shasha, Bruce Shapiro, Isidore Rigoutsos, and Kaizhong Zhang, "Finding Patterns in Three Dimensional Graphs: Algorithms and Applications to Scientific Data Mining", Research Report, Computer and Information Science Department, New Jersey Institute of Technology, CIS-99-04. Also submitted to IEEE Transaction on Knowledge and Data Engineering.

Xiong Wang and Jason T.L. Wang, "Fast Similarity Search in Three-Dimensional Structure Databases", Submitted to The Journal of Chemical Information and Computer Sciences.

Xiong Wang and Jason T.L. Wang, "Implementation and Evaluation of An Index Structure for Data Clustering", to appear in Knowledge and Information Systems: An International Journal.

Jason T.L. Wang, Xiong Wang, King-Ip Lin, Dennis Shasha, Bruce A. Shapiro, and Kaizhong Zhang, "Evaluating A Class of Distance-Mapping Algorithms for Data Mining and Clustering", Proc. of the Fifth ACM SIGKDD International Conference on Knowledge Discovery and Data Mining, pages 307 – 311, August 1999, San Diego, California, U.S.A.

Xiong Wang and Jason T. L. Wang, "Fast Similarity Search in Databases of 3D Objects", Proc. of the 10th IEEE International Conference on Tools with Artifical Intelligence, pages 16 – 23, November 1998, Taipei, Taiwan.

Yanling Yang, Kaizhong Zhang, Xiong Wang, Jason T.L. Wang and Dennis Shasha, "An Approximate Oracle for Distance in Metric Spaces", In M. Farach-Colton, editor, Combinatorial Pattern Matching, pages 104 – 117, Lecture Notes in Computer Science, Springer-Verlag, 1998.

Xiong Wang, Jason T.L. Wang, Dennis Shasha, Bruce Shapiro, Sitaram Dikshitulu, Isidore Rigoutsos and Kaizhong Zhang, "Automated Discovery of Active Motifs in Three Dimensional Molecules", Proc. of the Third International Conference on Knowledge Discovery and Data Mining, pages 89 – 95, August 1997, Newport Beach, California.

Xiong Wang and Jason T.L. Wang, "approximate Substructure Search in a Database of 3D Graphs", Proc. of the Third Joint Conference on Information Sciences, pages 12 – 15, March 1997, Research Triangle Park, North Carolina.

Xiong Wang and Baile Shi, "Query Optimization in a Knowledge Base System", Proc. of the Second Far-East Workshop on Future Database Systems, pages 327 – 330, April 1992, Kyoto, Japan.

This work is dedicated to
my wife and parents

ACKNOWLEDGMENT

First of all, I would like to thank my advisor Dr. Jason T. L. Wang for his patience, encouragement and help. He was always there to answer whatever question I had at any time. I wish also to thank Dr. Dennis Shasha, whose comments have been so inspiring. Their dedication to the academic career sets an example for me. I appreciate the cooperation with Dr. Kaizhong Zhang, Dr. Isidore Rigoutsos and Dr. Bruce Shapiro. Working with them has been so exciting.

I am grateful to Dr. James McHugh, Dr. David Nassimi, Dr. Frank Shih, and Dr. Euthimios Panagos for their serving in my dissertation committee.

Finally, I thank my wife and my parents, without whose love and support this accomplishment will not be possible.

TABLE OF CONTENTS

Chapter **Page**

LIST OF TABLES

LIST OF TABLES

LIST OF FIGURES

CHAPTER 1
INTRODUCTION

In recent years, much effort has been spent in the study of non-traditional data types, such as sequences [25, 41, 81, 84, 85], trees [12, 73, 75, 91, 103], graphs [90, 104], and high dimensional objects. These data types arise frequently in many scientific domains. For example, in molecular biology, they are used to represent DNA and protein structures [12, 81, 84, 85]. How to efficiently process these data types poses a challenging problem to the data management community.

This dissertation focuses on information retrieval, discovery, and clustering in high dimensional databases and metric spaces. In the first part of the dissertation, we introduce an approach to approximate pattern discovery in a database of three dimensional graphs (or objects) [96]. Our approach is an extension of the geometric hashing technique invented by Lamden and Wolfson for tackling computer vision problems [48, 49, 99]. Given a database $\mathcal{D}$ of 3D graphs, an *active pattern* is a substructure that occurs in many graphs. For example, in three dimensional molecules these patterns are called active motifs. Our algorithm tries to discover patterns that approximately occur in multiple graphs. A pattern is said to occur in a graph approximately if it matches a substructure of the graph, possibly in the presence of rotation, translation and node relabel/insert/delete in either the substructure or the pattern. Our algorithm finds many applications in for example drug design [26] and molecular biology [58].

Databases in these domains are often large in size. In order to find all interesting patterns, one needs to consider lots of possible substructures. Thus the efficiency of the algorithm is critical. Our approach employing geometric hashing is shown empirically to be very efficient. We then extend the algorithm to process a class of similarity queries in databases of 3D objects. We applied our query processing algorithms to 226 chemical compounds obtained from a drug database maintained in the National Cancer Institute, and a set of synthetic graphs. The experimental results showed that our technique is 100 times faster than the exhaustive search method when the data set has over 600 objects while achieving the same recall.

In the second part of the dissertation, we present an index structure, called *MetricMap*, that takes a set of objects and a distance metric and then maps those objects to a k-dimensional pseudo-Euclidean space in such a way that the distances among objects are approximately preserved. Our approach employs sampling and the calculation of eigenvalues and eigenvectors. The index structure is a useful tool for clustering and visualization in data intensive applications [101]. *MetricMap* differs from another data mining index structure, *FastMap*, proposed by Faloutsos and Lin, in the algorithm it uses for embedding and the target space it chooses. *FastMap* embeds the objects in a Euclidean space, whereas *MetricMap* embeds them in a pseudo-Euclidean space [33, 50]. We compare the two index structures according to two criteria: relative error and clustering accuracy [92, 97]. For relative error, we show that (i) *FastMap* gives a lower relative error than *MetricMap* for Euclidean distances, (ii) *MetricMap* gives a lower relative error than *FastMap* for non-Euclidean distances (i.e., general distance metrics), and (iii) combining the two reduces the error yet further. A similar result is obtained when comparing the accuracy of clustering. These results hold for different data sizes. The main qualitative conclusion is that these two index structures capture complementary information about distance metrics and therefore can be used together to great benefit. The net effect is that multi-day computations can be done in minutes.

In Chapter 2, we present the framework for finding patterns in 3D graphs and its application to the discovery of motifs in proteins and chemical compounds. Chapter 3 extends the algorithm to process a class of similarity queries in databases of 3D graphs. Chapter 4 describes the *MetricMap* index structure and its performance in approximating distances for both artificial data and real data. Chapter 5 compares *FastMap* with *MetricMap*, builds some complementary index structures, and compares the relative performance of these index structures. Chapter 6 describes the toolkit containing the programs for pattern discovery and similarity retrieval in 3D graphs using the geometric hashing technique as well as the *MetricMap* index structure. Chapter 7 concludes the dissertation and discusses future work.

CHAPTER 2

FINDING PATTERNS IN THREE DIMENSIONAL GRAPHS: ALGORITHMS AND AN APPLICATION TO DATA MINING

2.1 Introduction

In this Chapter, we introduce an approach for finding patterns in a database of 3D graphs. Given a database $\mathcal{D}$ of 3D graphs, An active pattern is a common substructure that occurs in more than one graph. For example, in three dimensional molecules these patterns are called active motifs. Our algorithm tries to discover patterns that approximately occur in more than one graph. A pattern is said to occur in a graph approximately if it matches a substructure of the graph approximately in the presence of rotation, translation and node relabel/insert/delete in either the substructure or the pattern. This is an extension of the traditional substructure match in scientific and biochemical databases [66]. Our approach is based on the geometric hashing technique.

The rest of the chapter is organized as follows. Section 2.2 is a survey of related work. Section 2.3 formalizes the pattern discovery problem. Section 2.4 presents the theoretical framework of our approach and describes the pattern-finding algorithm in detail. Section 2.5 evaluates the performance and efficiency of the pattern-finding algorithm. Section 2.6 discusses the applications of our approach to classifying proteins and clustering compounds. Section 2.7 concludes the chapter.

2.2 Related Work

There are several groups working on pattern finding (or knowledge discovery) in molecules and graphs. Conklin *et al.* [15, 16, 17], for example, represented a molecular structure as an image, which comprised a set of parts with their 3D coordinates and a set of relations that were preserved for the image. The authors used an incremental, divisive approach to discover the "knowledge" from a dataset, that is, to build a subsumption hierarchy that summarized and classified the dataset. The algorithm relied on a measure of similarity among molecular images that was defined in terms of their largest common subimages.

In [20], Djoko *et al.* developed a system, called SUBDUE, that utilized the minimum description length principle to find repeatedly occurring substructures in a graph. Once a substructure was found, the substructure was used to simplify the graph by replacing instances of the substructure with a pointer to the discovered substructure. In [19], Dehaspe *et al.* used DATALOG to represent compounds and applied data mining techniques to predicting chemical carcinogenicity. Their techniques were based on Mannila and Toivonen's algorithm [51] for finding interesting patterns from a class of sentences in a database.

In contrast to the above work, we use the geometric hashing technique to find approximately common patterns in a set of 3D graphs without prior knowledge of their structures, positions, or occurrence frequency. The geometric hashing technique used here originated from the work of Lamdan and Wolfson for model based recognition in computer vision [49]. Several researchers attempted to parallelize the technique based on various architectures, such as the Hypercube and the Connection Machine [9, 65, 63]. It was observed that the distribution of the hash table entries might be skewed. To balance the distribution of the hash function values, delicate rehash functions were designed [63]. There were also efforts exploring the uncertainty existing in the geometric hashing algorithms [34, 70].

Recently, Rigoutsos *et al.* employed geometric hashing and magic vectors for substructure matching in a database of chemical compounds [66]. The magic vectors were bonds among atoms; the choice of them was domain dependent and was based on the type of each individual graph. We extend the work in [66] by providing a framework for discovering approximately common substructures in a set of 3D graphs, and applying our techniques to both compounds and proteins. Our approach differs from [66] in that instead of using the magic vectors, we store a coordinate system in a hash table entry. Furthermore we establish a theory for detecting and eliminating false matches occurring in the hashing.

Geometric hashing technique was first introduced in late 80's for model based recognition in computer vision [49]. The key observation behind the technique is as follows. Suppose D is an object consisting of a set of points in the two dimensional space R^2. Given any three points P_1, P_2 and P_3 in D that are not collinear, a coordinate system can be formed using P_1 as the origin, $\vec{P_1, P_2}$ as X-axis and $\vec{P_1, P_3}$ as Y-axis. Any other point P in D has a set of coordinates (x, y) with respect to this coordinate system (Fig. 2.1(a)). Now suppose under certain rigid rotation or translation P_1, P_2, P_3 and P become P_1', P_2', P_3' and P'. P_1', P_2' and P_3' will still be non-collinear and they can form another coordinate system. Notice that the coordinates of P' with respect to this new coordinate system is still (x, y) (Fig. 2.1(b)).

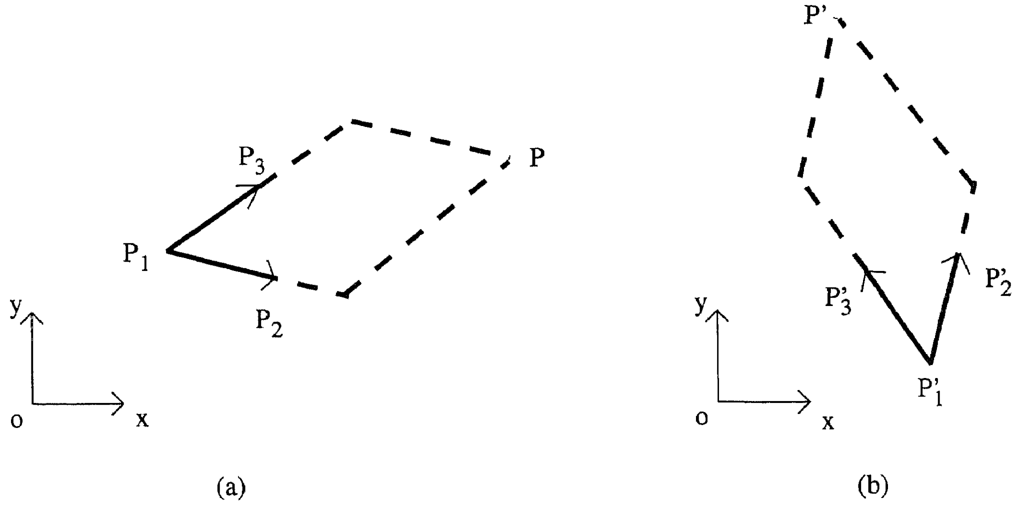

Figure 2.1 The reference system and affine coordinates.

Thus these coordinates are geometric invariant. Using the original terminologies, any triplet of points P_1, P_2 and P_3 in D that are non-collinear is called a *reference system* RS, and the coordinates of any point P in D with respect to RS is called the *affine coordinates* of P w.r.t. RS.

The geometric hashing algorithm is composed of two phases. In the preprocessing phase, every ordered triplet of points in D that are not collinear is used as an RS, and the affine coordinates (x, y) of every other point in D are computed with respect to the RS. RS is then entered into the hash table at each (x, y) location. For an object with n points, there are $(n-3) \times \binom{n}{3}$ entries in the hash table. This process is done for every data object D. In the recognition phase, given a query object Q, every triplet of points in Q is taken to be a reference system, and the affine coordinates of all other points in Q are computed with respect to the reference system to index into the hash table and "vote" for all RS's found there. A histogram for the RS's is created for each data object. If the number of the votes for any RS is sufficiently high, that RS and the corresponding data object are collected as a hypothesis. A verification process is then used to identify the correct answers. Suppose there is a substructure match between the query object and the data object and a triplet of points tri_Q in the query object Q matches an RS in a data object. This RS will get high score in the voting process when triplet tri_Q is chosen as the reference system during the recognition phase.

Due to the arrangement of hash table, the voting can be done for all data objects and all RS's in each data object simultaneously. Both phases of the algorithm have nice features for parallel processing. Algorithms for parallel geometric hashing have been developed on several different architectures, such as the Hypercube SIMD and the Connect Machine, e.g. model CM-2, CM-5 [9, 63, 65]. All these algorithms achieved fine-grain data parallelism.

However, nothing is perfect. The original geometric hashing algorithm has its drawbacks. Since every triplet of points in the data object is used as a reference system, the records in the hash table are highly redundant. Furthermore, in the presence of uncertainty, affine representations are not invariant with respect to the Cartesian coordinate system. In [34] the authors provided a precise analysis of affine point matching, obtaining an expression for the range of affine-invariant values consistent with bounded uncertainty. This analysis revealed that the range of affine-invariant values depends on the original positions of the points. The effect of this phenomenon is twofold. If it happened in the preprocessing phase when the data objects were hashed, it would degrade the performance rapidly [34]. Intuitively, due to uncertainty, the error causes the point entries in the hash table to blur into regions, making the table denser and increasing the chances that a random point (i.e. a point does not really belong to any data objects) will appear to be a hypothesis for a match [70]. One the other hand, if it happened in the recognition phase when the query object was processed, it would cause both false positive and false negative votes. In [70] the author analyzed the effect of this phenomenon in the presence of Gaussian noise.

In [38] the authors discussed the problem of self-affine shapes. A self-affine shape consists smaller, affine copies of itself or its parts. When geometric hashing is applied to scenes with lots of self-affine shapes, there is a large proportion of four-point combinations that produce the same affine-invariant coordinates, yielding severe spikes in the histogram, which may cause the geometric hashing method to malfunction [38]. The authors then introduced an alternative approach called similarity hashing. Like geometric hashing, similarity hashing operates on combinations of four points. Each group of four points $A, B, CandD$ forms two line segments $\overline{AB}$ and $\overline{CD}$. The two line segments $\overline{AB}$, $\overline{CD}$ are related by two parameters: scale and orientation. Assume $||\overline{AB}|| \geq ||\overline{CD}||$, the scale $s : 0 < s \leq 1$ is the ratio of the lengths of the two line segments

$$s = \frac{||\overline{CD}||}{||\overline{AB}||}$$

The orientation $\theta : -\frac{\pi}{2} \leq \theta < \frac{\pi}{2}$ is given by the minimum angle that $\overline{AB}$ rotates to become parallel to $\overline{CD}$. Their experiments demonstrated the ability of this approach at detecting morphological self-similarity, and producing the parameters of the self-similarity transformation, which helped in the process of fractal image compression.

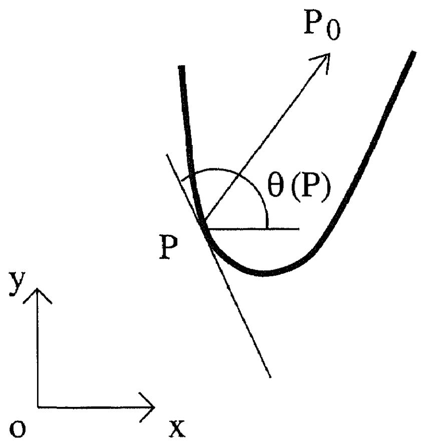

Figure 2.2 The generalized Hough transform.

It is interesting to compare the geometric hashing techniques with the generalized Hough transform [6, 39]. The generalized Hough transform is also composed of two phases. We describe here the Hough transform applying to a set of curves. Given are a set of data curves and a query curve, our goal is to find those data curves that best match the query curve. In the preprocessing phase, a data curve is processed as follows (Fig. 2.2).

1. Arbitrarily choose a reference point P_0;
2. for each point P on the curve do the following:
   - (a) calculate the angle $\theta(P)$ tangent at P;
   - (b) store the vector $\vec{P, P_0}$ at location $\theta(P)$ of a hash table.

In the recognition phase, for each point P on the query curve, the angle tangent at P is used as index to access the hash table. Every reference point P_0 at that location gets one vote. A histogram for the reference point is created for each data curve, and then analyzed to find matches.

Both the geometric hashing technique and the generalized Hough transform technique use similar object representation schemes and both of them utilize a look up table to improve the performance.

Comparing with the original geometric hashing technique, our approach reduces redundancy significantly and is more adjustable to noise. When dealing with approximate substructure matching, our approach is also more flexible than both the original geometric hashing technique and the generalized Hough transform technique.

2.3 3D Graphs in the Euclidean Space

Three dimensional (3D) graphs occur frequently in scientific disciplines. In chemistry, for example, chemical compounds are 3D graphs [66]. In biology, the tertiary structures of proteins are also 3D graphs [16, 27]. Each node of such graphs is an undecomposable or atomic unit and has a 3D coordinate.[1] Each node has a label, which is not necessarily unique in a graph. Node labels are chosen from a domain-dependent alphabet Σ. In chemical compounds, for example, the alphabet includes the names of all atoms. A node can be identified by a unique, user-assigned number in the graph. Edges in the graph are links between the atomic units. We consider in the chapter the graphs to be connected [53]; otherwise we focus on the connected components of the graphs.

A graph can be divided into one or more *rigid* substructures. A rigid substructure is a subgraph in which there are no internal rotations; that is, the relative positions of nodes in the substructure are fixed.[2] The precise definition of

[1]More precisely, the 3D coordinate indicates the location of the center of the atomic unit.

[2]Note that the rigid substructure as a whole can be rotated (we refer to this as a "whole-structure" rotation or simply a rotation when the context is clear). That is to say, the relative position of a node in the substructure and a node outside the substructure can be changed under the rotation.

a "substructure" is application dependent. For example, in chemical compounds, a ring is a rigid substructure. Thus if we consider a chemical compound as a 3D graph in which each atom is a node and each bond is an edge, a block [53] of the graph could be a rigid substructure; two rigid substructures may be connected by an edge and they may be rotatable with respect to each other around the edge. On the other hand, in a protein that itself as a whole is a rigid structure, a residue or a combination of multiple residues as illustrated in Section 2.4 could be a rigid substructure.

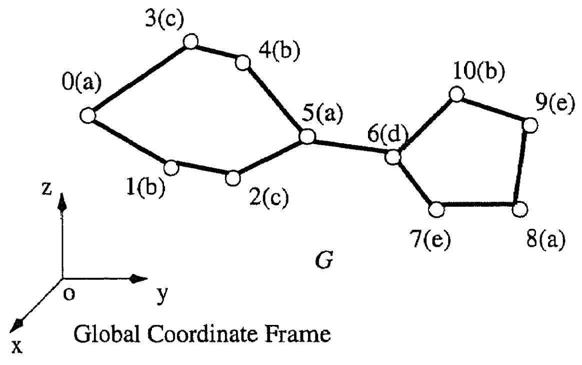

Figure 2.3 A data graph G.

Example 2.1 Consider the graph G in Fig. 2.3. Each node is associated with a unique number, with its label being enclosed in parentheses. Table 2.1 shows the 3D coordinates of the nodes in the graph with respect to the Global Coordinate Frame. We divide the graph into two rigid substructures: Str_0 and Str_1. Str_0 consists of nodes numbered 0, 1, 2, 3, 4, 5 as well as edges connecting the nodes (Fig. 2.4(a)). Str_1 consists of nodes numbered 6, 7, 8, 9, 10 as well as edges connecting them (Fig. 2.4(b)). The two substructures are rotatable with respect to each other around the edge $\{5, 6\}$ that connects Str_0 and Str_1. Note that a rigid substructure is not necessarily complete. For example, in Fig. 2.4(a), there is no edge connecting the node numbered 1 and the node numbered 3. □

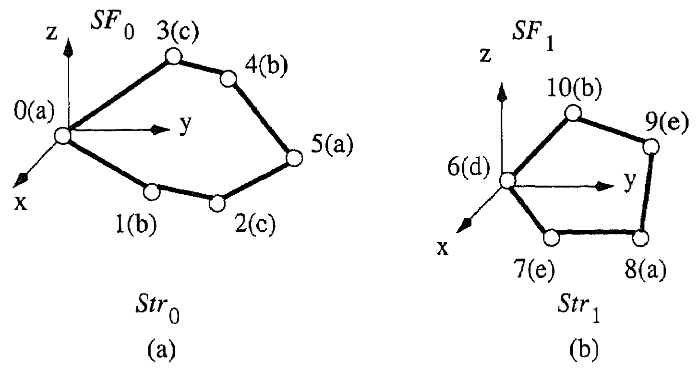

Figure 2.4 The substructures of the data graph in Fig. 2.3

Table 2.1 Identifiers, labels and global coordinates of the nodes of the graph in Fig. 2.3

Node identifier	Node label	Node coordinates
0	a	(1.0178, 1.0048, 2.5101)
1	b	(1.2021, 2.0410, 2.0020)
2	c	(1.3960, 2.9864, 2.0006)
3	c	(0.7126, 2.0490, 3.1921)
4	b	(0.7610, 2.7125, 3.0124)
5	a	(1.0097, 3.6478, 2.2660)
6	d	(1.1329, 4.5002, 2.2024)
7	e	(1.5309, 5.2026, 1.7191)
8	a	(1.4529, 6.1015, 1.5712)
9	e	(1.0356, 6.0030, 2.2820)
10	b	(0.7359, 5.0571, 2.6857)

We attach a local coordinate frame SF_0 (SF_1, respectively) to substructure Str_0 (Str_1, respectively). For instance, let us focus on the substructure Str_0 in Fig. 2.4(a). We attach a local coordinate frame to Str_0 whose origin is the node numbered 0. This local coordinate frame is represented by three basis points P_{b_1}, P_{b_2} and P_{b_3}, with coordinates $P_{b_1}(x_0, y_0, z_0)$, $P_{b_2}(x_0+1, y_0, z_0)$ and $P_{b_3}(x_0, y_0+1, z_0)$, respectively. The origin is P_{b_1} and the three basis vectors are $\vec{V}_{b_1,b_2}$, $\vec{V}_{b_1,b_3}$, and $\vec{V}_{b_1,b_2} \times \vec{V}_{b_1,b_3}$. Here, $\vec{V}_{b_1,b_2}$ represents the vector starting at point P_{b_1} and ending at point P_{b_2}. $\vec{V}_{b_1,b_2} \times \vec{V}_{b_1,b_3}$ stands for the cross product of the two corresponding vectors. We refer to this coordinate frame as Substructure Frame 0, or SF_0. Note that, the basis vectors of SF_0 are orthonormal. That is, the length of each vector is 1 and the angle between any two basis vectors has 90 degrees. Also note that, for any node numbered i in the substructure Str_0 with global coordinate $P_i(x_i, y_i, z_i)$, we can find a local coordinate of the node i with respect to SF_0, denoted P_i', where

$$P_i' = \vec{V}_{b_1,i} = (x_i - x_0, y_i - y_0, z_i - z_0) \tag{2.1}$$

2.3.1 Patterns in 3D Graphs

We consider a pattern to be a rigid substructure that may occur in a graph after allowing for an arbitrary number of rotations and translations as well as a small number (specified by the user) of edit operations in the pattern or in the graph. There are three types of edit operations: relabeling a node, deleting a node and inserting a node. Relabeling a node v means to change the label of v to any valid label that differs from its original label. Deleting a node v from a graph means to remove the corresponding atomic unit from the 3D Euclidean space and make the edges touching v connect with one of its neighbors v'. (This amounts to contraction of the edge between v and v' [29].) Inserting a node v into a graph means to add the corresponding atomic unit to the 3D Euclidean space and make a node v' and a subset of its neighbors become the neighbors of v.[3] Graph G matches graph G' with n mutations if by applying an arbitrary number of rotations and translations as well as n node insert, delete or relabeling operations, one can transform G to G'. A substructure P *approximately occurs* in a graph G (or G approximately contains P) within n mutations if P matches some subgraph of G with n mutations or fewer where n is chosen by the user.

[3]Note that when a node v is inserted or deleted, the nodes surrounding v do not move, i.e., their coordinates remain the same. The three edit operations are extensions of the edit operations on sequences; they arise naturally in graph editing [29] and molecule evolution [69]. As shown in Section 2.4, based on these edit operations, our algorithm finds useful patterns that can be used to classify and cluster 3D molecules effectively.

Example 2.2 Consider the set $\mathcal{S}$ of three graphs in Fig. 2.5(a). Suppose only exactly coinciding substructures (without mutations) occurring in at least two graphs and having size greater than 3 are considered as "patterns." Then $\mathcal{S}$ contains one pattern shown in Fig. 2.5(b). If substructures having size greater than 4 and approximately occurring in all the three graphs within one mutation (i.e. one node delete, insert or relabeling is allowed in matching a substructure with a graph) are considered as "patterns," then $\mathcal{S}$ contains one pattern shown in Fig. 2.5(c). □

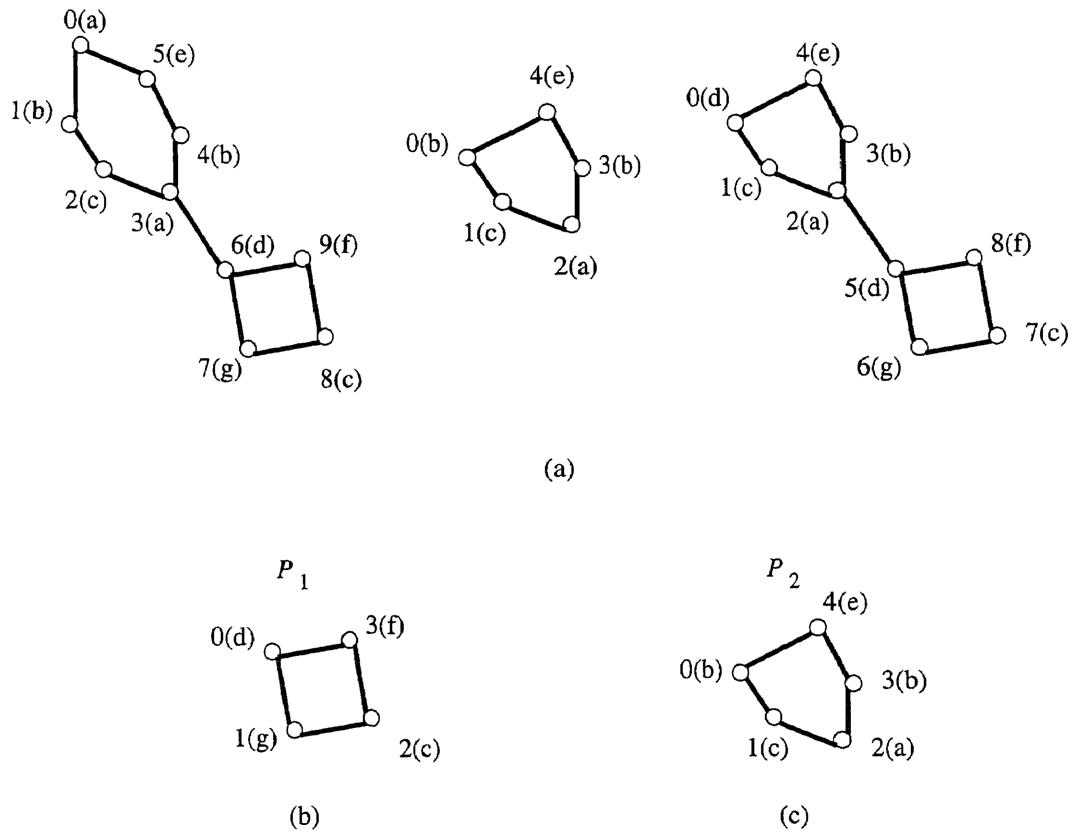

Figure 2.5 (a) The set $\mathcal{S}$ of three graphs; (b) the pattern exactly occurring in two graphs in $\mathcal{S}$; (c) the pattern approximately occurring, within one mutation, in all the three graphs.

Our strategy to find the patterns in a set of 3D graphs is to decompose the graphs into rigid substructures and then use the geometric hashing technique [49] to store the substructures in a disk-based table. We then evaluate the substructures in the hash table to find frequently occurring ones.

In [96], we applied the approach to the discovery of patterns in chemical compounds under a restricted set of edit operations including node insert and node delete, and tested the quality of the patterns by using them to classify the compounds. Here we extend the work in [96] by (i) considering more general edit operations including node insert, delete and relabeling; (ii) presenting the theoretical foundation and evaluating the performance and efficiency of our pattern-finding algorithm; (iii) applying the discovered patterns to classifying 3D proteins, which are much larger and more complicated in topology than chemical compounds; and (iv) presenting a technique to cluster 3D graphs based on the patterns occurring in them [98]. Classification and clustering are two important data mining operations in general and scientific disciplines [2, 3, 36, 86, 87, 105]; here we show experimentally that our techniques are useful for the scientific data mining applications.

2.4 Pattern-Finding Algorithm

2.4.1 Terminology

Let S be a set of 3D graphs. The occurrence number of a pattern P is the number of graphs in S that approximately contain P within the allowed number of mutations. Formally, the occurrence number of a pattern P (or the *activity* of P) with respect to mutation d and set S, denoted $occurrence\_no^d_S(P)$, is k if there are k graphs in S that contain P within d mutations. For example, consider Fig. 2.5 again. Let S contain the three graphs in Fig. 2.5(a). Then $occurrence\_no^0_S(P_1) = 2$; $occurrence\_no^1_S(P_2) = 3$.

Given a set S of 3D graphs, our algorithm finds all the patterns P where P approximately occurs in at least $Occur$ graphs in S within the allowed number of mutations Mut and $|P| \geq Size$, where $|P|$ represents the size, i.e., the number of nodes, of the pattern P. (Mut, $Occur$ and $Size$ are user-specified parameters.) One can use the patterns in several ways. For example, natural scientists may evaluate whether the patterns are in fact the active sites; computer scientists may use the patterns to classify or cluster molecules as demonstrated in Section 2.4.

Our algorithm proceeds in two phases to search for the patterns: (1) find candidate patterns from the graphs in $\mathcal{S}$; and (2) evaluate the activity of the candidate patterns to determine which of them satisfy the user-specified requirements. We describe each phase in turn below.

2.4.2 Phase (1) of the Algorithm

In phase (1) of the algorithm, we decompose the graphs into rigid substructures. Dividing a graph into substructures is necessary for two reasons. First, in dealing with some molecules such as chemical compounds in which there may exist two substructures that are rotatable with respect to each other, any graph containing the two substructures is not rigid. As a result, we decompose the graph into substructures having no rotatable components and consider the substructures separately. Second, our algorithm hashes node-triplets into a 3D table. When a graph as a whole is too large, as in the case of proteins, considering all combinations of three nodes in the graph may become prohibitive. Consequently, decomposing the graph into substructures and hashing node-triplets of the substructures can increase efficiency. For example, consider a graph of 20 nodes. There are $\binom{20}{3} = 1140$ node-triplets. On the other hand, if we decompose the graph into five substructures, each having four nodes, then there are only $5\times \binom{4}{3} = 20$ node-triplets.

There are several alternative ways to decompose 3D graphs into rigid substructures, depending on the application at hand and the nature of the graphs. The substructures may partition a graph or may overlap with one another. For example, to find patterns in a chemical compound, one can use a modified depth-first search algorithm for finding blocks to decompose the compound into substructures as described in [53, 96]. In this case, the substructures partition the compound.

Two substructures may be connected by one bond (edge); they may be rotatable with respect to each other around the bond (cf. Example 2.1). On the other hand, for a protein that itself forms a single rigid structure, one can decompose it into substructures of fixed size according to some order as illustrated in Section 2.4 or consider each residue as a rigid substructure. In these cases, two substructures may overlap or may be connected by multiple edges.

For the purposes of exposition, we describe our pattern-finding algorithm based on a partitioning strategy. Our approach assumes a notion of atomic unit which is the lowest level of description in the case of interest. Intuitively, atomic units are the fundamental building blocks, e.g. atoms in a molecule. Edges arise as bonds between atomic units. We break a graph into maximal size rigid substructures (recall that a rigid substructure is a subgraph in which there are no internal rotations; that is, the relative positions of nodes in the substructure are fixed). We use an approach similar to [53] that employs a depth-first search algorithm, referred to as DFB, to find blocks in graphs. Each block is a rigid substructure. We merge two rigid substructures B_1 and B_2 if they are not rotatable with respect to each other; that is, the relative position of a node $n_1 \in B_1$ and a node $n_2 \in B_2$ is fixed. The algorithm maintains a stack, denoted STK, which keeps the rigid substructures being merged. Fig. 2.6 shows the algorithm, which outputs a set of rigid substructures of a graph G. We then throw away the substructures P where $|P| < Size$. The remaining substructures constitute the candidate patterns generated from G. This pattern-generation algorithm runs in time linearly proportional to the number of edges in G.

2.4.3 Phase (2) of the Algorithm

Phase (2) of our pattern-finding algorithm consists of two subphases. In subphase A of phase (2), we hash the candidate patterns generated from the graphs in phase

```
Procedure Find_Rigid_Substructures
Input: Graph $G$.
Output: A set of maximal size rigid substructures generated from $G$.

$STK := \emptyset$;
while $G$ is not empty do
    begin
       locate the next block $B_1$ in $G$ using the DFB algorithm;
       delete $B_1$ from $G$; let the top entry of $STK$ be $B_2$;
       if ($STK$ is empty) or ($B_1$ and $B_2$ are not rotatable w.r.t. each other) then
          push the nodes of $B_1$ into $STK$;
       else begin
          pop out all nodes in $STK$,
          merge them and output the resulting substructure;
          push the nodes of $B_1$ into $STK$;
       end;
    end;
pop out all nodes in $STK$, merge them and output the resulting substructure;
```

Figure 2.6 Algorithm for finding rigid substructures in a graph.

(1) into a 3D table $\mathcal{H}$. In subphase B, we rehash each candidate pattern into $\mathcal{H}$ and evaluate its activity (recall that the activity is the number of approximate occurrences).

In processing a rigid substructure (pattern) of a 3D graph, we choose all three-node combinations, referred to as node-triplets, in the substructure and hash the node-triplets. We hash three-node combinations, because to fix a rigid substructure in the 3D Euclidean space one needs at least three nodes from the substructure and three nodes are sufficient provided they are not collinear. Notice that the proper order of choosing the nodes i, j, k in a triplet is significant. We determine the order of the three nodes by considering the triangle formed by them. The first node chosen always opposes the longest edge of the triangle and the third node chosen opposes the shortest edge. Thus, the order is unique if the triangle is not isosceles or equilateral, which usually holds when the coordinates are floating point numbers. In other cases, we store all configurations obeying the longest-shortest rule described above.

The labels of the nodes in a triplet form a label-triplet, which is encoded as follows. Suppose the three nodes chosen are v_1, v_2, v_3, in that order. We maintain all node labels in the alphabet Σ in an array $\mathcal{A}$. The code for the labels is an unsigned long integer, defined as $((L_1 \times Prime + L_2) \times Prime) + L_3$, where $Prime > |\Sigma|$ is a prime number, L_1, L_2 and L_3 are the indices for the node labels of v_1, v_2 and v_3, respectively, in the array $\mathcal{A}$. Thus the code of a label-triplet is unique. This simple encoding scheme reduces three label comparisons into one integer comparison.

Example 2.3 Consider again the graph G in Fig. 2.3. Suppose the node labels are stored in the array $\mathcal{A}$ as shown in Table 2.2. Suppose *Prime* is 1,009. Then, for example, for the three nodes numbered 2, 0 and 1 in Fig. 2.3, the code for the corresponding label-triplet is $((2 \times 1,009 + 0) \times 1,009) + 1 =$ 2,036,163. □

Table 2.2 The node labels of the graph in Fig. 2.3 and their indices in the array $\mathcal{A}$.

index	0	1	2	3	4
label	a	b	c	d	e

2.4.3.1 Subphase A of Phase (2) In this subphase, we hash the candidate patterns generated in phase (1) of the pattern-finding algorithm into a 3D table. For the purposes of exposition, consider the example substructure Str_0 in Fig. 2.4(a), which is assumed to be a candidate pattern. We choose any three nodes in Str_0 and calculate their 3D hash function values as follows. Suppose the chosen nodes are numbered i, j, k and have global coordinates $P_i(x_i, y_i, z_i)$, $P_j(x_j, y_j, z_j)$ and $P_k(x_k, y_k, z_k)$, respectively. Let l_1, l_2, l_3 be three integers where

$$\begin{aligned} l_1 &= ((x_i - x_j)^2 + (y_i - y_j)^2 + (z_i - z_j)^2) \times \mathit{Scale} \\ l_2 &= ((x_i - x_k)^2 + (y_i - y_k)^2 + (z_i - z_k)^2) \times \mathit{Scale} \\ l_3 &= ((x_k - x_j)^2 + (y_k - y_j)^2 + (z_k - z_j)^2) \times \mathit{Scale} \end{aligned}$$

Here $\mathit{Scale} = 10^p$ is a multiplier. Intuitively we round to the nearest pth position following the decimal point (here p is the last accurate position) and then multiply the numbers by 10^p. The reason for using the multiplier is that we want some digits following the decimal point to contribute to the distribution of the hash function values. We ignore the digits after the position p because they are inaccurate. (The multiplier is a parameter whose value is determined in experiments and is adjustable for different data.) Let

$$\begin{aligned} d_1 &= (l_1 + l_2) \bmod \mathit{Prime}_1 \bmod \mathit{Nrow} \\ d_2 &= (l_2 + l_3) \bmod \mathit{Prime}_2 \bmod \mathit{Nrow} \\ d_3 &= (l_3 + l_1) \bmod \mathit{Prime}_3 \bmod \mathit{Nrow} \end{aligned}$$

Prime_1, Prime_2 and Prime_3 are three prime numbers and Nrow is the cardinality of the hash table in each dimension. We use three different prime numbers in the hope that the distribution of the hash function values is not skewed even if pairs of l_1, l_2, l_3 are correlated. The node-triplet $[i, j, k]$ is hashed to the 3D bin with the address $h[d_1][d_2][d_3]$. Intuitively we use the squares of the lengths of the three edges connecting the three chosen nodes to determine the hash bin address. Stored in that bin are the graph identification number, the substructure identification number, and the label-triplet code. In addition, we store the coordinates of the basis points P_{b_1}, P_{b_2}, P_{b_3} of Substructure Frame 0 (SF_0) with respect to the three chosen nodes.

Specifically, suppose the chosen nodes i, j, k are not collinear. We can construct another local coordinate frame, denoted $LF[i, j, k]$, using $\vec{V}_{i,j}$, $\vec{V}_{i,k}$ and $\vec{V}_{i,j} \times \vec{V}_{i,k}$ as basis vectors. The coordinates of P_{b_1}, P_{b_2}, P_{b_3} with respect to the local coordinate frame $LF[i, j, k]$, denoted $SF_0[i, j, k]$, form a 3×3 matrix, which is calculated as follows (see Fig. 2.7):

$$SF_0[i,j,k] = \begin{pmatrix} \vec{V}_{i,b_1} \\ \vec{V}_{i,b_2} \\ \vec{V}_{i,b_3} \end{pmatrix} \times A^{-1} \tag{2.2}$$

where

$$A = \begin{pmatrix} \vec{V}_{i,j} \\ \vec{V}_{i,k} \\ \vec{V}_{i,j} \times \vec{V}_{i,k} \end{pmatrix} \tag{2.3}$$

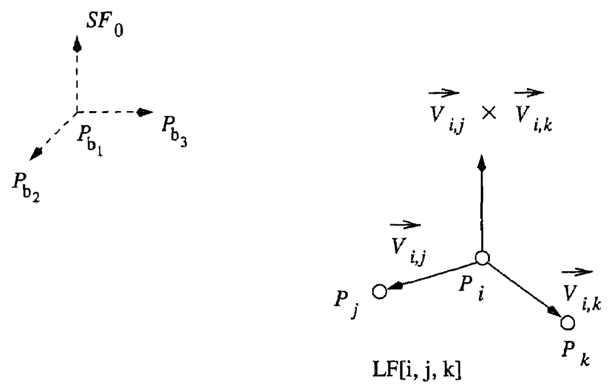

Figure 2.7 Calculation of the coordinates of the basis points P_{b_1}, P_{b_2}, P_{b_3} of Substructure Frame 0 (SF_0) with respect to the local coordinate frame $LF[i, j, k]$.

Thus suppose the graph in Fig. 2.3 has identification number 12. The hash bin entry for the three chosen nodes i, j, k is $(12, 0, Lcode, SF_0[i,j,k])$, where $Lcode$ is the label-triplet code. Since there are 6 nodes in the substructure Str_0, we have $\binom{6}{3} = 20$ node-triplets generated from the substructure and therefore 20 entries in the hash table for the substructure.

Example 2.4 Consider Table 2.1 again. The basis points of SF_0 of Fig. 2.4(a) have global coordinates

$$P_{b_1}(1.0178, 1.0048, 2.5101),$$

$$P_{b_2}(2.0178, 1.0048, 2.5101),$$

$$P_{b_3}(1.0178, 2.0048, 2.5101).$$

Fig. 2.8 shows the local coordinates, with respect to SF_0, of the nodes numbered 0, 1, 2, 3 and 4 in substructure Str_0 of Fig. 2.4(a).

$$P'_0(0.0000, 0.0000, 0.0000),$$

$$P'_1(0.1843, 1.0362, -0.5081),$$

$$P'_2(0.3782, 1.9816, -0.5095),$$

$$P'_3(-0.3052, 1.0442, 0.6820),$$

$$P'_4(-0.2568, 1.7077, 0.5023).$$

Figure 2.8 The local coordinates, with respect to SF_0, of nodes 0, 1, 2, 3, 4 in the substructure Str_0 of Fig. 2.4(a).

Now, suppose $Scale$, $Prime_1$, $Prime_2$, $Prime_3$ are 10, 1,009, 1,033 and 1,051 respectively, and $Nrow$ is 31. Thus, for example, for the nodes numbered 1, 2 and 3, the hash bin address is $h[25][12][21]$ and

$$SF_0[1,2,3] = \begin{pmatrix} -1.056731 & 0.357816 & 0.173981 \\ -0.875868 & 0.071949 & 0.907227 \\ -0.035973 & 0.417517 & 0.024041 \end{pmatrix} \tag{2.4}$$

As another example, for the nodes numbered 1, 4 and 2, the hash bin address is $h[24][0][9]$ and

$$SF_0[1,4,2] = \begin{pmatrix} 0.369457 & -1.308266 & -0.242990 \\ -0.043584 & -0.857105 & -1.006793 \\ 0.455285 & -0.343703 & -0.086982 \end{pmatrix} \tag{2.5}$$

Similarly, for the substructure Str_1, we attach a local coordinate frame SF_1 to the node numbered 6 as shown in Fig. 2.4(b). There are 10 hash table entries for Str_1, each having the form $(12, 1, Lcode, SF_1[l,m,n])$ where l, m, n are any three nodes in Str_1. $\square$

Recall that we choose the three nodes i, j, k based on the triangle formed by them—the first node chosen always opposes the longest edge of the triangle and the third node chosen opposes the shortest edge. Without loss of generality, let us assume that the nodes i, j, k are chosen in that order. Thus, $\vec{V}_{i,j}$ has the shortest length, $\vec{V}_{i,k}$ is the second shortest and $\vec{V}_{j,k}$ is the longest. We use node i as the origin, $\vec{V}_{i,j}$ as the X-axis and $\vec{V}_{i,k}$ as the Y-axis. Then construct the local coordinate frame $LF[i,j,k]$ using $\vec{V}_{i,j}$, $\vec{V}_{i,k}$ and $\vec{V}_{i,j} \times \vec{V}_{i,k}$ as basis vectors. Thus, we exclude the longest vector $\vec{V}_{j,k}$ when constructing $LF[i,j,k]$. Here is why.

The coordinates (x, y, z) of each node in a 3D graph have an error due to rounding. Thus the real coordinates for the node should be $(\overline{x}, \overline{y}, \overline{z})$, where $\overline{x} = x + \epsilon_1$, $\overline{y} = y + \epsilon_2$, $\overline{z} = z + \epsilon_3$ for three small decimal fractions $\epsilon_1, \epsilon_2, \epsilon_3$. After constructing $LF[i,j,k]$ and when calculating $SF_0[i,j,k]$, one may add or multiply the coordinates of the 3D vectors. We define the *accumulating error* induced by a calculation C, denoted $\Delta(C)$, as

$$\Delta(C) = |\overline{f} - f|$$

where $\overline{f}$ is the result obtained from C with the real coordinates and f is the result obtained from C with rounding errors.

Recall that in calculating $SF_0[i,j,k]$, the three basis vectors of $LF[i,j,k]$ all appear in the matrix A defined in Equation (2.3). Let $\overline{|\vec{V}_{i,j}|} = |\vec{V}_{i,j}| + \delta_1$, $\overline{|\vec{V}_{i,k}|} =$

$|\vec{V}_{i,k}| + \delta_2$, and $\overline{|\vec{V}_{j,k}|} = |\vec{V}_{j,k}| + \delta_3$. Let $\delta = \max\{|\delta_1|, |\delta_2|, |\delta_3|\}$. Notice

$$|\vec{V}_{i,j} \times \vec{V}_{i,k}| = |\vec{V}_{i,j}||\vec{V}_{i,k}| \sin\theta$$

where $|\vec{V}_{i,j}|$ is the length of $\vec{V}_{i,j}$, and θ is the angle between $\vec{V}_{i,j}$ and $\vec{V}_{i,k}$. Thus,

$$\begin{aligned}
\Delta(|\vec{V}_{i,j} \times \vec{V}_{i,k}|) &= |\overline{|\vec{V}_{i,j}||\vec{V}_{i,k}|} \sin\theta - |\vec{V}_{i,j}||\vec{V}_{i,k}| \sin\theta| \\
&= |(|\vec{V}_{i,j}| + \delta_1)(|\vec{V}_{i,k}| + \delta_2) \sin\theta - |\vec{V}_{i,j}||\vec{V}_{i,k}| \sin\theta| \\
&= |(|\vec{V}_{i,j}|\delta_2 + |\vec{V}_{i,k}|\delta_1 + \delta_1\delta_2)|| \sin\theta| \\
&\le (|\vec{V}_{i,j}||\delta_2| + |\vec{V}_{i,k}||\delta_1| + |\delta_1||\delta_2|)| \sin\theta| \\
&\le (|\vec{V}_{i,j}| + |\vec{V}_{i,k}| + \delta)\delta \\
&= U_1
\end{aligned}$$

Likewise,

$$\Delta(|\vec{V}_{i,j} \times \vec{V}_{j,k}|) \le (|\vec{V}_{i,j}| + |\vec{V}_{j,k}| + \delta)\delta = U_2$$

and

$$\Delta(|\vec{V}_{i,k} \times \vec{V}_{j,k}|) \le (|\vec{V}_{i,k}| + |\vec{V}_{j,k}| + \delta)\delta = U_3$$

Among the three upperbounds U_1, U_2, U_3, U_1 is the smallest. It's likely that the accumulating error induced by calculating the length of the cross product of the two corresponding vectors is also the smallest. Therefore we choose $\vec{V}_{i,j}$, $\vec{V}_{i,k}$ and exclude the longest vector $\vec{V}_{j,k}$ in constructing the local coordinate frame $LF[i, j, k]$, so as to minimize the accumulating error induced by calculating $SF_0[i, j, k]$.

2.4.3.2 Subphase B of Phase (2)

Let $\mathcal{H}$ be the resulting hash table obtained in subphase A of phase (2) of the pattern-finding algorithm. In subphase B, we evaluate the activity of each candidate pattern P by rehashing the node-triplets of P into $\mathcal{H}$. This way, we are able to match a node-triplet tri of P with a node-triplet tri' of another substructure (candidate pattern) P' stored in subphase A where tri and tri' have the same hash bin address. By counting the node-triplet matches, one can infer whether P matches P' and therefore whether P occurs in the graph from which P' is generated.

We associate each substructure with several counters, which are created and updated as illustrated by the following example. Suppose the two substructures (patterns) of graph G with identification number 12 in Fig. 2.3 have already been stored in the hash table $\mathcal{H}$ in subphase A. Suppose i, j, k are three nodes in the substructure Str_0 of G. Thus for this node-triplet, its entry in the hash table is $(12, 0, Lcode, SF_0[i, j, k])$. Now, in subphase B, consider another pattern P; we hash the node-triplets of P using the same hash function. Let u, v, w be three nodes in P that have the same hash bin address as i, j, k; that is, the node-triplet $[u, v, w]$ "matches" the node-triplet $[i, j, k]$. If the nodes u, v, w geometrically match the nodes i, j, k respectively, i.e., they have coinciding 3D coordinates after rotations and translations, we call the node-triplet match a *true match*; otherwise it is a *false match*. For a true match, let

$$SF_P = SF_0[i, j, k] \times \begin{pmatrix} \vec{V}_{u,v} \\ \vec{V}_{u,w} \\ \vec{V}_{u,v} \times \vec{V}_{u,w} \end{pmatrix} + \begin{pmatrix} P_u \\ P_u \\ P_u \end{pmatrix} \tag{2.6}$$

This SF_P contains the coordinates of the three basis points of the Substructure Frame 0 (SF_0) with respect to the global coordinate frame in which the pattern P is given. We compare the SF_P with those already associated with the substructure Str_0 (initially none is associated with Str_0). If the SF_P differs from the existing ones, a new counter is created, whose value is initialized to 1, and the new counter is assigned to the SF_P. If the SF_P is the "same" as an existing one with counter value Cnt,[4] and the code of the label-triplet of nodes i, j, k equals the code of the label-

[4]By saying SF_P is the same as an existing SF'_P, we mean that for each entry $e_{i,j}$, $1 \le i, j \le 3$, at the ith row and the jth column in SF_P and its corresponding entry $e'_{i,j}$ in SF'_P, $|e_{i,j} - e'_{i,j}| \le \epsilon$ where ϵ is an adjustable parameter depending on the data. In the examples presented in this chapter, $\epsilon = 0.01$.

triplet of nodes u, v, w, then Cnt is incremented by one. In general, a substructure may be associated with several different SF_P's, each having a counter.

We now present the theory supporting this algorithm. Theorem 2.1 below establishes a criterion based on which one can detect and eliminate a false match. Theorem 2.2 below justifies the procedure of incrementing the counter values.

Theorem 2.1 *Let P_{c_1}, P_{c_2} and P_{c_3} be the three basis points forming the SF_P defined in Equation (2.6), where P_{c_1} is the origin. $\vec{V}_{c_1,c_2}$, $\vec{V}_{c_1,c_3}$ and $\vec{V}_{c_1,c_2} \times \vec{V}_{c_1,c_3}$ are orthonormal vectors if and only if the nodes u, v and w geometrically match the nodes i, j and k, respectively.*

Proof (If) Let A be as defined in Equation (2.3) and let

$$B = \begin{pmatrix} \vec{V}_{u,v} \\ \vec{V}_{u,w} \\ \vec{V}_{u,v} \times \vec{V}_{u,w} \end{pmatrix} \tag{2.7}$$

Note that, if u, v and w geometrically match i, j and k, respectively, then $|B| = |A|$, where $|B|$ ($|A|$, respectively) is the determinant of the matrix B (matrix A, respectively). That is to say, $|A^{-1}||B| = 1$.

From Equation (2.2) and by the definition of the SF_P in Equation (2.6), we have

$$SF_P = \begin{pmatrix} \vec{V}_{i,b_1} \\ \vec{V}_{i,b_2} \\ \vec{V}_{i,b_3} \end{pmatrix} \times A^{-1} \times B + \begin{pmatrix} P_u \\ P_u \\ P_u \end{pmatrix} \tag{2.8}$$

Thus the SF_P basically transforms P_{b_1}, P_{b_2} and P_{b_3} via two translations and one rotation, where P_{b_1}, P_{b_2} and P_{b_3} are the basis points of the Substructure Frame 0 (SF_0). Since $\vec{V}_{b_1,b_2}$, $\vec{V}_{b_1,b_3}$ and $\vec{V}_{b_1,b_2} \times \vec{V}_{b_1,b_3}$ are orthonormal vectors, and translations and rotations do not change this property [80], we know that $\vec{V}_{c_1,c_2}$, $\vec{V}_{c_1,c_3}$ and $\vec{V}_{c_1,c_2} \times \vec{V}_{c_1,c_3}$ are orthonormal vectors.

(Only if) If u, v and w do not match i, j and k geometrically while having the same hash bin address, then there will be distortion in the aforementioned transformation. Consequently, $\vec{V}_{c_1,c_2}$, $\vec{V}_{c_1,c_3}$ and $\vec{V}_{c_1,c_2} \times \vec{V}_{c_1,c_3}$ will no longer be orthonormal vectors. □

Theorem 2.2 *If two true node-triplet matches yield the same SF_P and the codes of the corresponding label-triplets are the same, then the two node-triplet matches are augmentable, i.e., they can be combined to form a larger substructure match between P and Str_0.*

Proof Since three nodes are enough to set the SF_P at a fixed position and direction, all the other nodes in P will have definite coordinates under this SF_P. When another node-triplet match yielding the same SF_P occurs, it means that geometrically there is at least one more node match between Str_0 and P. If the codes of the corresponding label-triplets are the same, it means that the labels of the corresponding nodes are the same. Therefore the two node-triplet matches are augmentable (cf. Fig. 2.9). □

Thus, by incrementing the counter associated with the SF_P, we record how many true node-triplet matches are augmentable under this SF_P. Notice that in cases where two node-triplet matches occur due to reflections, the directions of the corresponding local coordinate systems are different, so are the SF_P's. As a result, these node-triplet matches are not augmentable.

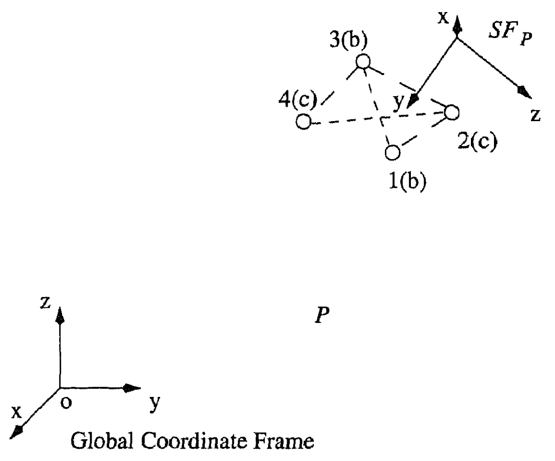

Figure 2.9 Augmenting two node-triplet matches.

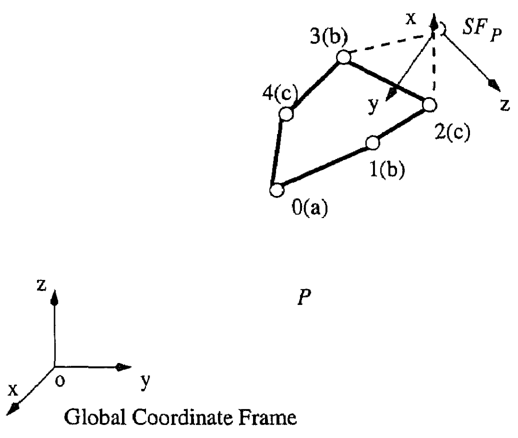

Figure 2.10 A substructure (pattern) P.

Example 2.5 Consider the pattern P in Fig. 2.10. In P, the nodes numbered 0, 1, 2, 3, 4 match, after rotation, the nodes numbered 5, 4, 3, 1, 2 in the substructure Str_0 in Fig. 2.4(a). The node numbered 0 in Str_0 does not appear in P (i.e. it is to be deleted). The labels of the corresponding nodes are identical. Thus, P matches Str_0 with 1 mutation, i.e., one node is deleted.

Now, suppose in P, the global coordinates of the nodes numbered 1, 2, 3 and 4 are

$$P_1(-0.269000, 4.153153, 2.911494),$$

$$P_2(-0.317400, 4.749386, 3.253592),$$

$$P_3(0.172100, 3.913515, 4.100777),$$

$$P_4(0.366000, 3.244026, 3.433268).$$

Refer to Example 2.4. For the nodes numbered 3, 4 and 2 of P, the hash bin address is $h[25][12][21]$, which is the same as that of nodes numbered 1, 2, 3 of Str_0, and

$$SF_P = \begin{pmatrix} -0.012200 & 5.005500 & 4.474200 \\ 0.987800 & 5.005500 & 4.474200 \\ -0.012200 & 4.298393 & 3.767093 \end{pmatrix} \tag{2.9}$$

The three basis vectors forming this SF_P are

$$\begin{aligned} \vec{V}_{c1,c2} &= (1.000000, 0.000000, 0.000000), \\ \vec{V}_{c1,c3} &= (0.000000, -0.707107, -0.707107), \\ \vec{V}_{c1,c2} \times \vec{V}_{c1,c3} &= (0.000000, 0.707107, -0.707107), \end{aligned}$$

which are orthonormal.

For the nodes numbered 3, 1 and 4 of P, the hash bin address is $h[24][0][9]$, which is the same as that of nodes numbered 1, 4, 2 of Str_0, and

$$SF_P = \begin{pmatrix} -0.012200 & 5.005500 & 4.474200 \\ 0.987800 & 5.005500 & 4.474200 \\ -0.012200 & 4.298393 & 3.767093 \end{pmatrix} \tag{2.10}$$

These two true node-triplet matches have the same SF_P, and therefore the corresponding counter associated with the substructure Str_0 of the graph 12 in Fig. 2.3 is updated to 2. After hashing all node-triplets of P, the counter value will be $\begin{pmatrix} 5 \\ 3 \end{pmatrix} = 10$, since all matching node-triplets have the same SF_P as in Equation (2.9) and the labels of the corresponding nodes are the same. □

Now consider again the SF_P defined in Equation (2.6) and the three basis points P_{c_1}, P_{c_2}, P_{c_3} forming the SF_P, where P_{c_1} is the origin. We note that for any node i in the pattern P with global coordinate $P_i(x_i, y_i, z_i)$, it has a local coordinate with respect to the SF_P, denoted P'_i, where

$$P'_i = \vec{V}_{c1,i} \times E^{-1} \tag{2.11}$$

Here E is the *base matrix* for the SF_P, defined as

$$E = \begin{pmatrix} \vec{V}_{c_1,c_2} \\ \vec{V}_{c_1,c_3} \\ \vec{V}_{c_1,c_2} \times \vec{V}_{c_1,c_3} \end{pmatrix} \tag{2.12}$$

and $\vec{V}_{c_1,i}$ is the vector starting at P_{c_1} and ending at P_i.

Remark If $\vec{V}_{c_1,c_2}$, $\vec{V}_{c_1,c_3}$ and $\vec{V}_{c_1,c_2} \times \vec{V}_{c_1,c_3}$ are orthonormal vectors, then $|E| = 1$. Thus a practically useful criterion for detecting false matches is to check whether or not $|E| = 1$. If $|E| \neq 1$, then $\vec{V}_{c_1,c_2}$, $\vec{V}_{c_1,c_3}$ and $\vec{V}_{c_1,c_2} \times \vec{V}_{c_1,c_3}$ are not orthonormal vectors, and therefore the nodes u, v and w do not match the nodes i, j and k geometrically (cf. Theorem 2.1).

Example 2.6 Refer to Example 2.5. The local coordinates, with respect to the SF_P in Equation (2.9), of nodes 3, 4 and 2 in P are

$$P'_3(0.184300, 1.036200, -0.508100),$$

$$P'_4(0.378200, 1.981600, -0.509500),$$

$$P'_2(-0.305200, 1.044200, 0.682000).$$

They match the local coordinates, with respect to SF_0, of nodes 1, 2 and 3 of the substructure Str_0 (cf. Fig. 2.8). Likewise, the local coordinate, with respect to the SF_P in Equation (2.9), of node 1 in P is

$$P'_1(-0.256800, 1.707700, 0.502300),$$

which matches the local coordinate, with respect to SF_0, of node 4 of the substructure Str_0 (cf. Fig. 2.8). □

Intuitively, our scheme is to hash node-triplets and match the triplets. Only if one triplet tri matches another tri' do we see how the substructure containing tri

matches the pattern containing tri'. Using Theorem 2.1, we detect and eliminate false node-triplet matches. Using Theorem 2.2, we record in a counter the number of augmentable true node-triplet matches. The following theorem says that the counter value needs to be large (i.e., there are a sufficient number of augmentable true node-triplet matches) in order to infer that there is a match between the corresponding pattern and substructure. The larger the Mut, the fewer node-triplet matches are needed.

Theorem 2.3 *Let Str be a substructure in the hash table $\mathcal{H}$ and let G be the graph from which Str is generated. Let P be a pattern where $|P| \geq Mut + 3$. After rehashing the node-triplets of P, suppose there is an SF_P associated with Str whose counter value $Cnt > \Theta_P$ where*

$$\Theta_P = \frac{(N-1) \times (N-2) \times (N-3)}{6} \tag{2.13}$$

and $N = |P| - Mut$. Then P matches Str within Mut mutations (i.e. P approximately occurs in G, or G approximately contains P, within Mut mutations).

Proof By Theorem 2.2, we increase the counter value only when there are true node-triplet matches that are augmentable under the SF_P. If there are $N-1$ node matches, then $Cnt \leq \Theta_P$. Therefore when $Cnt > \Theta_P$, there are at least N node matches between Str and P. □

Example 2.7 Refer to Example 2.5. Suppose the user-specified mutation number Mut is 1. The candidate pattern P in Fig. 2.10 has size $|P| = 5$. After rehashing the node-triplets of P, there is only one counter associated with the substructure Str_0 in Fig. 2.4(a); this counter corresponds to the SF_P in Equation (2.9) and the value of the counter, Cnt, is 10. Thus, Cnt is greater than $\Theta_P = (5-2)(5-3)(5-4)/6 = 1$.

By Theorem 2.3, P should match the substructure Str_0 within 1 mutation. This means that there are at least 4 node matches between P and Str_0. □

Thus, after rehashing the node-triplets of each candidate pattern P into the 3D table $\mathcal{H}$, we check the values of the counters associated with the substructures in $\mathcal{H}$. By Theorem 2.3, P approximately occurs in a graph G within Mut mutations if G contains a substructure Str and there is at least one counter associated with Str whose value $Cnt > \Theta_P$. If there are less than $Occur$ graphs in which P approximately occurs within Mut mutations, then we discard P. The remaining candidates are qualified patterns. Notice that Theorem 2.3 provides only the "sufficient" (but not the "necessary") condition for finding the qualified patterns. Due to the accumulating errors arising in the calculations, some node-triplets may be hashed to a wrong bin. As a result, the pattern-finding algorithm may miss some node-triplet matches and therefore miss some qualified patterns. In Section 2.3 we will show experimentally that the missed patterns are few compared with those found by exhaustive search.

Theorem 2.4 *Let the set $\mathcal{S}$ contain K graphs, each having at most N nodes. The time complexity of the proposed pattern-finding algorithm is $\mathcal{O}(KN^3)$.*

Proof For each graph in $\mathcal{S}$, phase (1) of the algorithm requires $\mathcal{O}(N^2)$ time to decompose the graph into substructures. Thus the time needed for phase (1) is $\mathcal{O}(KN^2)$. In subphase A of phase (2), we hash each candidate pattern P by considering the combinations of any three nodes in P, which requires time $\binom{|P|}{3} = \mathcal{O}(|P|^3)$. Thus the time needed to hash all candidate patterns is $\mathcal{O}(KN^3)$. In subphase B of phase (2), we rehash each candidate pattern, thus requiring the same time $\mathcal{O}(KN^3)$ totally. □

Table 2.3 Parameters in the pattern-finding algorithm and their base values used in the experiments.

Parameter	Value	Description
Mut	1	Allowed mutation between a pattern and a graph
$Occur$	3	Minimum occurrence number of an interesting pattern
$Size$	6	Minimum size of an interesting pattern
ϵ	0.01	Allowed error in comparing the entries of two coordinate matrices
$Scale$	10	the multiplier used in calculating the hash bin address
$Prime_1$	1009	the 1st prime number used in calculating the hash bin address
$Prime_2$	1033	the 2nd prime number used in calculating the hash bin address
$Prime_3$	1051	the 3rd prime number used in calculating the hash bin address
$Nrow$	101	the cardinality of the hash table along each dimension

2.5 Performance Evaluation

We carried out a series of experiments to evaluate the performance and the speed of our approach. The programs were written in the C programming language and run on a SunSPARC 20 workstation under the Solaris operating system version 2.4. Parameters used in the experiments can be classified into two categories: those related to data and those related to the pattern-finding algorithm. In the first category, we considered the size (in number of nodes) of a graph and the total number of graphs in a dataset. In the second category, we considered all the parameters described in Section 2.2, which are summarized in Table 2.3 together with the base values used in the experiments.

Two files were maintained: one recording the hash bin addresses and the other containing the entries stored in the hash bins. To evaluate the performance of the pattern-finding algorithm, we applied the algorithm to two sets of data: 1,000 synthetic graphs and 226 chemical compounds obtained from a drug database maintained in the National Cancer Institute. When generating the artificial graphs, we randomly generated the 3D coordinates for each node, with each coordinate being in the range [0, 100). The node labels were drawn randomly from the range A to E. The size of the rigid substructures in an artificial graph ranged from 4 to 10 and the size of the graphs ranged from 10 to 50. The size of the compounds ranged from 5 to 51.

In this section, we present experimental results to answer questions concerning the performance of the pattern-finding algorithm. For example, are all approximate patterns found, i.e., is the recall high? Are any uninteresting patterns found, i.e., is the precision high? In the next section, we study the applications of the algorithm and intend to answer questions such as whether graphs having some common phenomenological activity (e.g. they are proteins with the same function) share structural patterns in common and whether these patterns can characterize the graphs as a whole.

2.5.1 Effect of Data-Related Parameters

To evaluate the performance of the proposed pattern-finding algorithm, we compared it with exhaustive search. The exhaustive search procedure works by generating all candidate patterns as in phase (1) of the pattern-finding algorithm. Then the procedure examines if a pattern P approximately matches a substructure Str in a graph by permuting the node labels of P and checking if they match the node labels of Str. If so, the procedure performs translation and rotation on P and checks if P can geometrically match Str.

The speed of the algorithms was measured by the running time. The performance was evaluated using three measures: recall (RE), precision (PR), and the number of false matches, N_{fm}, arising during the hashing process. Recall is defined as

$$RE = \frac{RelevantPatternsFound}{TotalPatterns} \times 100\%$$

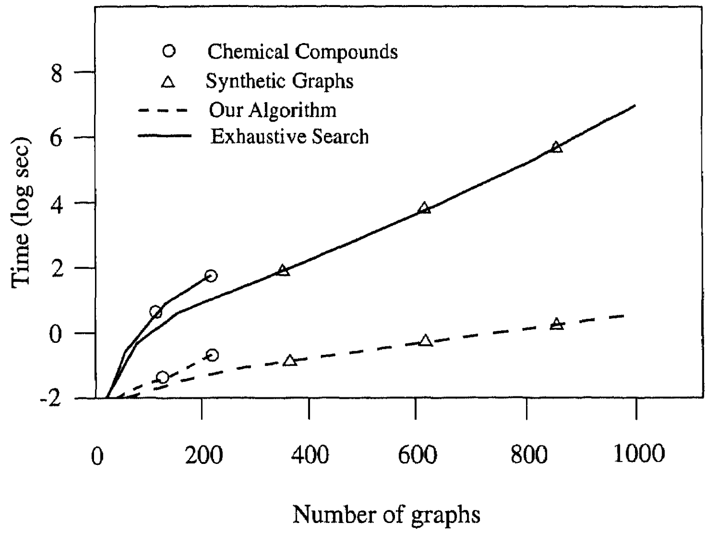

Figure 2.11 Running times as a function of the number of graphs.

Precision is defined as

$$PR = \frac{RelevantPatternsFound}{PatternsFound} \times 100\%$$

where $PatternsFound$ is the number of patterns found by the proposed algorithm, $RelevantPatternsFound$ is the number of patterns found that satisfy the user-specified parameter values, and $TotalPatterns$ is the number of patterns found by exhaustive search. One would like both RE and PR to be as high as possible.

Fig. 2.11 shows the running times of the algorithms as a function of the number of graphs and Fig. 2.12 shows the recall. The parameters used in the proposed pattern-finding algorithm had the values shown in Table 2.3. As can be seen from the figures, the proposed algorithm is 10,000 times faster than the exhaustive search method when the dataset has more than 600 graphs while achieving a very high ($> 97\%$) recall. Due to the accumulating errors arising in the calculations, some node-triplets may be hashed to a wrong bin. As a result, the proposed algorithm may miss some node-triplet matches in subphase B of phase (2) and therefore can not achieve a 100% recall. In these experiments, precision was 100%.

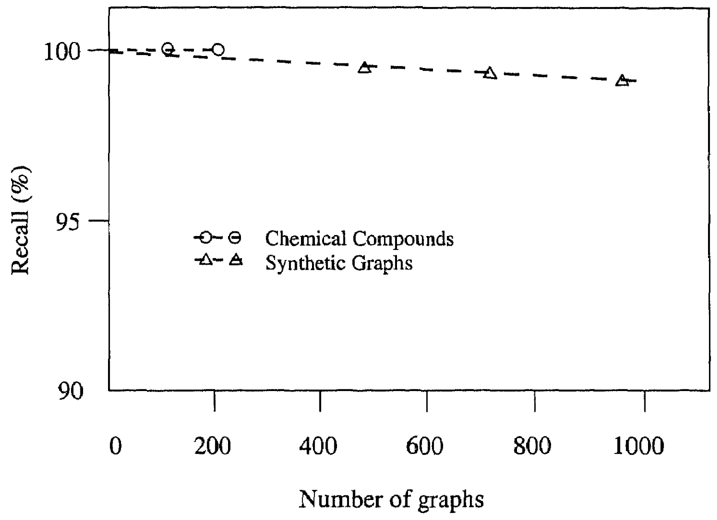

Figure 2.12 Recall as a function of the number of graphs.

Fig. 2.13 shows the number of false matches introduced by the proposed algorithm as a function of the number of graphs. For the chemical compounds, N_{fm} is small. For the synthetic graphs, N_{fm} increases as the number of graphs becomes large. Similar results were obtained when testing the size of graphs for both types of data.

2.5.2 Effect of Algorithm-Related Parameters

The purpose of this subsection is to analyze the effect of varying the algorithm-related parameter values on the performance of the proposed pattern-finding algorithm. To avoid the mutual influence of parameters, the analysis was carried out by fixing the parameter values related to data graphs—the 1,000 synthetic graphs and 226 compounds described above were used, respectively. In each experiment, only one algorithm-related parameter value was varied; the other parameters had the values shown in Table 2.3.

Figures 2.14, 2.15, and 2.16 show the recall as a function of *Size*, *Mut*, and *Scale*, respectively. In all the three figures, precision is 100%. From Fig. 2.14 and Fig. 2.15, we see that *Size* and *Mut* affect recall slightly. It was also observed

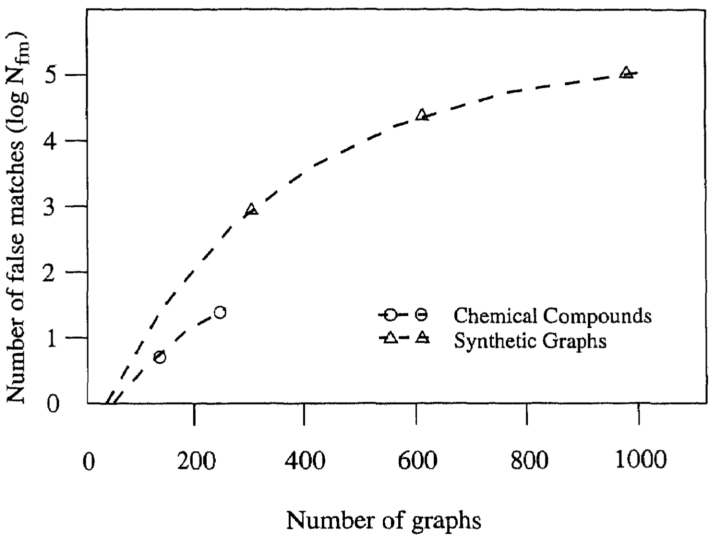

Figure 2.13 Number of false matches as a function of the number of graphs.

that the number of interesting patterns drops (increases, respectively) significantly as *Size* (*Mut*, respectively) becomes large. Fig. 2.16 shows that the pattern-finding algorithm yields a poor performance when *Scale* is large. In general, the digits after the 1st position on the right of the decimal point were found to be inaccurate for the tested graphs. Including those inaccurate values in calculating hash bin addresses may miss many node-triplet matches. This was why we set *Scale* to 10.

Figures 2.17 and 2.18 show the recall and precision as a function of ϵ. It can be seen that when ϵ is 0.01, precision is 100% and recall is greater than 97%. When ϵ becomes smaller (e.g. $\epsilon = 0.0001$), precision remains the same while recall drops. When ϵ becomes larger (e.g. $\epsilon = 10$), recall increases slightly while precision drops. This happens because some irrelevant node-triplet matches were included, rendering unqualified patterns returned as an answer. We also tested different values for *Occur*, *Nrow*, $Prime_1$, $Prime_2$ and $Prime_3$. It was found that varying these parameter values had little impact on the performance of the proposed algorithm.

Finally we examined the effect of varying the parameter values on generating false matches. Since few false matches were found for chemical compounds, the experiments focused on synthetic graphs. It was observed that only *Nrow* and *Scale*

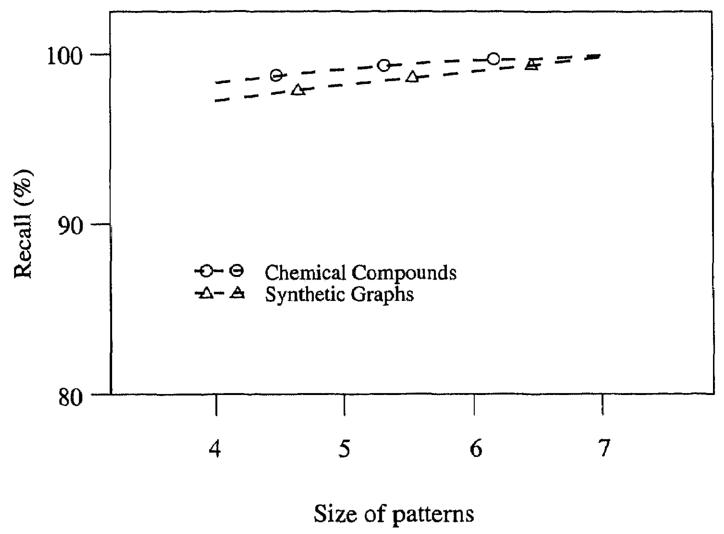

Figure 2.14 Effect of *Size*.

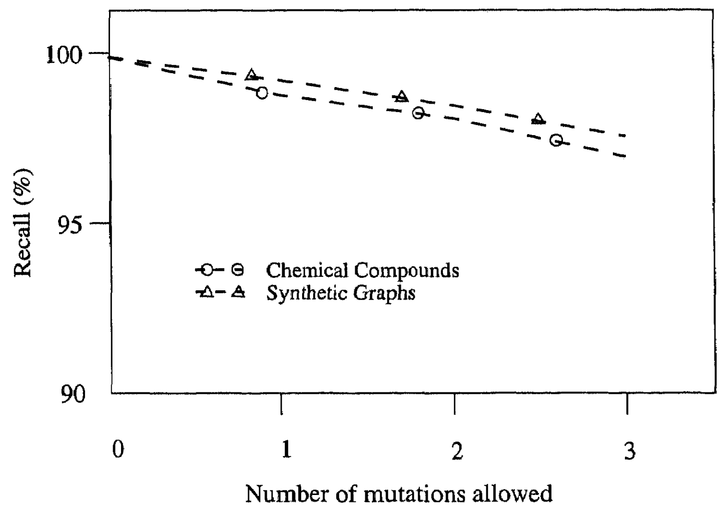

Figure 2.15 Effect of *Mut*.

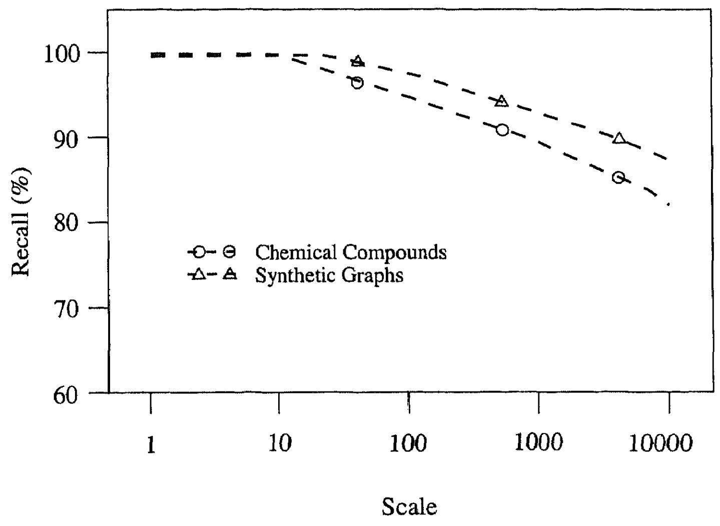

Figure 2.16 Impact of *Scale*.

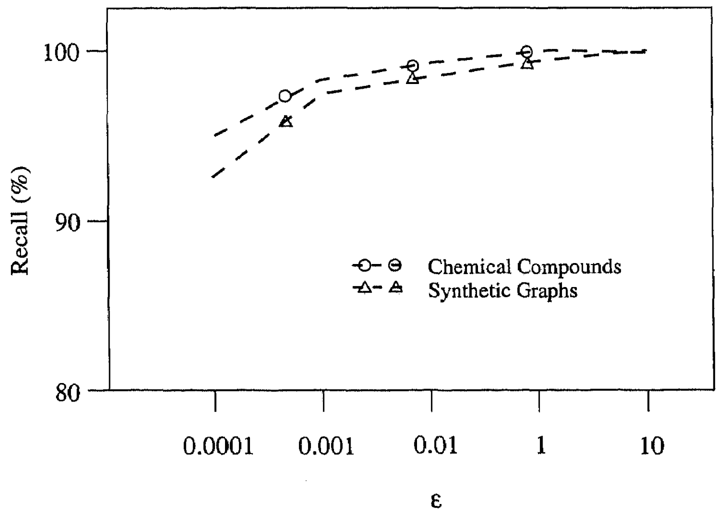

Figure 2.17 Recall as a function of ϵ.

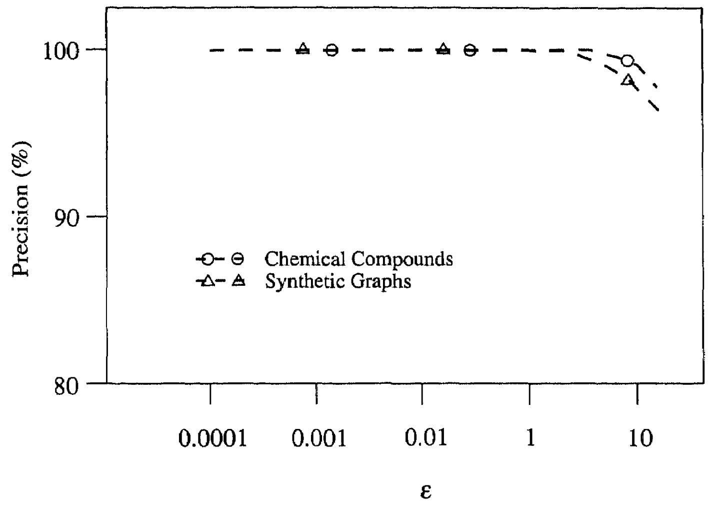

Figure 2.18 Precision as a function of ϵ.

affected the number of false matches. Fig. 2.19 shows N_{fm} as a function of *Scale* for *Nrow* = 101, 131, 167, 199, respectively. The larger the *Nrow*, the fewer entries in a hash bin, and consequently the fewer false matches. On the other hand, when *Nrow* is too large, the running times increase substantially, since one needs to spend a lot of time in reading the 3D table containing the hash bin addresses.

Examining Fig. 2.19, we see that *Scale* affects N_{fm} significantly. Taking an extreme case, when *Scale* = 1, a node-triplet with the squares of the lengths of the three edges connecting the nodes being 12.4567 is hashed to the same bin as a node-triplet with those values being 12.0000, although the two node-triplets do not match geometrically, cf. Section 2.3.1. On the other hand, when *Scale* is large (e.g. *Scale* = 10,000), the distribution of hash function values is less skewed, which reduces the number of false matches. It was observed that N_{fm} was largest when *Scale* was 100. This happens because with this *Scale* value, inaccuracy was being introduced in calculating hash bin addresses. A node-triplet being hashed to a bin might generate k false matches where k is the total number of node-triplets already stored in that bin—k would be large if the distribution of hash function values is skewed. With the

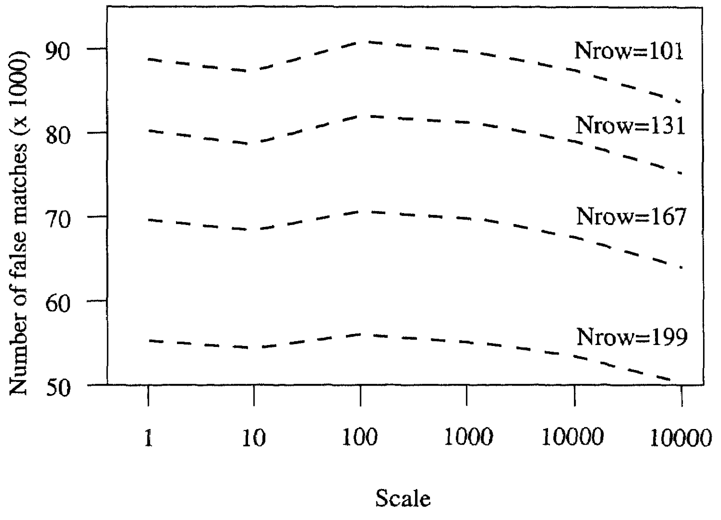

Figure 2.19 Number of false matches as a function of *Scale.*

data we tested, we found that setting *Scale* to 10 is the best overall for both recall and precision.

2.6 Data Mining Applications

One important application of pattern finding involves the ability to perform classification and clustering as well as other data mining tasks. In this section, we present two data mining applications of the proposed algorithm in scientific domains: classify proteins and cluster compounds.

2.6.1 Classifying Proteins

Proteins are large molecules, comprising hundreds of amino acids (residues). In each residue the C_α, C_β and N atoms form a backbone of the residue [61]. Following [82], we represent each residue by the three atoms. Thus if we consider a protein as a 3D graph, each node of the graph is an atom. Each node has a label, which is the name of the atom and is not unique in the protein. We assign a unique number to identify a node in the protein, where the order of numbering is obtained from the Protein Data Bank (PDB) at Brookhaven National Laboratory [1, 8].

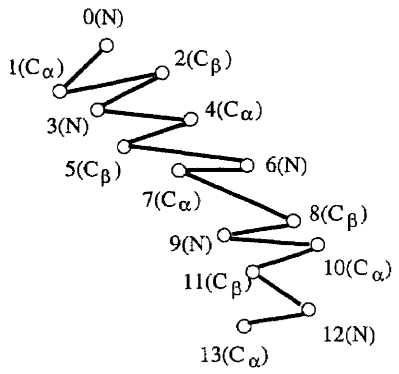

(a)

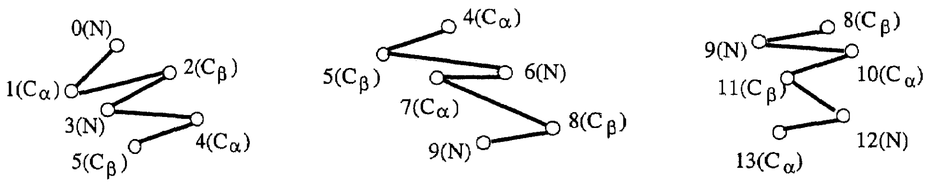

(b)

Figure 2.20 (a) A 3D protein. (b) The three substructures of the protein in (a).

In the experiments we examined two families of proteins chosen from PDB pertaining to RNA-directed DNA Polymerase and Thymidylate Synthase. Each family contains proteins having the same functionality in various organisms. We decompose each protein into consecutive substructures, each substructure containing 6 nodes. Two adjacent substructures overlap by sharing the two neighboring nodes on the boundary of the two substructures (see Fig. 2.20). Thus each substructure is a portion of the polypeptide chain backbone of a protein where the polypeptide chain is made up of residues linked together by peptide bonds. The peptide bonds have strong covalent bonding forces that make the polypeptide chain rigid. As a consequence, the substructures used by our algorithm are rigid. Notice that in the proteins there are other atoms such as O and H (not shown in Fig. 2.20) lying between two residues. Since these atoms are not as important as C_α, C_β and N in determining the structure of a protein, we do not consider them here. Table 2.4

Table 2.4 Statistics concerning the proteins and motifs found in them.

Family	Number of proteins	Maximum protein size	Minimum protein size	Number of motifs	Minimum motif size	Maximum motif size
RNA-directed DNA Polymerase	45	1,812	146	42	6	6
Thymidylate Synthase	37	2,128	1,000	33	6	6

summarizes the number of proteins in each family, their sizes and the frequently occurring patterns (or motifs) discovered from the proteins. The parameter values used were as shown in Table 2.3; 2,784 false matches were detected and eliminated during the process of finding the motifs.

To evaluate the quality of the discovered motifs, we applied them to classifying the proteins using the 10-way cross-validation scheme. That is, each family was divided into 10 groups of roughly equal size. Specifically, the RNA-directed DNA Polymerase family, referred to as family 1, contained five groups each having 5 proteins and five groups each having 4 proteins. The Thymidylate Synthase family, referred to as family 2, contained seven groups each having 4 proteins and three groups each having 3 proteins. Ten tests were conducted. In each test, a group was taken from a family and used as test data; the other nine groups were used as training data for that family. We applied our pattern-finding algorithm to each training dataset to find motifs (the parameter values used were as shown in Table 2.3). Each motif M found in family i was associated with a weight d where

$$d = r_i - r_j \qquad\qquad 1 \leq i, j \leq 2, \quad i \neq j$$

Here r_i is M's occurrence number in the training dataset of family i. Intuitively, the more frequently a motif occurs in its own family and the less frequently it occurs in the other family, the higher its weight is. In each family we collected all the motifs having a weight greater than one and used them as the characteristic motifs of that family.

When classifying a test protein Q, we first decomposed Q into consecutive substructures as described above. The result was a set of substructures, say, $Q^1, \ldots, Q^p$. Let $n_i^k, 1 \le i \le 2, 1 \le k \le p$, denote the number of characteristic motifs in family i that matched Q^k within one mutation. Each family i obtained a score N_i where

$$N_i = \frac{\sum_{k=1}^{p} n_i^k}{m_i}$$

and m_i is the total number of characteristic motifs in family i. The protein Q was classified into the family i with maximum N_i. If the scores were 0 for both families (i.e. the test protein did not have any substructure that matched any characteristic motif), then the "no-opinion" verdict was given. This algorithm is similar to those used in [84, 96] to classify chemical compounds and sequences.

As in Section 2.3, we use recall (RE_c) and precision (PR_c) to evaluate the effectiveness of our classification algorithm. Recall is defined as

$$RE_c = \frac{TotalNum - \sum_{i=1}^{2} NumLoss_c^i}{TotalNum} \times 100\%$$

where $TotalNum$ is the total number of test proteins and $NumLoss_c^i$ is the number of test proteins that belong to family i but are not assigned to family i by our algorithm (they are either assigned to family j, $j \neq i$, or they receive the "no-opinion" verdict). Precision is defined as

$$PR_c = \frac{TotalNum - \sum_{i=1}^{2} NumGain_c^i}{TotalNum} \times 100\%$$

where $NumGain_c^i$ is the number of test proteins that do not belong to family i but are assigned by our algorithm to family i. With the 10-way cross validation scheme, the average RE_c over the ten tests was 92.7% and the average PR_c was 96.4%. It was found that 3.7% test proteins on average received the "no-opinion" verdict during the classification. We repeated the same experiments using other parameter values and obtained similar results, except that larger Mut values (e.g., 3) generally yielded lower RE_c.

2.6.2 Clustering Compounds

In addition to classifying proteins, we have developed an algorithm for clustering 3D graphs based on the patterns occurring in the graphs and have applied the algorithm to grouping compounds. Given a collection $\mathcal{S}$ of 3D graphs, the algorithm first uses the procedure depicted in Section 2.2 to decompose the graphs into rigid substructures. Let $\{Str_p | p = 0, 1, ..., N-1\}$ be the set of substructures found in the graphs in $\mathcal{S}$ where $|Str_p| \geq Size$. Using the proposed pattern-finding algorithm, we examine each graph G_q in $\mathcal{S}$ and determine whether each substructure Str_p approximately occurs in G_q within Mut mutations. Each graph G_q is represented as a bit string of length N, i.e., $G_q = (b_q^0, b_q^1, ..., b_q^{N-1})$, where

$$b_q^p = \begin{cases} 1 & \text{if } Str_p \text{ occurs in } G_q \text{ within } Mut \text{ mutations} \\ 0 & \text{otherwise} \end{cases}$$

The distance between two graphs G_x and G_y, denoted $d(G_x, G_y)$, is defined as the Hamming distance [37] between their bit strings. The algorithm then uses the well known average-group method [44] to cluster the graphs in $\mathcal{S}$, which works as follows.

Initially, every graph is a cluster. The algorithm merges two nearest clusters to form a new cluster, until there are only K clusters left where K is a user-specified parameter. The distance between two clusters C_1 and C_2 is given by

$$\frac{1}{|C_1||C_2|} \sum_{G_x \in C_1, G_y \in C_2} |d(G_x, G_y)| \tag{2.14}$$

where $|C_i|$, $i = 1, 2$, is the size of cluster C_i. The algorithm requires $O(N^2)$ distance calculations where N is the total number of graphs in $\mathcal{S}$.

Table 2.5 Statistics concerning the chemical compounds and patterns found in them.

Group	Number of compounds	Minimum compound size	Maximum compound size	Number of patterns	Minimum pattern size	maximum pattern size
aromatic	36	12	42	58	5	13
bicyclic-alkanes	26	16	40	53	5	11
photo-synthesis	36	31	44	114	5	11

We applied this algorithm to clustering chemical compounds. Ninety eight compounds were chosen from the Merck Index that belonged to three groups pertaining to aromatic, bicyclicalkanes and photosynthesis. The data was created by the CORINA program that converted 2D data (represented in SMILES string) to 3D data (represented in PDB format) [67]. Table 2.5 lists the number of compounds in each group, their sizes and the patterns discovered from them. The parameter values used were $Size = 5$, $Occur = 1$, $Mut = 2$; the other parameters had the values shown in Table 2.3.

To evaluate the effectiveness of our clustering algorithm, we applied it to finding clusters in the compounds. The parameter value K was set to 3, as there were three groups. As in the previous sections, we use recall (RE_r) and precision (PR_r) to evaluate the effectiveness of the clustering algorithm. Recall is defined as

$$RE_r = \frac{TotalNum - \sum_{i=1}^{K} NumLoss_r^i}{TotalNum} \times 100\%$$

where $NumLoss_r^i$ is the number of compounds that belong to group G_i, but are assigned by our algorithm to group G_j, $i \neq j$, and $TotalNum$ is the total number of compounds tested. Precision is defined as

$$PR_r = \frac{TotalNum - \sum_{i=1}^{K} NumGain_r^i}{TotalNum} \times 100\%$$

where $NumGain_r^i$ is the number of compounds that do not belong to group G_i, but are assigned by our algorithm to group G_i. Our experimental results indicated that $RE_r = PR_r = 99\%$. Out of the 98 compounds, only one compound in the photosynthesis group was assigned incorrectly to the bicyclicalkanes group. We experimented with other parameter values and obtained similar results.[5]

2.7 Conclusion

In this chapter we have presented an algorithm for finding patterns in 3D graphs. A pattern here is a rigid substructure that may occur in a graph after allowing for an arbitrary number of rotations and translations as well as a small number of edit operations in the pattern or in the graph. We used the algorithm to find approximately common patterns in a set of synthetic graphs, chemical compounds and proteins. Our experimental results demonstrated the good performance of the proposed algorithm and its usefulness for pattern discovery. We then developed classification and clustering algorithms using the patterns found in the graphs, and applied them to classifying proteins and clustering compounds. Empirical study showed high recall and precision rates for both classification and clustering, indicating the significance of the patterns.

Our pattern-finding algorithm rehashes each candidate pattern P to evaluate P's activity. This rehashing may hit the same page several times and may cause page faults. Alternatively, one can proceed through the hash table $\mathcal{H}$ bin by bin to calculate the number of occurrences of the patterns. With the sequential scan, one has to store the node numbers for each node-triplet in its hash table entry in order to calculate SF_P values. When scanning the hash table $\mathcal{H}$, one has to keep, in a separate table $\mathcal{T}$, the SF_P values for every pair of patterns that have node-triplet matches;

[5]The *Occur* value was fixed at 1 in these experiments because of the fact that all the compounds were represented as binary bit strings.

each SF_P is associated with a counter. While scanning $\mathcal{H}$, the algorithm accesses $\mathcal{T}$ to update the counter values. When $\mathcal{T}$ is large, this updating may also cause page faults. In our experiments, we observed that when the patterns share many common substructures and when there exist many nonaugmentable node-triplet matches (i.e., these matches yield different SF_P's each having a counter with value 1), $\mathcal{T}$ becomes much larger than $\mathcal{H}$. As a consequence, rehashing is faster than sequential scan. On the other hand, when relatively fewer common substructures exist among the patterns, sequential scan is more efficient.

We have implemented the techniques presented in this chapter and are combining them with the algorithms for acyclic graph matching [104] into a toolkit. We use the toolkit to find patterns in various types of graphs arising in different domains. The toolkit can be obtained from the authors and is also accessible at `http://www.cis.njit.edu/~discdb` on the Web.

CHAPTER 3

FAST SIMILARITY SEARCH IN DATABASES OF 3D GRAPHS

3.1 Introduction

3D graph detection and recognition have been discussed in many domains, including computer vision [10, 52, 56, 68], image processing [43, 62, 100], pattern matching [14, 35], knowledge discovery [13, 59], and information retrieval [46, 47, 76]. We extend our algorithms in the previous chapter to deal with the problem of similarity search in databases of 3D graphs [95].

Given a database $\mathcal{D}$ of 3D graphs and a target graph Q, the similarity search problem (also known as the good-match retrieval problem [93]) is to find the graphs G in $\mathcal{D}$ that approximately match Q, possibly in the presence of rotation, translation, node insert, delete and relabeling in G or Q. This type of retrieval arises in many applications, including multimedia computing [79], image processing [18, 21, 71], environmental databases [30, 64], and molecular biology [40]. In such domains, a (dis)similarity metric is often used to measure the difference of two graphs. We adopt the *edit distance* to measure the difference of two 3D graphs. The distance measure is an extension of the widely used edit distance for strings [83], trees [88, 91] and 2D graphs [104].

The rest of this chapter is organized as follows. In the following subsection we list the similarity search problem and related queries. Section 3.2 discusses some additional preliminaries extended from the last chapter. Section 3.3 presents the approach which is an extension of our pattern finding algorithm. Section 3.4 reports some experimental results.

3.1.1 Similarity Search and Related Queries

The queries we are concerned with are categorized as follows: Given a target Q and a database $\mathcal{D}$ of 3D graphs,

- (similarity search or good-match retrieval [93]) find the graphs in $\mathcal{D}$ that approximately match Q, i.e., those that are within some distance, say ϵ, of Q;
- (k-closest retrieval) find the k graphs, for some k, in $\mathcal{D}$ that are closest to Q;
- (best-match retrieval [74]) find the closest (i.e., most similar) graph of Q in $\mathcal{D}$;[1]
- (bad-match retrieval) find the graphs in $\mathcal{D}$ that are sufficiently dissimilar to Q, i.e., those that are beyond distance ϵ of Q;
- (k-farthest retrieval) find the k graphs in $\mathcal{D}$ that are farthest from Q;
- (worst-match retrieval [55]) find the farthest (i.e., most dissimilar) graph of Q in $\mathcal{D}$.

3.2 Preliminaries

Our approach is composed of two phases. In the preprocessing phase, data graphs are divided into rigid substructures. These substructures are hashed into a three dimensional disk-based hash table. In the on-line phase, we divide the target graph into rigid substructures and hash the substructures using the same hash function as used in the preprocessing phase. We then locate the substructures of the data graphs that match with the substructures of the target. The matched substructures are then augmented wherever appropriate, to form larger matches. To facilitate augmentation, we maintain a common edge table, which lists pairs of data substructures that are connected by a common edge.

[1]This query is a special case for the k-closest retrieval where $k = 1$. The latter retrieves not only the closest graph, but the ith, $i = 2, \ldots, k$, closest graph of Q in $\mathcal{D}$.

3.2.1 The Common Edge Table

When a graph is large, processing it in its entirety would be costly in both time and space. Our strategy is to decompose the graph into rigid substructures, where the substructures are rotatable with respect to each other around a common edge. We decompose a data graph G into substructures using a modified depth-first search algorithm for finding blocks [53]. Starting at the node with the largest degree, the algorithm finds all the blocks in G. Clearly the blocks with more than one edge are rigid substructures. The algorithm identifies these blocks and combines them with neighboring blocks consisting of a single edge. (We do not glue two substructures that are rotatable with respect to each other.) The algorithm runs in time linearly proportional to the number of edges in G. The result is a collection $\mathcal{C}$ of rigid substructures where any two substructures in $\mathcal{C}$ are connected by at most one common edge. In each substructure, a node is distinguished and used as the origin of the local coordinate frame attached to the substructure (cf. Fig. 2.4).

We maintain a table of common edges. Each tuple in the table has the form

$$(O.id, Str_x, Str_y, Str_x.P_{b_1}, Str_y.P_{b_1}, Str_x.EP_1, Str_y.EP_2)$$

where $O.id$ is a graph identification number, Str_x and Str_y are two rigid substructures in the graph, $Str_x.P_{b_1}$ and $Str_y.P_{b_1}$ are the node numbers of the origins of the local coordinate frames attached to the two substructures respectively, and $Str_x.EP_1$ and $Str_y.EP_2$ are the node numbers of the end points of the common edge between Str_x and Str_y. For example, consider the data graph in Fig. 2.3 again and its rigid substructures in Fig. 2.4. Suppose the identification number of the graph is 12 and the nodes numbered 0 and 6 are chosen as the origins of the local coordinate frames attached to Str_0 and Str_1 respectively. Then there is a tuple $(12, Str_0, Str_1, 0, 6, 5, 6)$ in the common edge table, indicating the fact that Str_0 and Str_1 are connected via the common edge $\{5, 6\}$.

3.2.2 Encoding Node and Label Triplets

In addition to encoding label-triplets like in Chapter 2, we also encode the node-triplets.

Suppose the three nodes chosen are v_1, v_2, v_3, in that order. We encode this node-triplet as follows. The code for the node-triplet is an unsigned long integer, defined as $((N_1 \times 1000 + N_2) \times 1000) + N_3$, where N_1, N_2 and N_3 are the node numbers of v_1, v_2 and v_3, respectively. Here 1000 is a parameter value adjustable for different domains. As long as the number of nodes in a graph is less than 1000, the code of a node-triplet is unique.

Thus, for example, for the nodes numbered 1, 2 and 3, the code for this node-triplet is $((1 \times 1000 + 2) \times 1000) + 3 = 1002003$ and the code for the corresponding label-triplet is $((1 \times 1000 + 2) \times 1000) + 2 = 1002002$. $\square$

3.3 Our Approach

After explaining the basic concepts, we now turn to the description of the proposed approach. Our approach is composed of the preprocessing phase and the on-line search phase. We first present the algorithm used in the preprocessing phase. Then we discuss the on-line phase, followed by the algorithm used to augment substructure matches. Finally we describe the algorithms for fast similarity search and related queries.

3.3.1 Preprocessing Phase

We choose all node-triplets in a data substructure and hash them into a 3D disk-based hash table just like in Chapter 2. The only difference is that we also include the code of the node-triplets in the hash table.

Thus, for example, the hash table entry for the three chosen nodes i, j, k from the substructure Str_0 is now $(12, 0, Ncode, Lcode, SF_0[i, j, k])$, where $Ncode$ is the node-triplet code and $Lcode$ is the label-triplet code.

3.3.2 On-Line Phase

To facilitate detecting substructure matches, we associate a node_match_list and a relabeling_counter with each substructure in the data graphs. Given a target graph Q, we divide Q into rigid substructures and hash the substructures using the same hash function as in the preprocessing phase. Then we update the node_match_list and relabeling_counter as illustrated below. Let us focus on the substructure Str_0 of the data graph with identification number 12 shown in Fig. 2.4(a). Suppose i, j, k are three nodes in the substructure Str_0. Then its entry in the hash table is $(12, 0, Ncode, Lcode, SF_0[i, j, k])$. Let u, v, w be three nodes in the target graph Q that have the same hash address as i, j, k (i.e. the node-triplet $[u, v, w]$ hits the substructure Str_0). Calculate

$$Str_0.SF_Q = SF_0[i, j, k] \times \begin{pmatrix} \vec{V}_{u,v} \\ \vec{V}_{u,w} \\ \vec{V}_{u,v} \times \vec{V}_{u,w} \end{pmatrix} + \begin{pmatrix} P_u \\ P_u \\ P_u \end{pmatrix}$$

Intuitively, $Str_0.SF_Q$ contains the coordinates of the three basis points of the Substructure Frame 0 (SF_0) with respect to the global coordinate frame in which the target graph Q is given.

We decode $Ncode$ to get i, j, k and add them into the node_match_list of Str_0. Intuitively, this records that i geometrically matches u (i.e. they have the same 3D coordinate), j geometrically matches v and k geometrically matches w. We also decode $Lcode$ and determine whether these geometrically matching nodes have the same label. If not, the relabeling_counter is updated to reflect the fact that there is a relabeling between the geometrically matching nodes. In general, there may be several node-triplets of Q that hit Str_0. We update the node_match_list and relabeling_counter of Str_0 only if these matching node-triplets yield the same $Str_0.SF_Q$.

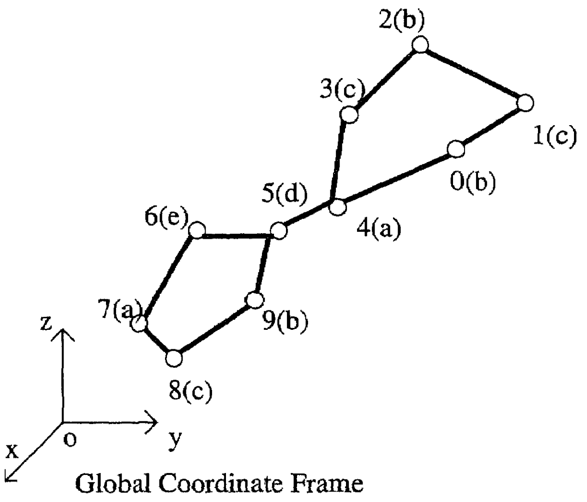

Figure 3.1 A target graph Q.

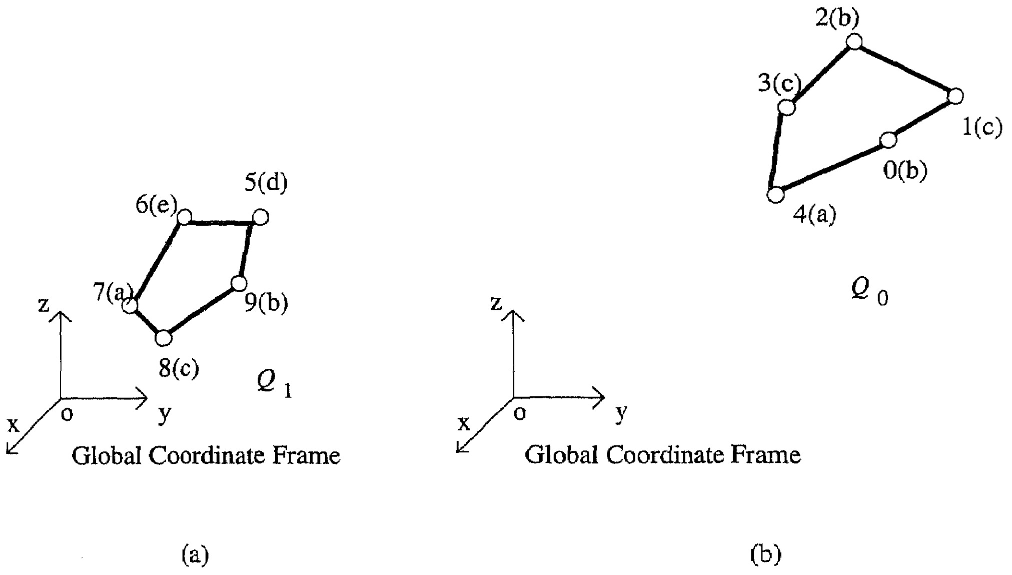

Figure 3.2 The two substructure from the target graph in Fig. 3.1

Example 3.1 Consider the target graph Q in Fig. 3.1 Q contains two rigid substructure Q_0 and Q_1 in Fig. 3.2. Table 3.1 lists the node labels and global

Table 3.1 Node labels and global coordinates for the target graph in Fig. 3.1

node No.	label	global coordinates
0	b	(-0.269000,4.153153,2.911494)
1	c	(-0.317400,4.749386,3.253592)
2	b	(0.172100,3.913515,4.100777)
3	c	(0.366000,3.244026,3.433268)
4	a	(-0.020300,2.964012,2.777921)
5	d	(0.102900,2.316302,2.220155)
6	e	(0.500900,1.477885,2.065228)
7	a	(0.422900,0.737686,1.534191)
8	c	(0.005600,1.309948,1.101230)
9	b	(-0.294100,2.264259,1.484623)

coordinates of the nodes in Q. In Q_0, the nodes numbered 0, 1, 2, 3, 4 match, after rotation, the nodes numbered 4, 3, 1, 2, 5 in the substructure Str_0 in Fig. 2.4(a). The node numbered 0 in Str_0 does not appear in Q_0 (i.e. it is to be deleted). Thus, for example, for the nodes numbered 2, 3 and 1 in Q_0, the bucket address in the 3-dimensional hash table is $h[25][12][21]$ and

$$Str_0.SF_Q = \begin{pmatrix} -0.012200 & 5.005500 & 4.474200 \\ 0.987800 & 5.005500 & 4.474200 \\ -0.012200 & 4.298393 & 3.767093 \end{pmatrix}$$

For the nodes numbered 2, 0 and 3 in Q_0, the bucket address is $h[24][0][9]$ and

$$Str_0.SF_Q = \begin{pmatrix} -0.012200 & 5.005500 & 4.474200 \\ 0.987800 & 5.005500 & 4.474200 \\ -0.012200 & 4.298393 & 3.767093 \end{pmatrix}$$

Referring to Example 2.4 and Example 2.5, these two matches (hits) have the same $Str_0.SF_Q$, and therefore the node_match_list for the substructure Str_0 of data graph 12 includes the nodes 1, 2, 3, and 4. After hashing all node-triplets of Q_0, the node_match_list of Str_0 will include the nodes 1, 2, 3, 4 and 5 (cf. Fig. 3.3(a)). Since all the matching nodes have the same labels, the relabeling_counter of Str_0 is 0.

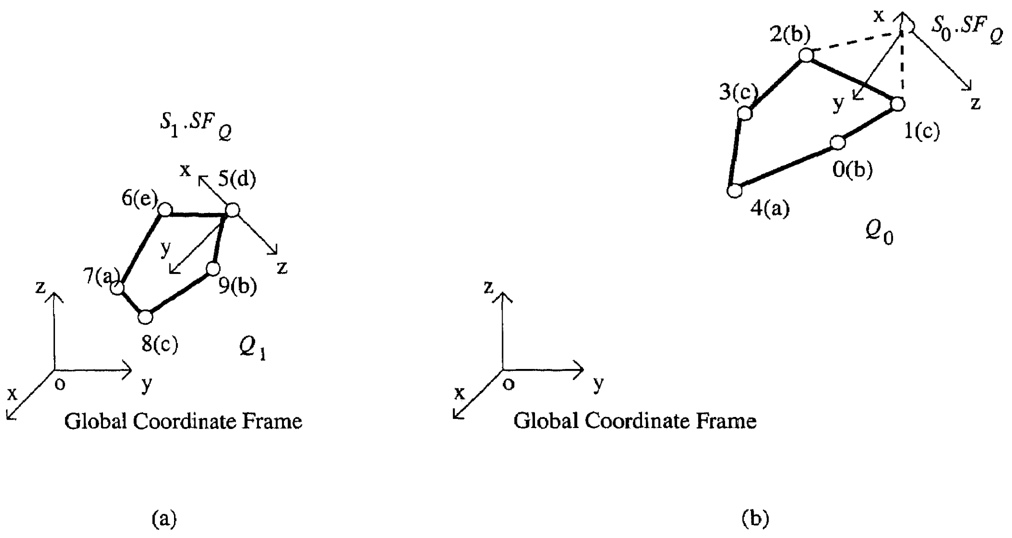

Figure 3.3 The matches between the substructures of the target and data graphs

Note that, for any node i in the substructure Q_0 with global coordinate $P_i(x_i, y_i, z_i)$, it has a local coordinate with respect to $Str_0.SF_Q$, denoted P_i', where

$$P_i' = \vec{V}_{c_1,i} \times Str_0.E$$

Here P_{c_1} is the origin of $Str_0.SF_Q$ and $Str_0.E$ is the base matrix of $Str_0.SF_Q$. Thus, for example, the local coordinates, with respect to $Str_0.SF_Q$, of nodes 2, 3 and 1 in Q_0 are

$$P_2'(0.184300, 1.036200, -0.508100)$$

$$P_3'(0.378200, 1.981600, -0.509500)$$

$$P_1'(-0.305200, 1.044200, 0.682000)$$

They match the local coordinates, with respect to SF_0, of nodes 1, 2 and 3 of the substructure Str_0 in Example 2.1 (cf. Fig. 2.8). Likewise, the local coordinate, with respect to $Str_0.SF_Q$, of node 0 in Q_0 is

$$P_0'(-0.256800, 1.707700, 0.502300)$$

which matches the local coordinate, with respect to SF_0, of node 4 of the data graph in Example 2.1 (cf. Fig. 2.8).

Similarly, in Q_1 the nodes numbered 5, 6, 7, 8, 9 match, after rotation, the nodes numbered 6, 7, 8, 9, 10 in the substructure Str_1 in Fig. 2.4(b). The node_match_list of substructure Str_1 includes nodes 6, 7, 8, 9 and 10 after hashing all node-triplets in Q_1 (cf. Fig. 3.3(b)). The relabeling_counter for Str_1 is 1, since the label of the node numbered 8 in Q_1 differs from the node numbered 9 in Str_1. □

3.3.3 Augmenting Substructure Matches

Substructure matches with the same graph identification number may be augmented by utilizing the common edge table. Suppose that, in the common edge table, there is a tuple

$$(O.id, Str_x, Str_y, Str_x.P_{b_1}, Str_y.P_{b_1}, Str_x.EP_1, Str_y.EP_2)$$

for two substructures Str_x and Str_y in a data graph. Let SF_x represent the local coordinate frame attached to Str_x and SF_y represent the local coordinate frame attached to Str_y. Suppose that, after hashing all node-triplets of the target graph Q, $Str_x.SF_Q$ ($Str_y.SF_Q$, respectively) contains the coordinates of the three basis points of SF_x (SF_y, respectively) with respect to the global coordinate frame in which the target graph Q is given. The base matrix for $Str_x.SF_Q$ ($Str_y.SF_Q$, respectively) is $Str_x.E$ ($Str_y.E$, respectively). $Str_x.P_{c_1}$ ($Str_y.P_{c_1}$, respectively) is the origin of $Str_x.SF_Q$ ($Str_y.SF_Q$ respectively).

Let

$$Str_x.EP_1' = \vec{V}_{Str_x.P_{b_1}, Str_x.EP_1} \times Str_x.E + Str_x.P_{c_1}$$

$$Str_x.EP_2' = \vec{V}_{Str_x.P_{b_1}, Str_y.EP_2} \times Str_x.E + Str_x.P_{c_1}$$

$$Str_y.EP_1' = \vec{V}_{Str_y.P_{b_1}, Str_x.EP_1} \times Str_y.E + Str_y.P_{c_1}$$

$$Str_y.EP_2' = \vec{V}_{Str_y.P_{b_1}, Str_y.EP_2} \times Str_y.E + Str_y.P_{c_1}$$

where $\vec{V}_{Str_x.P_{b_1}, Str_x.EP_1}$ ($\vec{V}_{Str_x.P_{b_1}, Str_y.EP_2}$, respectively) represents the coordinate of $Str_x.EP_1$ ($Str_y.EP_2$, respectively) with respect to the local coordinate frame SF_x, and $\vec{V}_{Str_y.P_{b_1},Str_x.EP_1}$ ($\vec{V}_{Str_y.P_{b_1},Str_y.EP_2}$, respectively) represents the coordinate of $Str_x.EP_1$ ($Str_y.EP_2$, respectively) with respect to the local coordinate frame SF_y. Intuitively, $Str_x.EP'_1$ contains the coordinates of the first end node of the common bond between Str_x and Str_y with respect to the global coordinate frame in which the target graph Q is given when matching Str_x with Q. This $Str_x.EP'_1$ is calculated by considering the local coordinate frame Substructure Frame $Str_x.SF_Q$. $Str_y.EP'_1$ contains the coordinates of the first end node of the common bond between Str_x and Str_y with respect to the global coordinate frame in which the target graph Q is given when matching Str_y with Q. This $Str_y.EP'_1$ is calculated by considering the local coordinate frame Substructure Frame $Str_y.SF_Q$.

Suppose the substructure Q_1 of Q matches the substructure Str_x of the graph G and the substructure Q_2 of Q matches the substructure Str_y of G. The two substructure matches are said to be *augmentable* if Q_1 (Str_x, respectively) is connected with Q_2 (Str_y, respectively) via a common bond and the two substructures are rotatable with respect to the common bond. The following proposition establishes the condition under which the two substructure matches are augmentable.

Proposition 3.1 *$Str_x.EP'_1 = Str_y.EP'_1$ and $Str_x.EP'_2 = Str_y.EP'_2$ if and only if the two substructure matches are augmentable.*

Proof The proof follows by observing that when two substructures are rotated around the common edge, the relative positions of all the nodes in one substructure with respect to the other substructure are changed except the two end points of the common edge. $\square$

Thus if the two substructure matches are augmentable, we can glue the two substructures of data graph G (target Q, respectively) to form a larger substructure S (K, respectively), thus obtaining a match between S and K. The node_match_list of S is the union of the node_match_list of Str_x and the node_match_list of Str_y. The relabeling_counter of S is the sum of the relabeling_counter of Str_x and the relabeling_counter of Str_y.

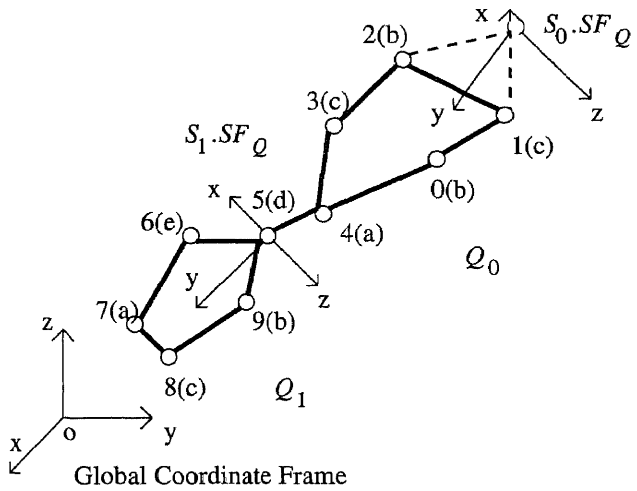

Figure 3.4 Augmenting substructure matches

Example 3.2 In Example 3.1, The node_match_list of substructure Str_0 includes the nodes 1, 2, 3, 4 and 5 after hashing all node-triplets of Q_0. The relabeling_counter of Str_0 is 0. The node_match_list of substructure Str_1 includes nodes 6, 7, 8, 9 and 10 after hashing all node-triplets in Q_1. The relabeling_counter of Str_0 is 1. There is a tuple $(12, Str_0, Str_1, 0, 6, 5, 6)$ in the common edge table. Therefore we calculate

$$\begin{aligned}\vec{V}_{P_0,P_5} &= (1.0097, 3.6478, 2.2660) - (1.0178, 1.0048, 2.5101) \\ &= (-0.0081, 2.6430, -0.2441)\end{aligned}$$

$$Str_0.SF_Q = \begin{pmatrix} -0.012200 & 5.005500 & 4.474200 \\ 0.987800 & 5.005500 & 4.474200 \\ -0.012200 & 4.298393 & 3.767093 \end{pmatrix}$$

$$Str_0.E = \begin{pmatrix} 1.000000 & 0.000000 & 0.000000 \\ 0.000000 & -0.707107 & -0.707107 \\ 0.000000 & 0.707107 & -0.707107 \end{pmatrix}$$

$$Str_0.c_1 = (-0.012200, 5.005500, 4.474200)$$

$$Str_0.EP_1' = \vec{V}_{P_0,P_5} \times Str_0.E + Str_0.c_1 = (-0.020300, 2.964012, 2.777921)$$

Similarly,

$$Str_0.EP_2' = \vec{V}_{P_0,P_6} \times Str_0.E + Str_0.c_1 = (0.102900, 2.316302, 2.220155)$$

$$Str_1.EP_1' = \vec{V}_{P_6,P_5} \times Str_0.E + Str_1.c_1 = (-0.020300, 2.964012, 2.777921)$$

$$Str_1.EP_2' = \vec{V}_{P_6,P_6} \times Str_0.E + Str_1.c_1 = (0.102900, 2.316302, 2.220155)$$

Since

$$Str_0.EP_1' = Str_1.EP_1'$$

and

$$Str_0.EP_2' = Str_1.EP_2'$$

the two substructure matches are augmentable. We glue Str_0 and Str_1 to form G in Fig. 2.3 and glue Q_0 and Q_1 to form Q in Fig. 3.4. The node_match_list of G now includes nodes 1, 2, 3, 4, 5, 6, 7, 8, 9 and 10, meaning that these nodes match nodes in Q geometrically. The relabeling_counter of G is 1, meaning that there is a relabeling operation (i.e. changing e to c) when matching G with Q. □

3.3.4 Query Processing Algorithms

By consulting the common edge table, one can augment small substructure matches to form larger substructure matches whenever appropriate. Then we can obtain the node_match_list and relabeling_counter of the data graph G. The size of node_match_list of G shows the number of nodes in G that match with nodes in Q geometrically. The relabeling_counter of G shows among those geometrically matching nodes, how many need to be relabeled. Thus, the node_match_list and relabeling_counter together show the distance between G and Q.

Formally, let n be the number of nodes in the node_match_list, m be the value of relabeling_counter, and $|G|$ ($|Q|$, respectively) be the size of the data graph G

Table 3.2 Similarity queries and the algorithms to process them

query type	**data graphs returned**
good-match	the graphs G where $\Delta(G,Q) \leq \epsilon$
k-closest	the k graphs G with the smallest $\Delta(G,Q)$'s
best-match	the graph G with the smallest $\Delta(G,Q)$
bad-match	the graphs G where $\Delta(G,Q) > \epsilon$
k-farthest	the k graphs G with the largest $\Delta(G,Q)$'s
worst-match	the graph G with the largest $\Delta(G,Q)$

(target graph Q, respectively). We have

Proposition 3.2 *The distance between G and Q is $\Delta(G,Q)$ where $\Delta(G,Q) = m + |G| + |Q| - 2n$.*

Proof When matching G with Q, there are $|G|-n$ node deletes, $|Q|-n$ node inserts and m node relabeling, and hence the result follows. □

Example 3.3 The data graph G in Fig. 2.3 has size $|G| = 11$ and the target graph Q in Fig. 3.1 has size $|Q| = 10$. After the augmentation as explained in Example 3.2, the number of nodes in the node_match_list is 10 and the relabeling_counter is 1. Thus the distance between G and Q is $\Delta(G,Q) = 1 + 11 + 10 - 2 \times 10 = 2$. Referring to Fig. 2.3 and Fig. 3.1 we see that in matching G with Q we deleted one node (i.e. deleted the node numbered 0 in G) and relabel another node (i.e. changed the label e of node 9 in G to the label c of node 8 in Q). □

Thus, after hashing the target graph, we can check the node_match_list and relabeling_counter for each graph in the database and calculate $\Delta(G,Q)$. Table 3.2 summarizes the algorithms for processing the six types of queries described in Section 3.1.

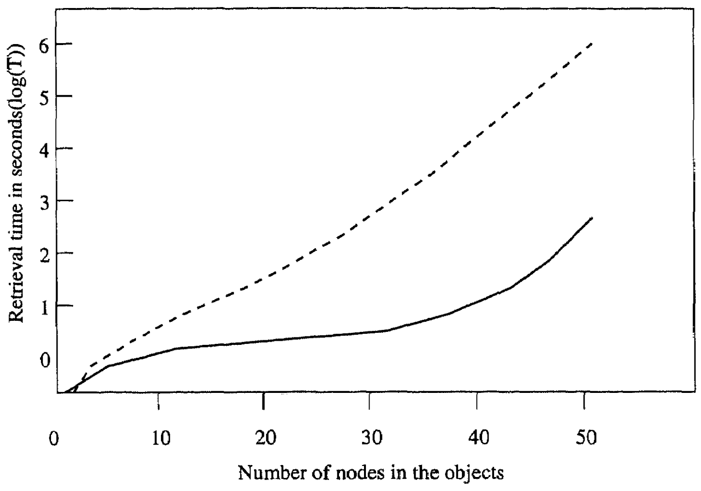

Figure 3.5 Impact of the decomposition/augmentation processes as a function of the size of graphs

3.4 Experimental Results

We have implemented the proposed algorithms using the C programming language on a SunSPARC 20 workstation running Solaris version 2.4. Two files are maintained: one recording the bucket addresses and the other containing all hash table entries. We applied the algorithms to 226 3D molecular structures obtained from a database maintained in the National Cancer Institute. The number of nodes (atoms) in the molecules range from 5 to 51. It takes 9 seconds to hash all the 226 molecules in the preprocessing phase. In order to demonstrate the advantage of decomposition/augmentation, we studied two cases. In the first case, we hashed and retrieved a molecule in its entirety. In the second case, we decomposed the molecules to substructures and augmented the substructure matches during the retrieval. In Fig. 3.5, the dashed line represents the retrieval time without the decomposition/augmentation processes. The solid line represents the retrieval time with the processes. It can be seen that the decomposition/augmentation processes speed up the retrieval by a factor of 100 when the graphs have 30 nodes and 1,000 when the graphs have 50 nodes. Fig. 3.6 compares the performance of our technique with exhaustive search. By exhaustive search, we mean that in the preprocessing

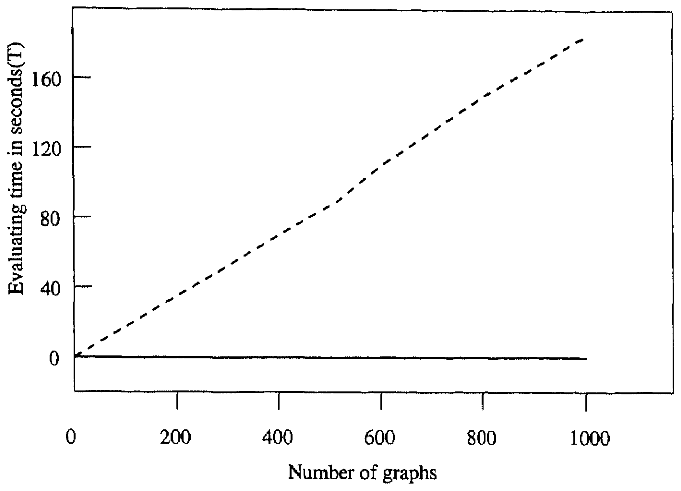

Figure 3.6 Performance comparison between our method and the exhaustive search technique

phase we sort and store the lengths of the three edges of the triangle formed by any node-triplet in a three dimensional array. We also store the local coordinate system $LF[i, j, k]$. In the on-line phase, we find node-triplet matches by searching the array. It can be seen that our technique is 100 times faster than the exhaustive search method when the data set has over 600 graphs while achieving the same recall.

CHAPTER 4

AN APPROXIMATE ORACLE FOR DISTANCE IN METRIC SPACES

4.1 Introduction

Consider a database of objects $\mathcal{D} = \{p_0, p_1, \ldots, p_k\}$ and a function d where for any $p_i, p_j \in \mathcal{D}$, $d(p_i, p_j)$ (or $d_{i,j}$ for short) represents the distance between p_i and p_j. In this chapter, we present a data structure for distance estimation, assuming only that the pairwise distances between the objects in $\mathcal{D}$ are given and the distance function d is a pseudo-metric. That is, for any $0 \leq i, j, l \leq k$, $d_{i,i} = 0$, $d_{i,j} \geq 0$, $d_{i,j} = d_{j,i}$ (symmetry) and $d_{i,l} \leq d_{i,j} + d_{j,l}$ (triangle inequality) [45]. The proposed data structure contributes to the processing of various pattern-matching based queries, including nearest neighbor search [78], which finds the objects closest to a given target, ϵ-range search, which finds the objects within distance ϵ of the target, and so on. Such retrieval operations arise in many applications including vision [31], data mining [24], computational biology [87], document processing [78] and multimedia information management [7].

The rest of the chapter is organized as follows. Section 3.2 is a survey of related work. Section 3.3 describes how to map data objects to vectors in a pseudo-Euclidean space with a reasonably low dimension that preserves the distance function approximately. In practice, such a mapping can be done in the off-line phase. Section 3.4 shows how to project a given target, possibly arriving in the on-line phase, onto the same vector space. Section 3.5 describes applications of our approach and reports some experimental results on the performance of the proposed data structure.

4.2 Related Work

Data structures for distance calculations and their applications to pattern-matching based query processing have been studied in the past. A common assumption is that

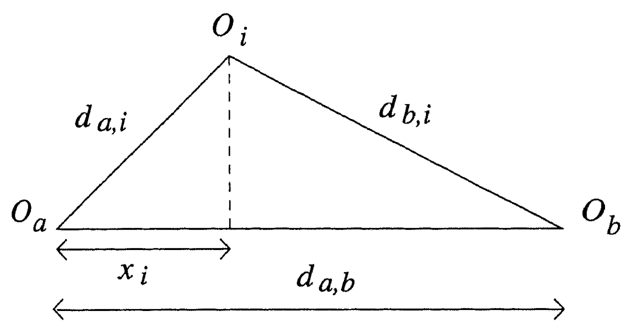

Figure 4.1 Illustration of the projection method used in *FastMap*.

calculating the distance between two objects is the dominating cost, which should be minimized. Common techniques include using the triangle inequality to prune the search space or mapping the objects to a Euclidean space where the cost incurred by computing Euclidean distances is negligible. For example, in [24], Faloutsos and Lin proposed the *FastMap* approach to solving the ϵ-range search problem. The authors mapped all objects (including the target) to vectors in a Euclidean space and used the Euclidean distances between vectors to approximate the target-object distances. The mapping is based on the Cosine Law of any triangle (cf. Fig.4.1). That is in any triangle $O_aO_iO_b$, we have

$$d_{b,i}^2 = d_{a,i}^2 + d_{a,b}^2 - 2x_i d_{a,b}$$

The approach is composed of two phases. In the preprocessing phase, the set of data objects are mapped to a k dimensional Euclidean space. Given a set of objects O_i $i = 1, \ldots, N$, and a distance function d. Pretending that the objects are indeed points in n dimensional space; choose a pair of objects to be the *pivot objects*; consider a $(n-1)$ dimensional hyper-plane $\mathcal{H}$ that is perpendicular to the line (O_a, O_b); project the objects on this hyper-plane. Let O_i' stand for the projection of O_i (for $i = 1, \ldots, N$). On the hyper-plane $\mathcal{H}$, the Euclidean distance d' can be calculated as

$$(d'(O'_i, O'_j))^2 = (d(O_i, O_j))^2 - (x_i - x_j)^2 \; i, j = 1, \ldots, N$$

Thus the problem is the same as the original one, with the dimension decreased by one. This process can be done $k \leq n$ times, and each object O_i is represented by a vector $(x_i^1, \ldots, x_i^k)$.

In the on-line search phase, the query object O_q is mapped into a k dimensional vector using the same set of 'pivot objects', with the appropriate distance function each time. The Euclidean distances of the k dimensional vectors are then used to approximate the distances of the objects.

The approximation can find all the qualifying data objects by examining the vectors within some distance of the target vector in the Euclidean space. However if the dimension of the Euclidean space is chosen inappropriately, many unqualified data objects appear to qualify according to the data structure. In contrast to *FastMap*, we map objects to a pseudo-Euclidean space [33]. This technique yields fewer false positives than *FastMap*.

In [7], Berchtold *et al.* described a parallel method for nearest-neighbor search in high-dimensional feature space. The FQ tree proposed by Baeza-Yates *et al.* [5] is a cluster structure which based on only the distance function. Given a set of objects each identified by a key in $\mathcal{K}$, and a distance function. The clustering starts by picking up a value k_r from $\mathcal{K}$, grouping those objects whose keys have the same distance to k_r together. k_r was then associated with an internal node and those groups became children of this node. This process was repeated for each of those subsets until the subsets are smaller than a pre-defined size. The unique feature of the FQ tree is that it has the same key at each level of the tree, i.e. for all nodes at the same level the same key is chosen to partition further. The key which associates with a level can be chosen from the objects or can be chosen especially to optimize the tree structure.

When processing a query object, starting at the root of the tree, the searching algorithm compares the key of the query object with the key associated with each node and utilizes the triangle inequality to prune the search space.

Similarly, the technique described in [74] employed an approximate distance map to guide the search and exploited the triangle inequality to prune the search space.

Another well known technique that reduces dimensionality in the Euclidean space is the Discrete Fourier Transform (DFT). In [4], the author used DFT to mapped time sequences to a lower-dimensionality space. An important observation is that the Fourier transform preserves the Euclidean distance in the time or frequency domain. The assumption for this technique to succeed is that for most sequences of practical interest, only the first few frequencies are strong.

There are other related techniques [28]. However, none of the work considered mapping objects to a high precision pseudo-Euclidean space.

4.3 Mapping Data Objects to a Vector Space

We are given a database of $k+1$ objects $\mathcal{D}$, a distance function d, which is a pseudo-metric, and pairwise distances $d_{i,j}$, for all $0 \leq i, j \leq k$. Thus, ($\mathcal{D}$, d) is a pseudo-metric space [45]. We first describe how to map the $k+1$ objects to a k-dimensional pseudo-Euclidean space, R^k. Then Section 3.3.2 establishes an orthogonal basis for R^k. Section 3.3.3 considers a lower dimension space R^n, $n \leq k$, by ignoring those dimensions dim_j where after mapping all the objects of $\mathcal{D}$ to R^k, the differences among the j^{th} components of the corresponding vectors are small. To further reduce the dimension, Section 3.3.4 considers an orthonormal basis and Section 3.3.5 establishes an m-dimensional pseudo-Euclidean space R^m, $m \ll k$. The objects corresponding to the dimensions of R^m are chosen as *reference objects.* These reference objects will be compared with the target in the very beginning of the on-line phase, so that the calculated distances can be used for projecting the target onto R^m.

4.3.1 Pseudo-Euclidean Space R^k

Our notation is mainly based on [32, 50]. In addition, we will use the following notations:

We use $\{a_i\}_{1\leq i\leq n}$, or simply $\{a_i\}$ when the context is clear, to represent $\{a_1, \ldots, a_n\}$ where a_i's are vectors. Let c_i's be real numbers.

$$(c_i)_{1\leq i\leq n} = \begin{pmatrix} c_1 \\ c_2 \\ \vdots \\ c_n \end{pmatrix}$$

$$(c_{i,j})_{1\leq i\leq m, 1\leq j\leq n} = \begin{pmatrix} c_{1,1} & c_{1,2} & \cdots & c_{1,n} \\ c_{2,1} & c_{2,2} & \cdots & c_{2,n} \\ \vdots & & & \vdots \\ c_{m,1} & c_{m,2} & \cdots & c_{m,n} \end{pmatrix}$$

$$diag(c_i)_{1\leq i\leq n} = \begin{pmatrix} c_1 & 0 & \cdots & 0 \\ 0 & c_2 & \cdots & 0 \\ \vdots & & & \vdots \\ 0 & 0 & \cdots & c_n \end{pmatrix}$$

We define a mapping α as follows:

$$\alpha : \mathcal{D} \rightarrow R^k$$

such that

$$\alpha(p_0) = a_0 = (0, \ldots, 0)$$

$$\alpha(p_i) = a_i = (0, \ldots, 1_{(i)}, \ldots, 0)\ 1 \leq i \leq k$$

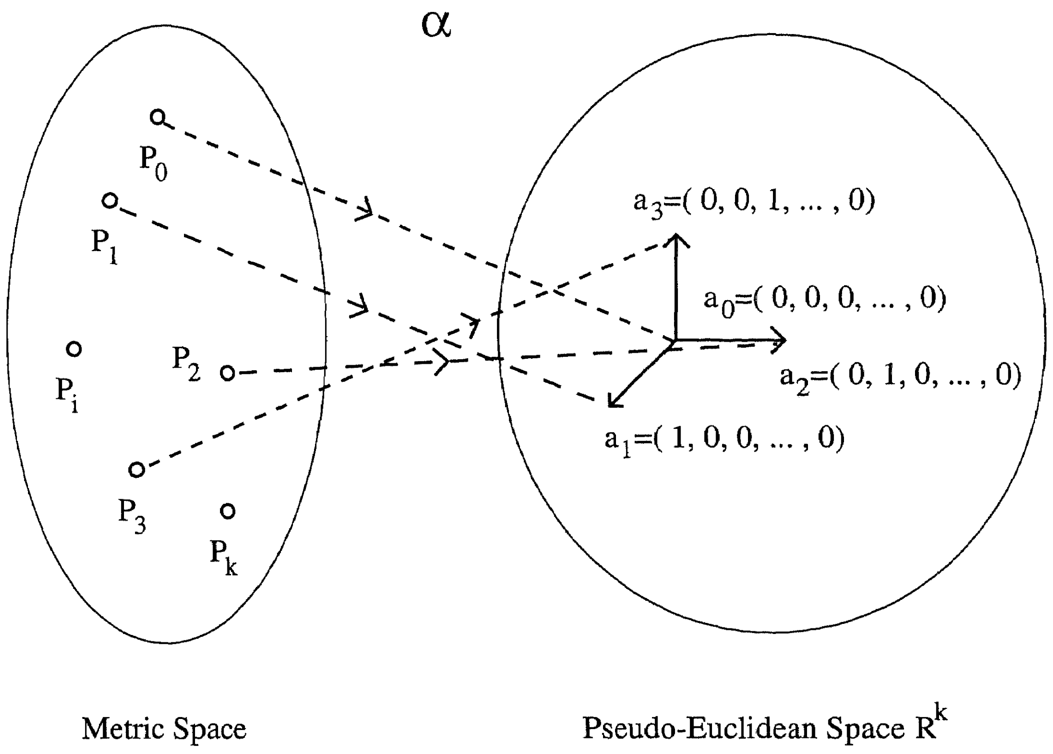

Figure 4.2 The mapping α.

Let

$$M(\psi_{<a>}) = (m_{i,j})_{1\leq i,j\leq k}$$

where

$$m_{i,j} = (d_{i,0}^2 + d_{j,0}^2 - d_{i,j}^2)/2 \; 1 \leq i,j \leq k$$

Fig. 4.2 illustrate the mapping α between the pseudo-metric space $\mathcal{D}$ and the k-dimensional pseudo-Euclidean space R^k.

We define another mapping ψ as follows:

$$\psi : R^k \times R^k \to R$$

such that

$$\psi(x,y) = x^T M(\psi_{<a>})y$$

where x^T is the transpose of vector x. Notice that $\psi(a_i, a_j) = m_{i,j}$. ψ is a *symmetric bilinear form* of R^k. $M(\psi_{<a>})$ is the matrix of ψ w. r. t. the basis $\{a_i\}_{1\leq i\leq k}$. The vector space R^k equipped with the symmetric bilinear form ψ is called a *pseudo-Euclidean space* [33]. For any two vectors $x, y \in R^k$, $\psi(x, y)$ is called the *inner product* of x and y, and $||x - y||^2 = \psi(x - y, x - y)$ is called the *squared distance* between x and y.

4.3.2 ψ-Orthogonal Basis $\{e_i\}$

Since the matrix $M(\psi_{<a>})$ is real symmetric, there is an orthogonal matrix $Q = (q_{i,j})_{1 \le i,j \le k}$ and a diagonal matrix $D = diag(\lambda_i)_{1 \le i \le k}$ such that

$$Q^T M(\psi_{<a>}) Q = D \tag{4.1}$$

where Q^T is the transpose of Q, $\lambda_i' s$ are eigenvalues of $M(\psi_{<a>})$ arranged in some order, and columns of Q are the corresponding eigenvectors [32]. Let

$$(e_1, \ldots, e_k) = (a_1, \ldots, a_k)Q$$

or equivalently

$$(a_1, \ldots, a_k) = (e_1, \ldots, e_k)Q^T \tag{4.2}$$

Then $\{e_i\}_{1 \le i \le k}$ is another basis of R^k. Note that the coordinate of e_j w. r. t. $\{a_i\}_{1 \le i \le k}$ is the j^{th} column of matrix Q, and the coordinate of a_j w. r. t. $\{e_i\}_{1 \le i \le k}$ is the j^{th} row of Q. Thus through a matrix transformation, we find a ψ-Orthogonal Basis $\{e_i\}$ in R^k (see Fig. 4.3).

Since there will often be three different bases of a space in our discussion, we introduce a new notation, which is not common, but convenient. Let $x = (x^1, \ldots, x^k)$ be a vector and $\{a_i\}_{1 \le i \le k}$ be a basis of R^k. The coordinate of x w. r. t. $\{a_i\}_{1 \le i \le k}$ is denoted by $x_{<a>} = (x^i_{<a>})_{1 \le i \le k}$. Using this notation, the relation between $\{a_j\}$ and $\{e_j\}$ may be written as

$$e_{j<a>} = (q_{1,j}, \ldots, q_{k,j}) \; 1 \le j \le k$$

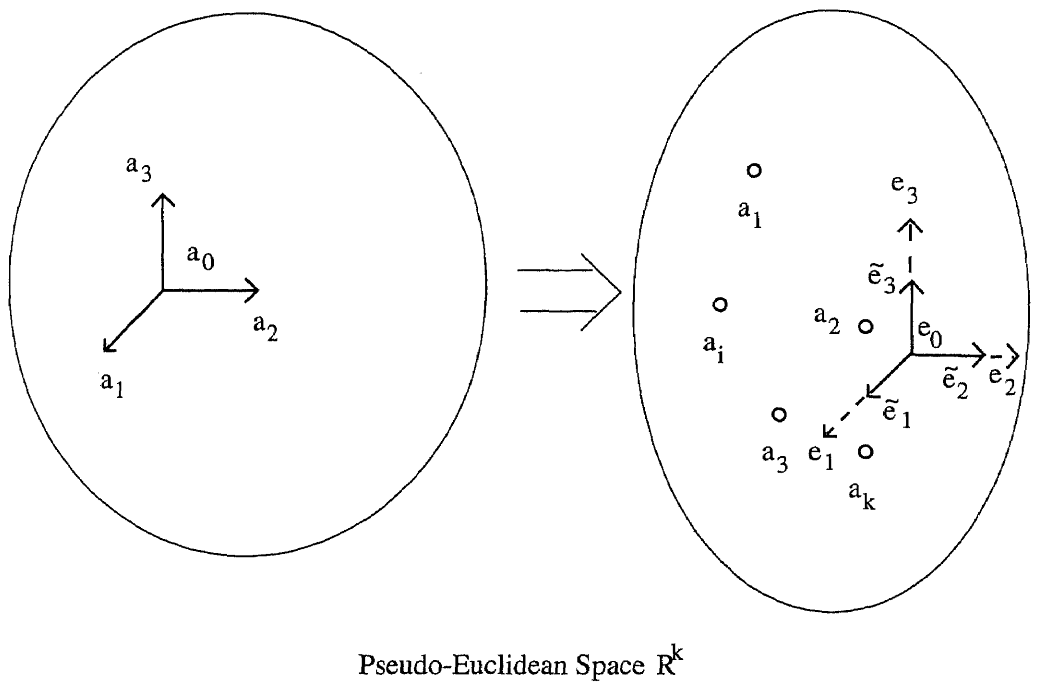

Figure 4.3 The ψ-Orthogonal Basis $\{e_i\}$ and the ϕ-Orthonormal Basis $\{\tilde{e}_i\}$.

and

$$a_{j<e>} = (q_{j,1}, \ldots, q_{j,k}) \; 1 \leq j \leq k$$

where $e_{j<a>}$ is the coordinate of e_j w. r. t. $\{a_i\}_{1 \leq i \leq k}$, and $a_{j<e>}$ is the coordinate of a_j w. r. t. $\{e_i\}_{1 \leq i \leq k}$. Let x be a vector in R^k. Then

$$(x^1_{<a>}, \ldots, x^k_{<a>}) = (x^1_{<e>}, \ldots, x^k_{<e>})Q^T \tag{4.3}$$

Therefore the matrix of the bilinear form ψ w. r. t. $\{e_i\}_{1 \leq i \leq k}$ is

$$M(\psi_{<e>}) = Q^T M(\psi_{<a>}) Q = D$$

That is, the basis $\{e_i\}_{1 \leq i \leq k}$ is *ψ-orthogonal.* Let x, y be two vectors in R^k. Then

$$\begin{aligned}\psi(x,y) &= x^T_{<a>}M(\psi_{<a>})y_{<a>} \\ &= x^T_{<e>}Q^T M(\psi_{<a>})Qy_{<e>} \\ &= x^T_{<e>}Dy_{<e>} \\ &= \Sigma_{i=1}^k \lambda_i x^i_{<e>} y^i_{<e>}\end{aligned}$$

$$||x-y||^2 = \Sigma_{i=1}^k \lambda_i (x^i_{<e>} - y^i_{<e>})^2 \qquad (4.4)$$

Especially, we have

$$\psi(a_i, a_j) = \Sigma_{l=1}^k \lambda_l q_{i,l} q_{j,l}$$

Remark. If the matrix $M(\psi_{<a>})$ has negative eigenvalues, the squared distance between two vectors in the pseudo-Euclidean space may be negative. That's why we never say the "distance" between vectors in a pseudo-Euclidean space. Furthermore, the fact that the squared distance between two vectors vanishes does not imply that these two vectors are the same. These situations cannot happen in a Euclidean space.

4.3.3 Pseudo-Euclidean Space R^n, $n \le k$

Assume that the eigenvalues of the matrix $M(\psi_{<a>})$ are ordered as follows: first n^+ positive eigenvalues, then n^- negative ones and finally zeroes. $n = n^+ + n^-$. Then

$$R^k = V \oplus R^0$$

where $\oplus$ denotes the direct sum of two subspaces: $V = R^{(n^+ + n^-)}$ is the subspace generated by $\{e_i\}_{1 \le i \le n}$, and R^0 is the subspace generated by $\{e_i\}_{n+1 \le i \le k}$ [50]. Let $\phi = \psi|_{V \times V}$. Then ϕ is a non-degenerate bilinear form over $V \times V$. The set of vectors $\{e_i\}_{1 \le i \le n}$ is a ϕ-orthogonal basis of subspace V.

Let x be a vector in R^k. We define the ψ-orthogonal projection

$$\Pi : R^k \to R^n$$

such that

$$\Pi(x^1_{<e>}, \dots, x^n_{<e>}, x^{n+1}_{<e>}, \dots, x^k_{<e>}) = (x^1_{<e>}, \dots, x^n_{<e>})$$

Fig. 4.4 illustrates the projection from R^k to R^n.

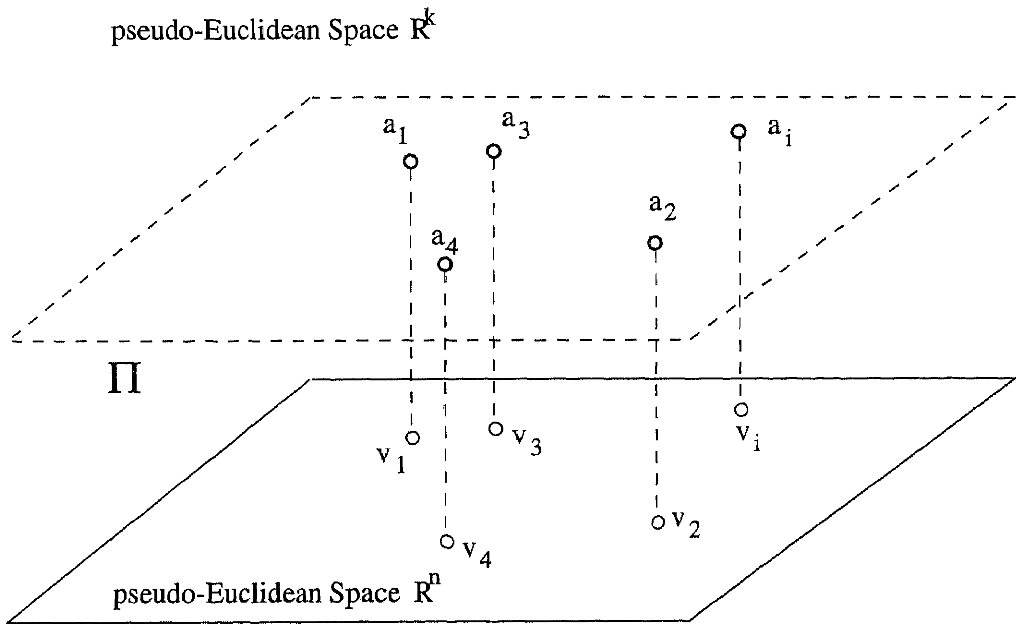

Figure 4.4 The projection from R^k to R^n.

Let v_j denote $\Pi(a_j)$. Let $Q_{[kn]}$ be the $k \times n$ matrix consisting of the first n columns of the orthogonal matrix Q, namely $Q_{[kn]} = (q_{i,j})_{1 \le i \le k, 1 \le j \le n}$. Then from the definition of Π and equation (4.2), we have

$$(v_1, \ldots, v_k) = (e_1, \ldots, e_n) Q^T_{[kn]} \tag{4.5}$$

i.e. the coordinate of v_j w. r. t. $\{e_i\}_{1 \le i \le n}$ includes the first n elements of the j^{th} row of the matrix Q, namely $v_{j<e>} = (q_{j,1}, \ldots, q_{j,n})$.

All the discussions about the inner product can now be summarized as follows:

$$\begin{aligned} \phi(v_i, v_j) &= \Sigma_{l=1}^{n} \lambda_l q_{i,l} q_{j,l} \\ &= \Sigma_{l=1}^{k} \lambda_l q_{i,l} q_{j,l} \\ &= \psi(a_i, a_j) \\ &= (d_{i,0}^2 + d_{j,0}^2 - d_{i,j}^2)/2 \end{aligned}$$

Thus, the vector representation of the pseudo-metric space $(\mathcal{D}, d)$ is the mapping

$$\beta : \mathcal{D} \to R^{(n^+, n^-)}$$

satisfying

$$\beta(p_0) = \Pi(\alpha(p_0)) = \Pi(a_0) = (0, \ldots, 0)_n$$

and

$$\beta(p_j) = \Pi(\alpha(p_j)) = \Pi(a_j) = v_j \; 1 \leq j \leq k$$

Definition 4.1. A vector representation ρ of the pseudo-metric space $(\mathcal{D}, d)$ is an *isometric representation* if for any $p_i, p_j \in \mathcal{D}$, $||\rho(p_i) - \rho(p_j)||^2 = d^2_{i,j}$. $\square$

From the above discussions, we have

Theorem 4.1. *The mapping β is an isometric representation of the pseudo-metric space $(\mathcal{D}, d)$ in the pseudo-Euclidean space $R^{(n^+ + n^-)}$. That is, for any pair of indices i, j, $0 \leq i, j \leq k$,*

$$||v_i - v_j||^2 = \phi(v_i - v_j, v_i - v_j) = d^2_{i,j}$$

Theorem 4.1 describes the relation between the distance d in the pseudo-metric space and the squared distance in the corresponding pseudo-Euclidean space, stating the fact that the mapping β preserves d.

4.3.4 ϕ-Orthonormal Basis $\{\tilde{e}_i\}$

Define $sign(\lambda_i)$ to be

$$sign(\lambda_i) = \begin{cases} 1 & \text{if } \lambda_i > 0 \\ 0 & \text{if } \lambda_i = 0 \\ -1 & \text{if } \lambda_i < 0 \end{cases}$$

Let $J = diag(sign(\lambda_i))_{1 \leq i \leq k}$ and $\tilde{D} = diag(d_i)_{1 \leq i \leq k}$, where

$$d_i = \begin{cases} |\lambda_i| & \text{if } \lambda_i \neq 0 \\ 1 & \text{otherwise} \end{cases}$$

Let $\tilde{Q} = Q \times \tilde{D}^{-1/2}$. Then,

$$\begin{aligned}\tilde{Q}^T M(\psi_{<a>})\tilde{Q} &= \tilde{D}^{-1/2}Q^T M(\psi_{<a>})Q\tilde{D}^{-1/2}\\ &= \tilde{D}^{-1/2}diag(\lambda_i)\tilde{D}^{-1/2}\\ &= J\end{aligned}$$

This means that the first n columns of the matrix $\tilde{Q}$ are ψ-orthonormal vectors.

Let

$$\tilde{e}_i = \frac{e_i}{\sqrt{d_i}}\ 1 \leq i \leq k$$

or equivalently

$$(\tilde{e}_1, \ldots, \tilde{e}_k) = (e_1, \ldots, e_k)\tilde{D}^{-1/2} \tag{4.6}$$

Then, the set of vectors $\{\tilde{e}_i\}_{1\leq i\leq n}$ is a *ϕ-orthonormal basis* of R^n (cf. Fig. 4.3). From equations (4.2) and (4.6), we have

$$(a_1, \ldots, a_k) = (\tilde{e}_1, \ldots, \tilde{e}_k)\tilde{D}^{1/2}Q^T \tag{4.7}$$

From equations (4.5) and (4.6), we have

$$(v_1, \ldots, v_k) = (\tilde{e}_1, \ldots, \tilde{e}_n)\tilde{D}^{1/2}_{[n]}Q^T_{[kn]} \tag{4.8}$$

where $\tilde{D}_{[n]}$ is the n^{th} leading principal submatrix of the matrix $\tilde{D}$, i.e. $\tilde{D}_{[n]} = diag(|\lambda_i|)_{1\leq i\leq n}$. The coordinate of v_j w. r. t. the basis $\{\tilde{e}_i\}_{1\leq i\leq n}$ includes the first n elements of the j^{th} row of the matrix $\tilde{T} = Q \times \tilde{D}^{1/2}$, i.e. $v_{j<\tilde{e}>} = (\sqrt{|\lambda_1|}q_{j,1}, \ldots, \sqrt{|\lambda_n|}q_{j,n})$. Let x, y be two vectors in R^n. Then

$$\psi(x,y) = \Sigma_{i=1}^n sign(\lambda_i)x^i_{<\tilde{e}>}y^i_{<\tilde{e}>}$$

and

$$||x-y||^2 = \Sigma_{i=1}^n sign(\lambda_i)(x^i_{<\tilde{e}>} - y^i_{<\tilde{e}>})^2$$

4.3.5 Pseudo-Euclidean Space R^m, $m < n$

In practice, the number of objects in $\mathcal{D}$, i.e. $k+1$, may be rather large. The dimension of R^n could still be large. From equation (4.4), we know that the eigenvalues represent the extension of variances of the objects in $\mathcal{D}$ in the corresponding dimension. To avoid dealing with a space of very high dimensionality, we ignore the dimensions along which the eigenvalues are small. Specifically, suppose the eigenvalues are sorted in descending order by their absolute values. Let $\{\lambda_i\}_{1\le i\le m}$ be the first m eigenvalues, $m < n$, $m = m^- + m^+$, $m^- \le n^-$ and $m^+ \le n^+$. The mapping

$$\gamma : \mathcal{D} \to R^{(m^+ + m^-)}$$

is the projection of the exact vector representation β onto the subspace spanned by the first m vectors in the ϕ-orthonormal basis. The first m elements of the i^{th} row of the corresponding $\tilde{T}$ would give the coordinates of $\gamma(p_i)$ for the reduced vector representation, i.e.

$$\gamma(p_i) = (\sqrt{|\lambda_1|}q_{i,1}, \ldots, \sqrt{|\lambda_m|}q_{i,m})$$

Let x,y be two vectors in R^n. Then

$$\varphi(x, y) = \Sigma_{i=1}^{m} sign(\lambda_i) x^i_{<\tilde{e}>} y^i_{<\tilde{e}>}$$

is the approximate representation of $\psi(x, y)$ for the corresponding vectors in R^m, and

$$\varphi(x - y, x - y) = \Sigma_{i=1}^{m} sign(\lambda_i)(x^i_{<\tilde{e}>} - y^i_{<\tilde{e}>})^2 \qquad (4.9)$$

is the approximate representation of $||x - y||^2$. Note that

$$||x - y||^2 - \varphi(x - y, x - y) = \Sigma_{i=m+1}^{n} \lambda_i (x^i_{<e>} - y^i_{<e>})^2$$

Let w_i be v_i projected onto R^m (cf. Fig. 4.5), i.e. $w_i = (\sqrt{|\lambda_1|}q_{i,1}, \ldots, \sqrt{|\lambda_m|}q_{i,m})$. We have

$$||w_i - w_j||^2 - \varphi(w_i - w_j, w_i - w_j) = \Sigma_{l=m+1}^{n} \lambda_l (q_{i,l} - q_{j,l})^2$$

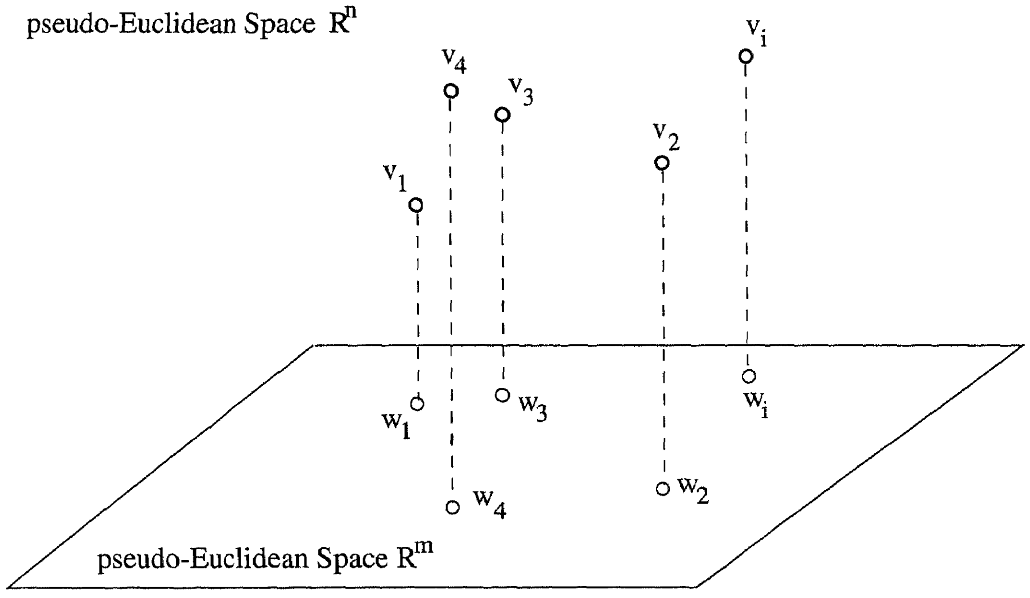

Figure 4.5 The projection from R^n to R^m.

Proposition 4.1. *Let* $\triangle_{i,j} = ||w_i - w_j||^2 - \varphi(w_i - w_j, w_i - w_j)$. *Then* $|\triangle_{i,j}| \leq 4|\lambda_{m+1}|$.

Proof. The result follows by observing that

$$\begin{aligned}
|\triangle_{i,j}| &\leq \Sigma_{l=m+1}^{n}|\lambda_l|(q_{i,l} - q_{j,l})^2 \\
&\leq |\lambda_{m+1}|\Sigma_{l=m+1}^{n}(q_{i,l} - q_{j,l})^2 \\
&\leq |\lambda_{m+1}|\Sigma_{l=m+1}^{n}2(|q_{i,l}|^2 + |q_{j,l}|^2) \\
&\leq 2|\lambda_{m+1}|\Sigma_{l=1}^{n}(|q_{i,l}|^2 + |q_{j,l}|^2) \\
&= 4|\lambda_{m+1}|
\end{aligned}$$

4.4 Projection of a Target Object

By now we have established an m dimensional pseudo-Euclidean space, and mapped the data objects to vectors in that space. To deal with the nearest neighbor search or ϵ-range search problem, when the target comes in, we map the target to the same pseudo-Euclidean space, and employ the distance between the vectors to approximate the distances between the target object and the data objects (see Fig. 4.6). In this section, we introduce the process for projecting the target to the pseudo-Euclidean space, no matter whether the target is embeddable to that space or not.

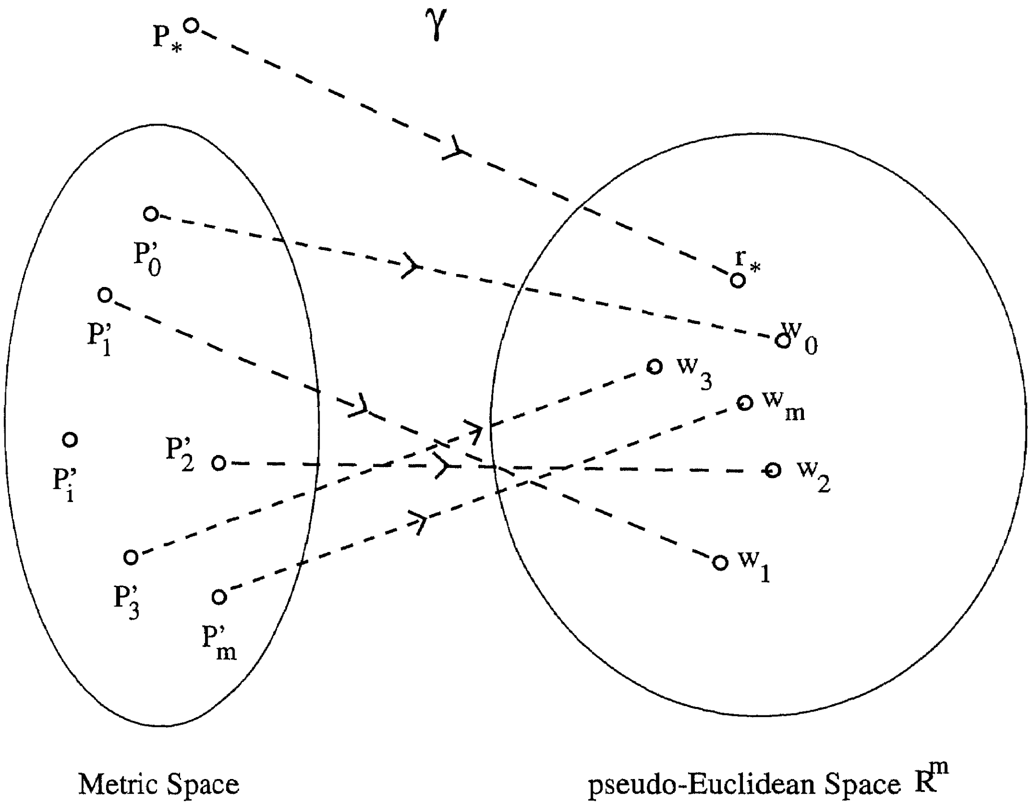

Figure 4.6 The projection of a target object.

4.4.1 Projection of an Embeddable Target

Now, suppose we are given a target p_*, and want to find the object in $\mathcal{D}$ that is closest to p_*. We project p_* onto R^m based on the distances between p_* and the reference objects ref_j, $0 \le j \le m$. To begin with, add p_* into $\mathcal{D}$. Let the distances between p_* and p_j be given as:

$$d_{*,j} = \pi(p_*, p_j) \; 0 \le j \le k$$

Assume that the new object p_* is isometrically represented by a vector $u_* \in R^k$, i.e.

$$||u_* - v_j||^2 = d^2_{*,j} \; 0 \le j \le k$$

or equivalently

$$\phi(u_*, v_j) = (d^2_{*,0} + d^2_{j,0} - d^2_{*,j})/2 \; 1 \le j \le k \tag{4.10}$$

$\phi(u_*, u_*) = d_{*,0}$. Let $Q_{[km]}$ be the matrix consisting of the first m columns of the matrix Q, namely $Q_{[km]} = (q_{i,j})_{1\le i\le k, 1\le j\le m}$. Let $\tilde{D}_{[m]}$ be the m^{th} leading principal submatrix of the matrix $\tilde{D}$, i.e., $\tilde{D}_{[m]} = diag(|\lambda_i|)_{1\le i\le m}$. Then from equations (4.5) and (4.8),

$$(w_1, \dots, w_k) = (e_1, \dots, e_m)Q^T_{[km]} = (\tilde{e}_1, \dots, \tilde{e}_m)\tilde{D}^{1/2}_{[m]}Q^T_{[km]} \tag{4.11}$$

Let r_* be the ϕ-orthogonal projection of u_* onto R^m. r_* can be represented as a linear combination of the set of vectors $\{w_i\}_{1\le i\le m}$, $r_* = \Sigma_{i=1}^m r_*^i w_i$. Taking the inner product of r_* and w_j, $1 \le j \le m$, we obtain $\phi(r_*, w_j) = \Sigma_{i=1}^m r_*^i \phi(w_i, w_j)$. Owing to the ϕ-orthogonality, $\phi(r_*, w_j) = \phi(u_*, w_j), 1 \le j \le m$. Hence

$$\Sigma_{i=1}^m r_*^i \phi(w_i, w_j) = \phi(u_*, w_j) \; 1 \le j \le m \tag{4.12}$$

Let the Gram matrix $G(w_1, w_2, \dots, w_m) = (\phi(w_i, w_j))_{1\le i,j\le m}$, $b = (\phi(u_*, w_j))_{1\le j\le m}$. Then equation (4.12) can be re-written as $G(w_1, w_2, \dots, w_m)r_* = b$. Since the determinant of $G(w_1, w_2, \dots, w_m)$ is not zero, i.e. the matrix is non-singular, $r_* = [G(w_1, w_2, \dots, w_m)]^{-1}b$.

Note that this equation gives the coordinate of r_* w. r. t. the basis $\{w_i\}_{1\le i\le m}$. To obtain the coordinate w. r. t. $\{e_i\}$ or $\{\tilde{e}_i\}$, we need the matrices of coordinate transformation. Let $Q_{[mm]}$ be the m^{th} leading principal submatrix of the orthogonal matrix Q. Then from equation (4.11),

$$(w_1, \dots, w_m) = (e_1, \dots, e_m)Q^T_{[mm]} = (\tilde{e}_1, \dots, \tilde{e}_m)\tilde{D}^{1/2}_{[m]}Q^T_{[mm]} \tag{4.13}$$

So,

$$r_{*<e>} = Q^T_{[mm]}[G(w_1, w_2, \dots, w_m)]^{-1}b$$

and

$$r_{*<\tilde{e}>} = \tilde{D}^{1/2}_{[m]}Q^T_{[mm]}[G(w_1, w_2, \dots, w_m)]^{-1}b \tag{4.14}$$

where $b = (\phi(u_*, w_j))_{1\le j\le m}$.

These equations can be further simplified. From equation (4.13), we know that the coordinate of w_i w. r. t. $\{e_j\}_{1\le j\le m}$ is the i^{th} row of $Q_{[mm]}$, i.e., $w_{i<e>} = (q_{i,1}, \ldots, q_{i,m})$. According to the formula for the inner product, $\phi(w_i, w_j)$ $= \Sigma_{l=1}^{m} \lambda_l q_{i,l} q_{j,l}$, $1 \le i, j \le m$. Therefore, $G(w_1, w_2, \ldots, w_m) = (\phi(w_i, w_j))_{1\le i,j\le m} = Q_{[mm]} D_{[m]} Q^T_{[mm]}$. Substituting this into equation (4.14),

$$\begin{aligned} r_{*<\tilde{e}>} &= \tilde{D}^{1/2}_{[m]} Q^T_{[mm]} (Q^T_{[mm]})^{-1} D^{-1}_{[m]} Q^{-1}_{[mm]} b \\ &= \tilde{D}^{1/2}_{[m]} D^{-1}_{[m]} Q^{-1}_{[mm]} b \\ &= J_{[m]} \tilde{D}^{-1/2}_{[m]} Q^{-1}_{[mm]} b \end{aligned}$$

Thus,

$$r_{*<\tilde{e}>} = J_{[m]} \tilde{D}^{-1/2}_{[m]} Q^{-1}_{[mm]} b \tag{4.15}$$

Note that, after computing m eigenvalues and eigenvectors, one obtains the matrices $Q_{[mm]}$ and $\tilde{D}_{[m]}$. However, in general we do not know how large $\phi(u_*, w_j)$ is. What we know is $\phi(u_*, v_j) = (d^2_{*,0} + d^2_{j,0} - d^2_{*,j})/2$, $1 \le j \le k$. Thus we have to use $\phi(u_*, v_j)$ as an approximate value of $\phi(u_*, w_j)$ to compute r_*. In other words, the formulae we use in practice are:

$$\overline{r}_{*<e>} = Q^T_{[mm]} [G(w_1, w_2, \ldots, w_m)]^{-1} \overline{b}$$

and

$$\overline{r}_{*<\tilde{e}>} = \tilde{D}^{1/2}_{[m]} Q^T_{[mm]} [G(w_1, w_2, \ldots, w_m)]^{-1} \overline{b} \tag{4.16}$$

where $\overline{b} = (\phi(u_*, v_j))_{1\le j\le m}$. Following the way to simplify $r_{*<\tilde{e}>}$, equation (4.16) can be simplified as

$$\overline{r}_{*<\tilde{e}>} = J_{[m]} \tilde{D}^{-1/2}_{[m]} Q^{-1}_{[mm]} \overline{b} \tag{4.17}$$

One may ask how well this works? The following three propositions estimate the error between $r_{*<\tilde{e}>}$ and $\overline{r}_{*<\tilde{e}>}$ when $\phi(u_*, v_i)$ is used in place of $\phi(u_*, w_i)$. All these propositions are based on the assumption that there is an object p_h in $\mathcal{D}$ that is very close to p_*. That is, if $\triangle_j = d_{*,j} - d_{h,j}$, $0 \le j \le k$, then there exists a small positive real number ϵ such that

$$|\triangle_j| \le \epsilon \; 0 \le j \le k \tag{4.18}$$

Proposition 4.2. $||u_* - a_h||_2 \le \overline{\epsilon}$, *where*

$$\overline{\epsilon} = \frac{\epsilon}{|\lambda_{min}|}[\Sigma_{j=1}^k (d_{h,0} + d_{h,j})^2]^{1/2}$$

λ_{min} *is the non-zero eigenvalue with the smallest absolute value in* $\{\lambda_i\}_{1 \le i \le n}$, *and* u_*, a_h *are the vector representations of* p_* *and* p_h, *respectively.*

Proof. Since p_* can be embedded isometrically into R^k,

$$||u_* - a_j||^2 = d_{*,j}^2 \; 0 \le j \le k$$

or equivalently

$$\psi(u_*, a_j) = (d_{*,0}^2 + d_{j,0}^2 - d_{*,j}^2)/2 \; 1 \le j \le k \tag{4.19}$$

Let $b_* = (b_*^j)_{1 \le j \le k}$ where $b_*^j = (d_{*,0}^2 + d_{j,0}^2 - d_{*,j}^2)/2 \; 1 \le j \le k$. Equation (4.19) can be written as $M(\psi_{<a>})u_{*<a>} = b_*$. Thus $(Q^T M(\psi_{<a>})Q)(Q^T u_{*<a>}) = Q^T b_*$. From equations (4.1) and (4.3), $Du_{*<e>} = Q^T b_*$. Since $\lambda_j = 0$, $n+1 \le j \le k$, $u_{*<e>}^j$, $n+1 \le j \le k$, can take any values. Let $\overline{D} = diag(\overline{\lambda_j})_{1 \le j \le k}$ where

$$\overline{\lambda_j} = \begin{cases} \lambda_j & \text{if } j < n \\ \lambda_n & \text{if } n \le j \le k \end{cases}$$

We choose those u^j, $1 \le j \le k$, that satisfy $\overline{D}u_{*<e>} = Q^T b_*$. Thus $u_{*<e>} = \overline{D}^{-1} Q^T b_*$. Similarly, $a_{h<e>} = \overline{D}^{-1} Q^T b_h$. Thus

$$||u_* - a_h||_2 \le ||\overline{D}^{-1}||_2 ||Q^T||_2 ||b_* - b_h||_2$$

Evaluating these norms, we get $||\overline{D}^{-1}||_2 \le \frac{1}{|\lambda_{min}|}$, $||Q^T||_2 = 1$,

$$\begin{aligned} ||b_* - b_h||_2 &= [\Sigma_{j=1}^k (b_*^j - b_h^j)^2]^{1/2} \\ &= [\Sigma_{j=1}^k \tfrac{1}{4}(d_{*,0}^2 - d_{*,j}^2 - d_{h,0}^2 + d_{h,j}^2)^2]^{1/2} \\ &= [\Sigma_{j=1}^k (d_{h,0}\triangle_0 - d_{h,j}\triangle_j + \tfrac{1}{2}\triangle_0^2 - \tfrac{1}{2}\triangle_j^2)^2]^{1/2} \end{aligned}$$

Omitting the infinitesimal of higher order and substituting inequality (4.18), we get

$$||b_* - b_h||_2 = \epsilon[\Sigma_{j=1}^k (d_{h,0} + d_{h,j})^2]^{1/2}$$

Hence

$$||u_* - a_h||_2 \leq \frac{\epsilon}{|\lambda_{min}|}[\Sigma_{j=1}^k (d_{h,0} + d_{h,j})^2]^{1/2}$$

□

Proposition 4.3. *For each i, $1 \leq i \leq k$,*

$$|\phi(u_*, v_i) - \phi(u_*, w_i)| \leq |\lambda_{m+1}|(1 + \bar{\epsilon})$$

Proof. Let $u_{*<e>} = (u^j)_{1\leq j\leq n}$. Since $v_{i<e>} = (q_{i,1}, \ldots, q_{i,n})$ (cf. equation (4.5)) and w_i is the projection of v_i to R^m, we obtain

$$\begin{aligned} |\phi(u_*, v_i) - \phi(u_*, w_i)| &= |\Sigma_{j=m+1}^n \lambda_j u^j q_{i,j}| \\ &= |\Sigma_{j=m+1}^n \lambda_j (q_{h,j} + \triangle v_j) q_{i,j}| \\ &\leq |\Sigma_{j=m+1}^n \lambda_j q_{h,j} q_{i,j}| + |\Sigma_{j=m+1}^n \lambda_j \triangle v_j q_{i,j}| \end{aligned}$$

where $\triangle v_j = u^j - q_{h,j}$, $1 \leq j \leq n$.

The first term on the right-hand side is easy to estimate. Since Q is orthogonal, $\Sigma_{j=1}^k q_{i,j}^2 = 1$, $1 \leq i \leq k$. Thus

$$\begin{aligned} |\Sigma_{j=m+1}^n \lambda_j q_{h,j} q_{i,j}| &\leq \Sigma_{j=m+1}^n |\lambda_j||q_{h,j}||q_{i,j}| \\ &\leq |\lambda_{m+1}|[\Sigma_{j=m+1}^n q_{h,j}^2]^{1/2}[\Sigma_{j=m+1}^n q_{i,j}^2]^{1/2} \\ &\leq |\lambda_{m+1}| \end{aligned}$$

Similarly,

$$\begin{aligned} |\Sigma_{j=m+1}^n \lambda_j \triangle v_j q_{i,j}| &\leq \Sigma_{j=m+1}^n |\lambda_j||\triangle v_j||q_{i,j}| \\ &\leq |\lambda_{m+1}|[\Sigma_{j=m+1}^n (\triangle v_j)^2]^{1/2}[\Sigma_{j=m+1}^n q_{i,j}^2]^{1/2} \\ &\leq |\lambda_{m+1}|[\Sigma_{j=m+1}^n (\triangle v_j)^2]^{1/2} \end{aligned}$$

By Proposition 4.2,

$$\begin{aligned}
[\Sigma_{j=m+1}^{n}(\triangle v_j)^2]^{1/2} &\leq [\Sigma_{j=1}^{k}(\triangle v_j)^2]^{1/2} \\
&= \|u_* - a_h\|_2 \\
&\leq \bar{\epsilon}
\end{aligned}$$

Hence $|\phi(u_*, v_i) - \phi(u_*, w_i)| \leq |\lambda_{m+1}|(1+\bar{\epsilon})$. □

Proposition 4.4.

$$\begin{aligned}
\|\triangle r_*\|_2 &= \|\bar{r}_{*<\hat{e}>} - r_{*<\hat{e}>}\|_2 \\
&\leq \sqrt{\tfrac{m}{|\lambda_m|}}|\lambda_{m+1}|(1+\bar{\epsilon})\|Q_{[mm]}^{-1}\|_2 \\
&\leq \sqrt{m|\lambda_{m+1}|}(1+\bar{\epsilon})\|Q_{[mm]}^{-1}\|_2
\end{aligned}$$

Proof. Subtracting equation (4.15) from (4.17),

$$\triangle r_* = J_{[m]}\tilde{D}_{[m]}^{-1/2}Q_{[mm]}^{-1}(\bar{b} - b)$$

Hence

$$\|\triangle r_*\|_2 \leq \|J_{[m]}\|_2\|\tilde{D}_{[m]}^{-1/2}\|_2\|Q_{[mm]}^{-1}\|_2\|\bar{b} - b\|_2 \tag{4.20}$$

Evaluating these norms, we get $\|J_{[m]}\|_2 = 1$, $\|\tilde{D}_{[m]}^{-1/2}\|_2 = \frac{1}{\sqrt{|\lambda_m|}}$. By Proposition 4.3,

$$\begin{aligned}
\|\bar{b} - b\|_2 &= [\Sigma_{i=1}^{m}(\phi(u_*, v_i) - \phi(u_*, w_i))^2]^{1/2} \\
&\leq [\Sigma_{i=1}^{m}(|\lambda_{m+1}|(1+\bar{\epsilon}))^2]^{1/2} \\
&= \sqrt{m}|\lambda_{m+1}|(1+\bar{\epsilon})
\end{aligned}$$

Substituting these into inequality (4.20), we get

$$\begin{aligned}
\|\triangle r_*\|_2 &\leq \sqrt{\tfrac{m}{|\lambda_m|}}|\lambda_{m+1}|(1+\bar{\epsilon})\|Q_{[mm]}^{-1}\|_2 \\
&\leq \sqrt{m|\lambda_{m+1}|}(1+\bar{\epsilon})\|Q_{[mm]}^{-1}\|_2
\end{aligned}$$

□

From these propositions, it can be seen that the error is negligible whenever m is not large and λ_{m+1} is small enough. It should be pointed out that the coordinates of $\{w_i\}_{1\le i\le k}$ are derived from $Q_{[km]}$, which are projections of the eigenvectors, whereas the coordinate of the target is calculated using equation (4.16) or (4.17). Thus, the projection of the target may be different from any of the objects in $\mathcal{D}$, even if the target is entirely the same as one of the objects of $\mathcal{D}$. Under this circumstance, one should calculate the coordinates of the objects of $\mathcal{D}$ using the formula (4.16) during the off-line phase.

Proposition 4.5. *If $\{\overline{w}_i\}_{1\le i\le k}$ are the coordinates calculated based on the formula (4.16), then $||\Delta w_i||_2 = ||\overline{w}_i - w_i||_2 \le \sqrt{m|\lambda_{m+1}|}||Q^{-1}_{[mm]}||_2$.*

Proof. By replacing u_* with v_i, $1 \le i \le k$, in equations (4.15) and (4.17), we get $w_{i<\hat{e}>} = J_{[m]}\tilde{D}^{-1/2}_{[m]}Q^{-1}_{[mm]}b_i$, $\overline{w}_{i<\hat{e}>} = J_{[m]}\tilde{D}^{-1/2}_{[m]}Q^{-1}_{[mm]}\overline{b_i}$, where $b_i = (\phi(v_i, w_j))_{1\le j\le m}$ and $\overline{b_i} = (\phi(v_i, v_j))_{1\le j\le m}$. Observe that

$$\begin{aligned}
||\overline{b_i} - b_i||_2 &= [\Sigma_{j=1}^m(\phi(v_i,v_j) - \phi(v_i,w_j))^2]^{1/2} \\
&= [\Sigma_{j=1}^m(\Sigma_{l=m+1}^n \lambda_l q_{i,l} q_{j,l})^2]^{1/2} \\
&\le [\Sigma_{j=1}^m(|\lambda_{m+1}|\Sigma_{l=m+1}^n |q_{i,l} q_{j,l}|)^2]^{1/2} \\
&\le \sqrt{m}|\lambda_{m+1}|
\end{aligned}$$

Thus $||\overline{w}_i - w_i||_2 = ||J_{[m]}||_2||\tilde{D}^{-1/2}_{[m]}||_2||Q^{-1}_{[mm]}||_2||\overline{b_i} - b_i||_2 \le \sqrt{m|\lambda_{m+1}|}||Q^{-1}_{[mm]}||_2$.

□

Note that this upper bound is just the first term of that for Δr_* in Proposition 4.4, which is reasonable, since $\epsilon = \overline{\epsilon} = 0$ in this case.

4.4.2 Projection of an Unembeddable Target

In many cases, the target will not be isometrically embedded into R^k. However, we still can derive a projection formula which is basically the same as equation (4.16).

The problem with an unembeddable target is that equation (4.10) in Section 3.4.1 does not hold. As a consequence, the projection formula of equation (4.14) can not be established. To address this problem, we construct a $(k+1)$-dimensional space with the target p_* as the $(k+1)^{th}$ dimension. Then we project all the $(k+2)$ objects (i.e. the $k+1$ data objects in $\mathcal{D}$, plus the target) onto R^m. The projection of the $(k+2)^{th}$ object establishes the formula for the target. We then introduce a new mapping η to connect R^{k+1} with R^k, thus resulting in a formula very similar to the previous one for an embeddable target.

To begin with, let us first establish a $(k+1)$-dimensional space. Let $\mathcal{D}_* = \mathcal{D} \cup \{p_*\}$ and $\alpha_* : \mathcal{D}_* \to R^{k+1}$, such that (i) $\alpha_*(p_0) = a_{*0} = (0, \ldots, 0, 0)$, (ii) $\alpha_*(p_j) = a_{*j} = (0, \ldots, 1_{(j)}, \ldots, 0, 0)$, $1 \leq j \leq k$, (iii) $\alpha_*(p_*) = a_{*(k+1)} = (0, \ldots, 0, 1)$. Next we define a symmetric bilinear form ψ_* over $R^{k+1} \times R^{k+1}$, such that (i) $\psi_*(a_{*i}, a_{*j}) = (d_{i,0}^2 + d_{j,0}^2 - d_{i,j}^2)/2$, $1 \leq i, j \leq k$, and (ii) $\psi_*(a_{*(k+1)}, a_{*j}) = (d_{*,0}^2 + d_{j,0}^2 - d_{*,j}^2)/2$, $1 \leq j \leq k$. Then define the matrix of the bilinear form w. r. t. $\{a_{*j}\}_{1 \leq j \leq k+1}$: $M_*(\psi_{*<a*>}) = (\psi_*(a_{*i}, a_{*j}))_{1 \leq i,j \leq k+1}$. Comparing the definition of ψ_* with that of ψ in Section 3.3.1, one can see that for each pair of subscripts i, j, $1 \leq i, j \leq k$, $\psi_*(a_{*i}, a_{*j}) = \psi(a_i, a_j)$. Moreover, the matrix $M(\psi_{<a>})$ is simply the k^{th} leading principal submatrix of $M_*(\psi_{*<a*>})$.

Analogously to how we dealt with ψ in Sections 3.3.2 through 3.3.5, we can compute the eigenvectors of the matrix $M_*(\psi_{*<a*>})$ to obtain a ψ_*-orthonormal basis, say $\{\tilde{e}_{*i}\}_{1 \leq i \leq k+1}$, of R^{k+1}. To derive a formula similar to equation (4.14) for an embeddable target, we need another ψ_*-orthonormal basis in R^{k+1}. We define a mapping $\eta : R^k \to R^{k+1}$ such that $\eta(x^1, \ldots, x^k) = (x^1, \ldots, x^k, 0)$, where $(x^1, \ldots, x^k)$ is the coordinate of a vector in R^k with respect to some basis of it.

Proposition 4.6. *Let $x_1, \ldots, x_l$ be vectors in R^k and let $c_1, \ldots, c_l$ be real numbers. If $\Sigma_{i=1}^l c_i x_i = 0$, then $\Sigma_{i=1}^l c_i \eta(x_i) = 0$.*

Proof. Let $x_i = (x_i^j)_{1\le j\le k}, 1 \le i \le l$. We have $\Sigma_{i=1}^l c_i x_i^j = 0, 1 \le j \le k$. Let $y_i = (y_i^j)_{1\le j\le k+1}, 1 \le i \le l$ and $\eta(x_i) = y_i, 1 \le i \le l$. By the definition of η, $y_i^j = x_i^j$, $1 \le j \le k$, $1 \le i \le l$ and $y_i^{k+1} = 0$, $1 \le i \le l$. Thus $\Sigma_{i=1}^l c_i y_i^j = 0, 1 \le j \le k+1$. Namely $\Sigma_{i=1}^l c_i y_i = 0$. □

Proposition 4.7. *Let x and y be two vectors in R^k. Then $\psi_*(\eta(x), \eta(y)) = \psi(x, y)$.*

Proof. By the definition of η,

$$\eta(x) = \begin{pmatrix} x \\ 0 \end{pmatrix}$$

$$\eta(y) = \begin{pmatrix} y \\ 0 \end{pmatrix}$$

$$M_*(\psi_{*<a*>}) = \begin{pmatrix} M(\psi_{<a>}) & M_1 \\ M_1^T & \psi_*(a_{*(k+1)}, a_{*(k+1)}) \end{pmatrix}$$

where $M_1 = (\psi_*(a_{*(k+1)}, a_{*j}))_{1\le j\le k}$. Thus

$$\begin{aligned} \psi_*(\eta(x), \eta(y)) &= \begin{pmatrix} x^T & 0 \end{pmatrix} \begin{pmatrix} M(\psi_{<a>}) & M_1 \\ M_1^T & \psi_*(a_{*(k+1)}, a_{*(k+1)}) \end{pmatrix} \begin{pmatrix} y \\ 0 \end{pmatrix} \\ &= x^T M(\psi_{<a>}) y = \psi(x, y) \end{aligned}$$

□

Consider the subspace R^n of R^k defined in Section 3.3.3. The mapping η associates R^n with a subspace, say R_*^n, in R^{k+1}. The space R^{k+1} can be represented as the direct sum of R_*^n and its ψ_*-orthogonal complement [50]. It follows that the union of a ψ_*-orthogonal basis of R_*^n and a ψ_*-orthogonal basis of its ψ_*-orthogonal complement will become a ψ_*-orthogonal basis of R^{k+1}. The subspace R^n is spanned by $\{\tilde{e}_i\}_{1\le i\le n}$. According to Proposition 4.6, the set of vectors $\{\eta(\tilde{e}_i)\}_{1\le i\le n}$ spans R_*^n. According to Proposition 4.7, $\{\eta(\tilde{e}_i)\}_{1\le i\le n}$ is ψ_*-orthonormal, since $\{\tilde{e}_i\}_{1\le i\le n}$ is ψ-orthonormal. Therefore, there is a ψ_*-orthonormal basis of R^{k+1} which includes $\{\eta(\tilde{e}_i)\}_{1\le i\le n}$ as a subset. The coordinate of a vector in R^{k+1} with respect to the basis mentioned above may be obtained from its coordinate w. r. t. $\{\tilde{e}_{*i}\}_{1\leq i\leq k+1}$, through multiplying the latter one by a certain non-singular matrix (i.e. through coordinate transformation).

Note that $a_{*j} = \eta(a_j)$, $1 \leq j \leq k$. According to Proposition 4.7 and equation (4.7),

$$(a_{*1}, \ldots, a_{*k}) = (\eta(\tilde{e}_1), \ldots, \eta(\tilde{e}_k))\tilde{D}^{1/2}Q^T$$

Therefore the coordinate of the projection of a_{*j} w. r. t. $\{\eta(\tilde{e}_i)\}_{1\leq i\leq k}$ is simply the coordinate of a_j w. r. t. $\{\tilde{e}_i\}_{1\leq i\leq k}$. In parallel with the introduction of the subspace R^n_*, we can introduce a subspace R^m_* of R^{k+1} from R^m in R^k, and then consider the projection of the target p_* onto R^m_*. Let w_j be the ψ-orthogonal projection of a_j onto R^m. Then $w_{*j} = \eta(w_j)$ is the ψ_*-orthogonal projection of a_{*j} onto R^m_*. Since the set of projections $\{w_j\}_{1\leq j\leq m}$ spans R^m, according to Proposition 4.6, the set of projections $\{w_{*j}\}_{1\leq j\leq m}$ spans R^m_*. Furthermore, from equation (4.13),

$$(w_{*1}, \ldots, w_{*m}) = (\eta(\tilde{e}_1), \ldots, \eta(\tilde{e}_m))\tilde{D}^{1/2}_{[m]}Q^T_{[mm]}$$

According to Proposition 4.7, the Gram matrix of $\{w_{*j}\}$ is simply the Gram matrix of $\{w_j\}$. Summarizing these results, we know that the coordinate of projecting a_{*j} onto R^m_* w. r. t. $\{\eta(\tilde{e}_i)\}_{1\leq i\leq m}$ can be computed using the equation:

$$r_{*<\eta(\tilde{e})>} = \tilde{D}^{1/2}_{[m]}Q^T_{[mm]}[G(w_1, \ldots, w_m)]^{-1}b_*$$

where the matrices $\tilde{D}_{[m]}$, $Q_{[mm]}$ and $G(w_1, \ldots, w_m)$ are the same as those in equation (4.16), and $b_* = (\psi_*(a_{*(k+1)}, w_{*j}))_{1\leq j\leq m}$. Again we don't know how large $\psi_*(a_{*(k+1)}, w_{*j})$ is. What we can do is to replace it by $\psi_*(a_{*(k+1)}, a_{*j})$, thus obtaining

$$\bar{r}_{*<\eta(\tilde{e})>} = \tilde{D}^{1/2}_{[m]}Q^T_{[mm]}[G(w_1, \ldots, w_m)]^{-1}\bar{b}_* \tag{4.21}$$

where $\bar{b}_* = (\psi_*(a_{*(k+1)}, a_{*j}))_{1\leq j\leq m}$. By comparing equation (4.16) with equation (4.21), we conclude that no matter whether or not the target is embeddable to R^k, one can always use the same formula to calculate the projection of the target, though the resulting coordinates are with respect to the same basis represented in different dimensional spaces (more precisely, with respect to $\{\tilde{e}_i\}_{1\leq i\leq m}$ and $\{\eta(\tilde{e}_i)\}_{1\leq i\leq m}$, respectively).

4.5 Experiments and Applications

We have implemented the proposed data structure and tested it on three datasets, containing 90 artificial objects, proteins and dictionary words respectively. The pairwise distances between the artificial objects are randomly generated over a uniform distribution between 0 and 350, and those for the proteins and dictionary words are calculated using the edit distance [83]. Let p, q be two objects in $\mathcal{D}$ and let x, y be their vectors in R^m. We define the *vector distance* between p and q, denoted $vecdist(p, q)$, to be

$$vecdist(p,q) = \begin{cases} \sqrt{\varphi(x-y, x-y)} & \text{if } \varphi(x-y,x-y) \geq 0 \\ -\sqrt{-\varphi(x-y,x-y)} & \text{otherwise} \end{cases}$$

where $\varphi(x-y, x-y)$ is the squared distance between x and y (cf. equation (4.9)). The measures used for evaluating the performance of the data structure are the *average absolute error* (Err_a), *standard deviation* (Dev_a), and *average relative error* (Err_r). Let $\delta(p,q) = |vecdist(p,q) - d(p,q)|$ and $\Delta = \sum_{p,q\in\mathcal{D}} \delta(p,q)$. There are (90, 2) = 4005 combinations of pairs of objects. $Err_a = \Delta/4005$, Dev_a $= \sqrt{(\sum_{p,q\in\mathcal{D}}(\delta(p,q) - Err_a)^2)/4005}$, and $Err_r = (\sum_{p,q\in\mathcal{D}}\delta(p,q)/\sum_{p,q\in\mathcal{D}} d(p,q)) \times 100\%$. Figure 4.7 Figure 4.8 and Figure 4.9 graph Err_a, Dev_a and Err_r respectively as a function of the dimension m of different pseudo-Euclidean spaces. The performance is data dependent, and as expected, the larger the m, the smaller the errors (i.e., the better performance the data structure has).

Our future work is concerned with the question: *if one wants correct results, then how can one use the data structure as an approximate oracle?* We have studied

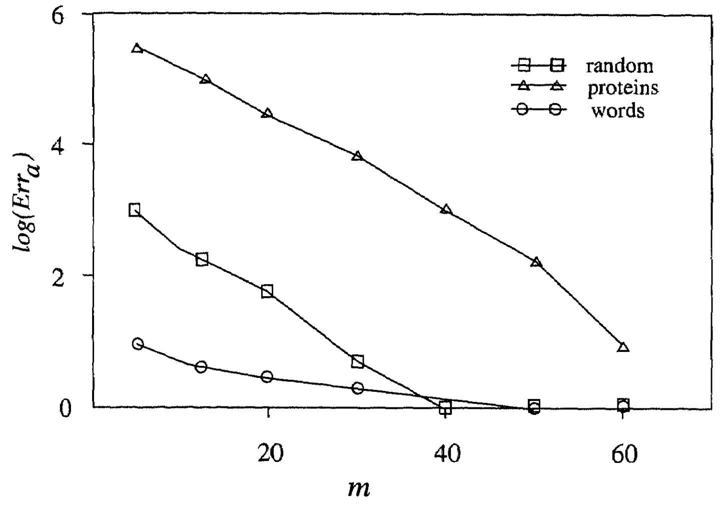

Figure 4.7 Average absolute errors as a function of the dimension m of the pseudo-Euclidean spaces.

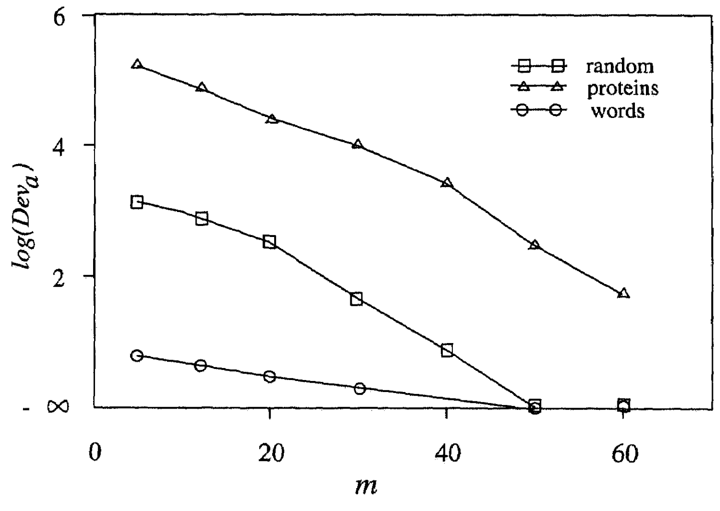

Figure 4.8 Standard deviations as a function of the dimension m of the pseudo-Euclidean spaces.

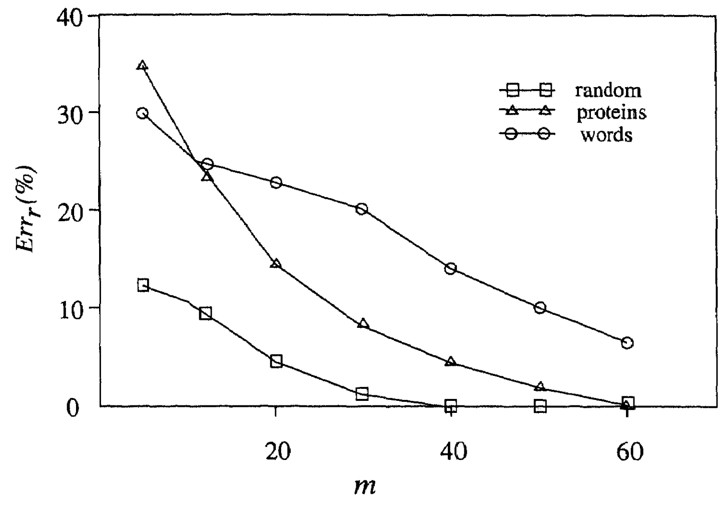

Figure 4.9 Average relative errors as a function of the dimension m of the pseudo-Euclidean spaces.

two applications. First, we partitioned the three datasets of 90 objects into clusters solely based on the oracle. (We omit the details here.) An object p is *mis-clustered* if, based on the oracle, p belongs to a cluster C, whereas based on the real distances between objects, p is not in C; or vice versa, i.e. when p really is in C, but the oracle indicates otherwise. Our experimental results showed that when the dimension m was 40, the number of mis-clustered objects was 9, 16 and 3 for artificial objects, proteins, and words, respectively (out of 90 in each case). This shows that the oracle offers an excellent first cut at clustering. In the second application, we solved the nearest neighbor search problem by using the oracle to approximate target-object distances in combination with the triangle inequality. It was estimated that the approach did fewer than half the comparisons needed in using the triangle inequality alone.

CHAPTER 5

AN EXPERIMENTAL EVALUATION OF DISTANCE-EMBEDDING DATA STRUCTURES

5.1 Introduction

In [24], Faloutsos and Lin proposed an index structure, called *FastMap*, for knowledge discovery, visualization and clustering in data intensive applications. The index structure takes a set of objects and a distance metric and maps the objects to points in a k-dimensional target space in such a way that the distances between objects are approximately preserved. One can then perform data mining and clustering operations on the k-dimensional points in the target space. Empirical studies indicated that *FastMap* works well for Euclidean distances [23, 24]. In a later paper, the inventors showed that a modification to *FastMap* could also help detect patterns using the time-warping distance (which is not even a metric, i.e., it doesn't satisfy the triangle inequality) [102].

In [101], we presented an index structure, called *MetricMap*, that works in a similar way as *FastMap*. In this chapter, we present the implementation of *MetricMap* and conduct experiments to compare the performance of *FastMap* and *MetricMap* based on both Euclidean distance and general distance metrics [92, 97].

A general distance metric is a function δ that takes pairs of objects into real numbers, satisfying the following properties: for any objects x, y, z, $\delta(x,x) = 0$ and $\delta(x,y) > 0, x \neq y$ (nonnegative definiteness); $\delta(x,y) = \delta(y,x)$ (symmetry); $\delta(x,y) \leq \delta(x,z) + \delta(z,y)$ (triangle inequality). Euclidean distance satisfies these properties. On the other hand, many general distance metrics of interest are not Euclidean, e.g. string edit distance as used in biology [69], document comparison [89] and the UNIX diff operator. Neither *FastMap* nor *MetricMap* (nor any other index structure that we know of) give guaranteed performance for general distance metrics. For this reason, an experimental analysis is worthwhile.

Section 5.2 surveys related work. Section 5.3 discusses the basic properties of *FastMap* and *MetricMap*. Sections 5.4 and 5.5 present experimental results. Sections 5.6 and 5.7 present discussions and conclusions of the chapter.

5.2 Related Work

Clustering is an important operation in data mining [2, 22, 87, 94]. Clustering algorithms can be broadly classified into two categories: *partitional* and *hierarchical* [42, 44]. A partitional algorithm partitions the objects into a collection of a user-specified number of clusters. A hierarchical algorithm is an iterative process, which either merges small clusters into larger ones, starting with atomic clusters containing single objects, or divides the set of objects into subunits, until some termination condition is met. These algorithms have been studied extensively by researchers in different communities, including statistics [28], pattern recognition [21, 42], machine learning [54], and databases. In particular, data intensive clustering algorithms include CLARANS [57], BIRCH [105], DBSCAN [22], STING [94], WaveCluster [77], CURE [36], CLIQUE [2], etc.

For example, the recently published CURE algorithm [36] utilizes multiple representatives for each cluster. The representatives are generated by selecting well scattered points from the cluster and then shrinking them toward the center of the cluster by a specified fraction. This enables the algorithm to adjust well to a geometry of clusters having non-spherical shapes and wide variances in size. CURE is designed to handle points (vectors) in k-d space only, not for general distance metric spaces, and therefore is considered as a *vector-based* clustering algorithm. It employs a combination of random sampling and partitioning to handle large datasets. The algorithm is a typical hierarchical one, which starts with each input point as a separate cluster, and at each successive step merges the closest pair of clusters.

By contrast, the popular K-means and K-medoid methods are partitional algorithms. The methods determine K cluster representatives and assign each object to the cluster with its representative closest to the object such that the sum of the distances squared between the objects and their representatives is minimized. The methods work for both Euclidean distance and general distance metrics, and therefore are considered as *distance-based* clustering algorithms. [44, 57, 105] presented extensions of the partitional methods for large and spatial databases, some of which are vector-based and some are distance-based.

In contrast to the above work, *FastMap* and *MetricMap* employ the approach of mapping objects to points in a k-dimensional (k-d) target space R^k and then cluster the points in R^k. The main benefit provided by this approach is that it saves time in distance computation. Calculating the actual distances among the objects is much more expensive than measuring the dissimilarities among the points in R^k.[1] This is particularly true for new, emerging applications in multimedia and scientific computing. As an example, comparing two RNA secondary structures may require a dynamic programming algorithm [75] or a genetic algorithm [72] that runs in seconds or minutes on current workstation. The presented mapping approach is useful not only for data mining and cluster analysis, but also for visualization and retrieval in large datasets [23, 24].

5.3 FastMap and MetricMap: A Brief Comparison

Consider a set of objects $\mathcal{D} = \{O_0, O_1, \ldots, O_{N-1}\}$ and a distance function d where for any two objects O_i, $O_j \in \mathcal{D}$, $d(O_i, O_j)$ (or $d_{i,j}$ for short) represents the distance between O_i and O_j. The function d can be Euclidean or a general distance metric. Both *FastMap* and *MetricMap* take the set of objects, some inter-object distances

[1]We use "dissimilarity", rather than "distance", in the discussion since there may be a negative dissimilarity value between two points in the target space.

and embed the objects in a k-d space R^k (k is user-defined), such that the distances among the objects are approximately preserved. The k-d point P_i corresponding to the object O_i is called the *image* of O_i. The k-d space containing the *images* is called *target space*.

The differences between the two index structures lie in the algorithm they use for embedding and the target space they choose. *FastMap* embeds the objects in a Euclidean space, whereas *MetricMap* embeds them in a pseudo-Euclidean space [33, 50]. Since it is less familiar, we review some properties of pseudo-Euclidean space and explain how the embedding is performed. Related proofs can be found in [24, 101].

5.3.1 The FastMap Algorithm

The basic idea of this algorithm is to project objects on a line (O_a, O_b) in an n-dimensional (n-d) space R^n for some unknown n, $n \geq k$. The line is formed by two *pivot objects* O_a, O_b, chosen as follows. First arbitrarily choose one object and let it be the second pivot object O_b. Let O_a be the object that is farthest apart from O_b. Then update O_b to be the object that is farthest apart from O_a. The two resulting objects O_a, O_b are pivots.

Consider an object O_i and the triangle formed by O_i, O_a and O_b (Figure 4.1). From the cosine law, one can get

$$d_{b,i}^2 = d_{a,i}^2 + d_{a,b}^2 - 2x_i d_{a,b} \tag{5.1}$$

Thus, the first coordinate x_i of object O_i with respect to the line (O_a, O_b) is

$$x_i = \frac{d_{a,i}^2 + d_{a,b}^2 - d_{b,i}^2}{2d_{a,b}} \tag{5.2}$$

Now we can extend the above projection method to embed objects in the target space R^k as follows. Pretending that the given objects are indeed points in R^n, we consider an $(n-1)$-d hyper-plane $\mathcal{H}$ that is perpendicular to the line (O_a, O_b), where O_a and O_b are two pivot objects. We then project all the objects onto this hyper-plane. Let O_i, O_j be two objects and let O_i', O_j' be their projections on the hyper-plane $\mathcal{H}$. It can be shown that the dissimilarity d' between O_i', O_j' is

$$(d'(O_i', O_j'))^2 = (d(O_i, O_j))^2 - (x_i - x_j)^2, \qquad i, j = 0, \ldots, N-1 \tag{5.3}$$

Being able to compute d' allows one to project on a second line, lying on the hyper-plane $\mathcal{H}$, and therefore orthogonal to the first line (O_a, O_b). We repeat the steps recursively, k times, thus mapping all objects to points in R^k.

The discussion thus far assumes that the objects are indeed points in R^n. If the assumption doesn't hold, $(d(O_i, O_j))^2 - (x_i - x_j)^2$ may become negative. For this case, Equation (5.3) is modified as follows:

$$d'(O_i', O_j') = -\sqrt{(x_i - x_j)^2 - (d(O_i, O_j))^2} \tag{5.4}$$

Let O_i, O_j be two objects in $\mathcal{D}$ and let $P_i = (x_i^1, \ldots, x_i^k)$, $P_j = (x_j^1, \ldots, x_j^k)$ be their images in the target space R^k. The dissimilarity between P_i and P_j, denoted $d_f(P_i, P_j)$, is calculated as

$$d_f(P_i, P_j) = \sqrt{\sum_{l=1}^{k} (x_i^l - x_j^l)^2} \tag{5.5}$$

Note that if the objects are indeed points in R^n, $n \geq k$, and the distance function d is Euclidean, then from Equation (5.3), *FastMap* guarantees a lower bound on inter-object distances. That is,

Proposition 5.1 $\quad d_f(P_i, P_j) \leq d(O_i, O_j)$.

Let $Cost_{fastmap}$ denote the total number of distance calculations required by *FastMap*. From Equations (5.2) and (5.3) and the way the pivot objects are chosen, we have

$$Cost_{fastmap} = 3Nk \tag{5.6}$$

where N is the size of the dataset and k is the dimensionality of the target space.

5.3.2 The MetricMap Algorithm

The algorithm works by first choosing a small sample $\mathcal{A}$ of $2k$ objects from the dataset. In choosing the sample, one can either pick it up randomly, or use the $2k$ pivot objects found by *FastMap*. The algorithm calculates the pairwise distances among the sampling objects and uses these distances to establish the target space R^k. The algorithm then maps all objects in the dataset to points in R^k.

Specifically, assume, without loss of generality, that $\mathcal{A} = \{O_0, \ldots, O_{2k-1}\}$. We define a mapping α as follows: $\alpha : \mathcal{A} \to R^{2k-1}$ such that $\alpha(O_0) = a_0 = (0, \ldots, 0)$, $\alpha(O_i) = a_i = (0, \ldots, 1_{(i)}, \ldots, 0)$, $1 \leq i \leq 2k-1$ (see Figure 5.1(a)). Intuitively we map O_0 to the origin and map the other sampling objects to vectors (points) $\{a_i\}_{1 \leq i \leq 2k-1}$ in R^{2k-1} so that each of the objects corresponds to a base vector in R^{2k-1}.

Let

$$M(\psi_{<a>}) = (m_{i,j})_{1 \leq i,j \leq 2k-1} \tag{5.7}$$

where

$$m_{i,j} = \frac{d_{i,0}^2 + d_{j,0}^2 - d_{i,j}^2}{2}, \qquad 1 \leq i, j \leq 2k-1 \tag{5.8}$$

Define the function ψ as follows: $\psi : R^{2k-1} \times R^{2k-1} \to R$ such that

$$\psi(x, y) = x^T M(\psi_{<a>}) y \tag{5.9}$$

where x^T is the transpose of vector x. Notice that $\psi(a_i, a_j) = m_{i,j}$, $1 \leq i, j \leq 2k-1$. The function ψ is called a *symmetric bilinear form* of R^{2k-1} [33]. $M(\psi_{<a>})$ is the matrix of ψ with respect to the basis $\{a_i\}_{1 \leq i \leq 2k-1}$. The vector space R^{2k-1} equipped with the symmetric bilinear form ψ is called a pseudo-Euclidean space. For any two points (vectors) $x, y \in R^{2k-1}$, $\psi(x, y)$ is called the *inner product* of x and y. The *squared distance* between x and y, denoted $||x - y||^2$, is defined as

$$||x - y||^2 = \psi(x - y, x - y) \tag{5.10}$$

This squared distance is used to measure the dissimilarity of two points in the pseudo-Euclidean space.

Since the matrix $M(\psi_{<a>})$ is real symmetric, there is an orthogonal matrix $Q = (q_{i,j})_{1 \le i,j \le 2k-1}$ and a diagonal matrix $D = diag(\lambda_i)_{1 \le i \le 2k-1}$ such that

$$Q^T M(\psi_{<a>}) Q = D \tag{5.11}$$

where Q^T is the transpose of Q, $\lambda_i s$ are eigenvalues of $M(\psi_{<a>})$ arranged in some order, and columns of Q are the corresponding eigenvectors [32]. Note that if the matrix $M(\psi_{<a>})$ has negative eigenvalues, the squared distance between two points in the pseudo-Euclidean space may be negative. That's why we never say the "distance" between points in a pseudo-Euclidean space.

Now we find a *ψ-orthogonal* basis of R^{2k-1}, $\{e_i\}_{1 \le i \le 2k-1}$, where

$$(e_1, \ldots, e_{2k-1}) = (a_1, \ldots, a_{2k-1})Q \tag{5.12}$$

or equivalently

$$(a_1, \ldots, a_{2k-1}) = (e_1, \ldots, e_{2k-1})Q^T \tag{5.13}$$

Each vector a_i, $1 \le i \le 2k-1$, can be represented as a vector in the space spanned by $\{e_i\}_{1 \le i \le 2k-1}$ and the coordinate of a_j with respect to $\{e_i\}_{1 \le i \le 2k-1}$ is the j^{th} row of Q (see Figure 5.1(b)). Each e_i corresponds to an eigenvector.

Suppose the eigenvalues are sorted in descending order by their absolute values, followed by the zero eigenvalues. The *MetricMap* algorithm reduces the dimensionality of R^{2k-1} to obtain the subspace R^k by removing the $k-1$ dimensions along which the eigenvalues $\lambda_i s$ of $M(\psi_{<a>})$ are zero or their absolute values are smallest (see Figure 5.1(c)). Notice that among the remaining k-dimensions, some may have negative eigenvalues. The algorithm then chooses $k+1$ objects, called the *reference objects*, that span R^k.

Once the target space R^k is established, the algorithm maps each object O_* in the dataset to a point (vector) P_* in the target space by comparing the object with the

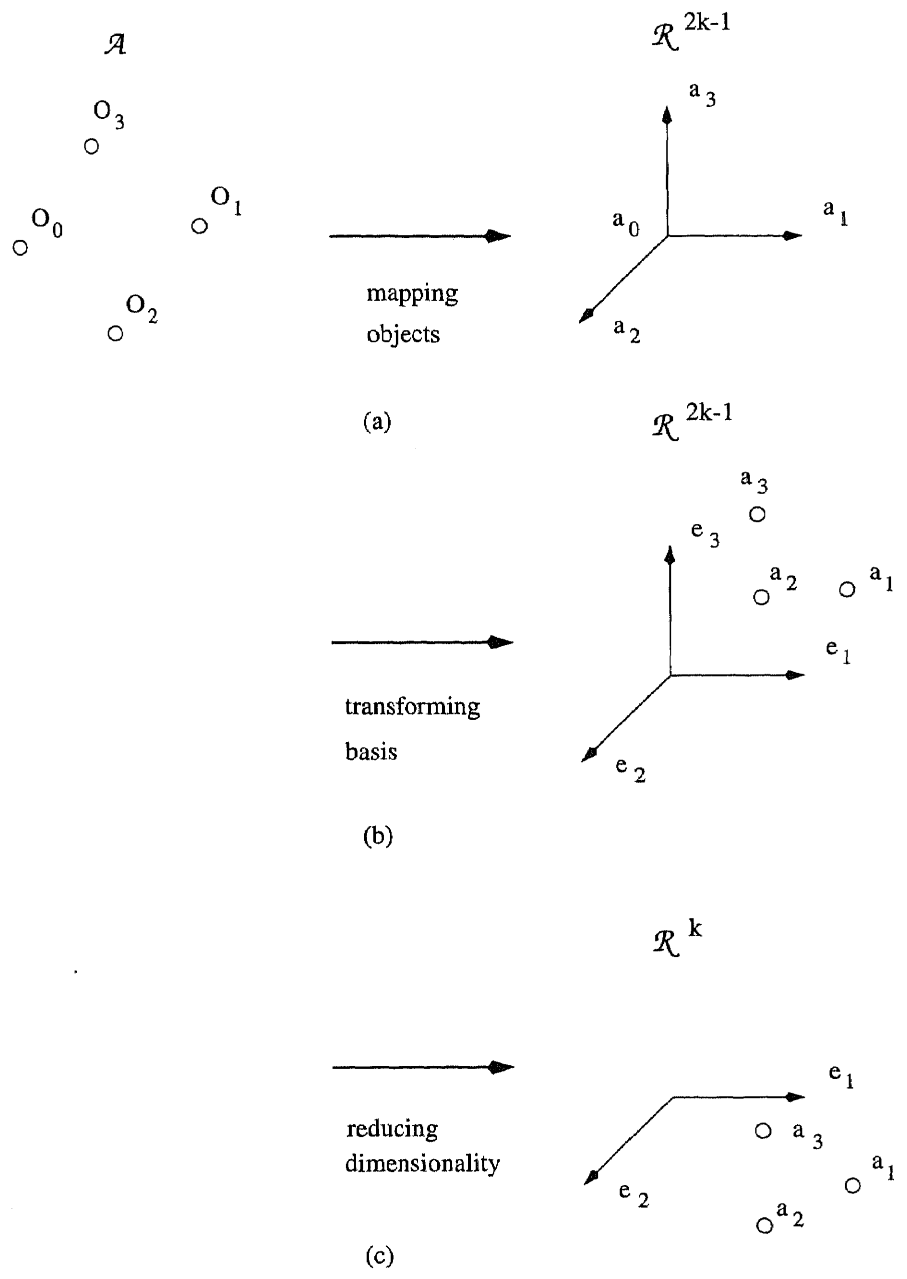

Figure 5.1 Illustration of the *MetricMap* algorithm ($k = 2$).

reference objects. The coordinate of P_* is calculated through matrix multiplication. Here is how.

Assume, without loss of generality, that the reference objects are $O_0, O_1, \ldots, O_k$. Let

$$b = (n_{*,j})_{1 \le j \le k} \tag{5.14}$$

where

$$n_{*,j} = \frac{d^2_{*,0} + d^2_{j,0} - d^2_{*,j}}{2}, \qquad 1 \le j \le k \tag{5.15}$$

Define

$$sign(\lambda_i) = \begin{cases} 1 & \text{if } \lambda_i > 0 \\ 0 & \text{if } \lambda_i = 0 \\ -1 & \text{if } \lambda_i < 0 \end{cases} \tag{5.16}$$

That is, $sign(\lambda_i)$ is the sign of the ith eigenvalue λ_i. Let $J = diag(sign(\lambda_i))_{1 \le i \le 2k-1}$ and $C = diag(c_i)\ _{1 \le i \le 2k-1}$ where

$$c_i = \begin{cases} |\lambda_i| & \text{if } \lambda_i \ne 0 \\ 1 & \text{otherwise} \end{cases} \tag{5.17}$$

Let $J_{[k]}$ be the k^{th} leading principal submatrix of the matrix J, i.e. $J_{[k]} = diag(sign(\lambda_i))_{1 \le i \le k}$. Let $C_{[k]}$ be the k^{th} leading principal submatrix of the matrix C, i.e. $C_{[k]} = diag(|\lambda_i|)_{1 \le i \le k}$. Let $Q_{[kk]}$ be the k^{th} leading principal submatrix of the orthogonal matrix Q, i.e. $Q_{[kk]} = (q_{i,j})_{1 \le i,j \le k}$. The coordinate of P_* in R^k, denoted $Coor(P_*)$, can be approximated as follows:

$$Coor(P_*) \approx J_{[k]} C_{[k]}^{-1/2} Q_{[kk]}^{-1} b \tag{5.18}$$

Let O_i, O_j be two objects in $\mathcal{D}$ and let $P_i = (x_i^1, \ldots, x_i^k)$, $P_j = (x_j^1, \ldots, x_j^k)$ be their images in R^k. Let

$$\Delta(P_i, P_j) = \sum_{l=1}^{k} sign(\lambda_l)(x_i^l - x_j^l)^2 \tag{5.19}$$

The dissimilarity between P_i and P_j, denoted $d_m(P_i, P_j)$, is approximated by

$$d_m(P_i, P_j) \approx \begin{cases} \sqrt{\Delta(P_i, P_j)} & \text{if } \Delta(P_i, P_j) \ge 0 \\ -\sqrt{-\Delta(P_i, P_j)} & \text{otherwise} \end{cases} \tag{5.20}$$

Note that if the objects are points in R^n, $n \geq k$, and the distance function d is Euclidean, then as in *FastMap*, *MetricMap* guarantees a lower bound on inter-object distances. That is,

Proposition 5.2 $\quad d_m(P_i, P_j) \leq d(O_i, O_j)$.

To see this, note that in the Euclidean spaces, the bilinear form ψ is positive definite, because for any non-zero vector x, $x^T M(\psi_{<a>})x$ is positive [60]. This implies that all the non-zero eigenvalues are positive. When projecting the points from R^n onto R^k, the images have fewer coordinates. From Equations (5.19) and (5.20), we conclude that the dissimilarity between two images is less than or equal to the distance between the corresponding objects.

Let $Cost_{metricmap}$ denote the total number of distance calculations required by *MetricMap*. From equations (5.7), (5.8) and (5.11), we see that to calculate the eigenvalues of $M(\psi_{<a>})$, one needs to calculate the pairwise distances $d_{i,j}$, $0 \leq i, j \leq 2k-1$. This requires $(2k)^2 = 4k^2$ distance calculations. From equations (5.14), (5.15) and (5.18), we see that to embed each object O_* in R^k, one needs to calculate the distances from O_* to the $k+1$ reference objects. Notice that if O_* is a sampling object, its distances to the reference objects need not be recalculated, since they are part of the distances $d_{i,j}$, $0 \leq i, j \leq 2k-1$ that are already computed. Totally there are N objects in the dataset, and therefore

$$Cost_{metricmap} = 4k^2 + (N - 2k)(k+1) \tag{5.21}$$

Comparing Equations (5.6) and (5.21), since $N \geq k$, $Cost_{metricmap} \leq Cost_{fastmap}$.

5.4 Precision of Embedding

We conducted a series of experiments to evaluate the precision of embedding by calculating the errors induced by the index structures. The index structures were implemented in C and C++ under the UNIX operating system run on a SPARC 20. Four sets of distances were generated: synthetic Euclidean, synthetic non-Euclidean, protein and RNA. The last three were general distance metrics, so satisfied the triangle inequality, but were not Euclidean.

5.4.1 Data

In creating synthetic Euclidean distances, we generated N n-dimensional vectors. Each vector was generated by choosing n real numbers randomly and uniformly from the interval $[LowBound..Hig\text{-}\ hBound]$. We then calculated the pairwise distances among the vectors. In creating synthetic non-Euclidean distances, we generated the pairwise distances among N objects randomly and uniformly in the interval $[MinDistance..MaxDistance]$, keeping only those objects that satisfied the triangle inequality as in [74]. Table 5.1 summarizes the parameters and base values used in the experiments.

In generating protein distances, we selected a set of 230 kinase sequences obtained from the protein database in the Cold Spring Harbor Laboratory. We used the string edit distance to measure the dissimilarity of two proteins [69]. The inter-protein distances were in the interval (1..2573).

In generating RNA distances, we used 200 RNA secondary structures obtained from the virus database in the National Cancer Institute. The RNA secondary structures were created by first choosing two phylogenetically related mRNA sequences, rhino 14 and cox5, from GenBank [11] pertaining to the human rhinovirus and coxsackievirus. The 5' non-coding region of each sequence was folded and 100

Table 5.1 Parameters and base values used in the experiments for evaluating the precision of embedding.

Parameter	Value	Description
k	15	Dimensionality of the target space
N	3,000	Number of objects in the dataset
n	20	Dimensionality of synthetic vectors in Euclidean space
LowBound	0	Smallest possible value for each coordinate of the synthetic vectors
HighBound	100	Largest possible value for each coordinate of the synthetic vectors
MinDistance	1	Minimum distance between objects for the synthetic non-Euclidean data
MaxDistance	100	Maximum distance between objects for the synthetic non-Euclidean data

secondary structures of that sequence were collected. The structures were then transformed into trees and their pairwise distances were calculated as described in [75, 91]. The trees had between 70 and 180 nodes. The distances for rhino 14's trees and cox5's trees were in the interval (1..75) and (1..60), respectively. The distances between rhino 14's trees and cox5's trees were in the interval (43..94). The secondary structures (trees) for each sequence roughly formed a cluster.

5.4.2 Experimental Results

Let O_i, O_j be two objects in $\mathcal{D}$ and let P_i, P_j be their images in R^k. The dissimilarity between P_i, P_j embedded by *FastMap*, denoted $d_f(P_i, P_j)$, was as in Equation (5.5). The dissimilarity between P_i, P_j embedded by *MetricMap*, denoted $d_m(P_i, P_j)$, was as in Equation (5.20). To understand whether the index structures might complement each other, we considered three combinations of the index structures: *AvgMap*, *MinMap* and *MaxMap*, with the dissimilarities d_a, d_n, d_x defined as follows:

$$d_a(P_i, P_j) = \frac{d_f(P_i, P_j) + d_m(P_i, P_j)}{2} \quad (5.22)$$

$$d_n(P_i, P_j) = \min\{d_f(P_i, P_j), d_m(P_i, P_j)\} \quad (5.23)$$

$$d_x(P_i, P_j) \;=\; \max\{d_f(P_i, P_j), d_m(P_i, P_j)\} \tag{5.24}$$

We collectively refer to all these index structures as *mappers*. In building the mappers, we used random sampling objects for *MetricMap* to establish the target space (cf. Section 5.3.2). Note here that the mappers have the same cost $O(Nk)$ asymptotically, cf. Equations (5.6) and (5.21).

The measure used for evaluating the precision of embedding was the *average relative error* (Err_r), defined as

$$Err_r = \frac{\sum_{O_i,O_j \in \mathcal{D}} |d(O_i, O_j) - |d_s(P_i, P_j)||}{\sum_{O_i,O_j \in \mathcal{D}} d(O_i, O_j)} \times 100\% \tag{5.25}$$

where $s = f, m, a, n, x$, respectively. One would like this percentage to be as low as possible. The lower Err_r is, the better performance the corresponding mapper has.

Figure 5.2 graphs Err_r as a function of the dimensionality of the target space, k, for the synthetic Euclidean data. The parameters have the values shown in Table 5.1. We see that for all the mappers, Err_r drops as k increases. Err_r approaches 0 when $k = 19$. *FastMap* performs better than *MetricMap*, but *MaxMap* dominates in all situations. From Proposition 5.1 and Proposition 5.2, both *FastMap* and *MetricMap* underestimate inter-object distances, so *MaxMap* gives the lowest average relative error among all the mappers.

We next examined the scalability of the results. Figure 5.3 compares *FastMap*, *MetricMap* and *MaxMap* for varying N, Figure 5.4 compares the three mappers for varying n, and Figure 5.5 plots Err_r as a function of (*HighBound*/*LowBound*) for the three mappers. In each figure, only one parameter is tuned and the other parameters have the values shown in Table 5.1. The *LowBound* in Figure 5.5 is fixed at 1. It can be seen that Err_r depends on the dimensionality of vectors n, but is independent of the dataset size N and coordinate ranges of the vectors. *MaxMap* consistently beats the other two mappers in all these figures.

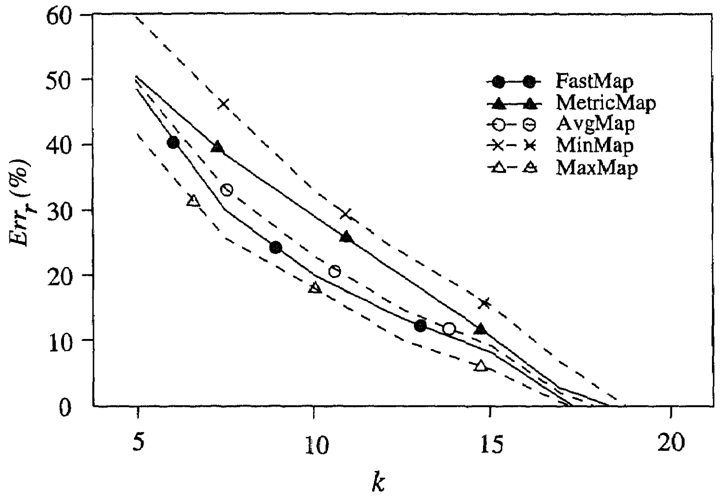

Figure 5.2 Average relative errors of the mappers as a function of the dimensionality of the target space for synthetic Euclidean data.

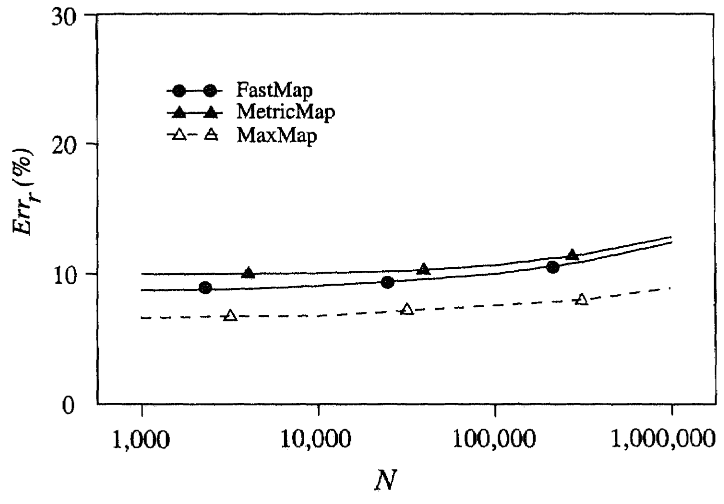

Figure 5.3 Effect of dataset size for synthetic Euclidean data.

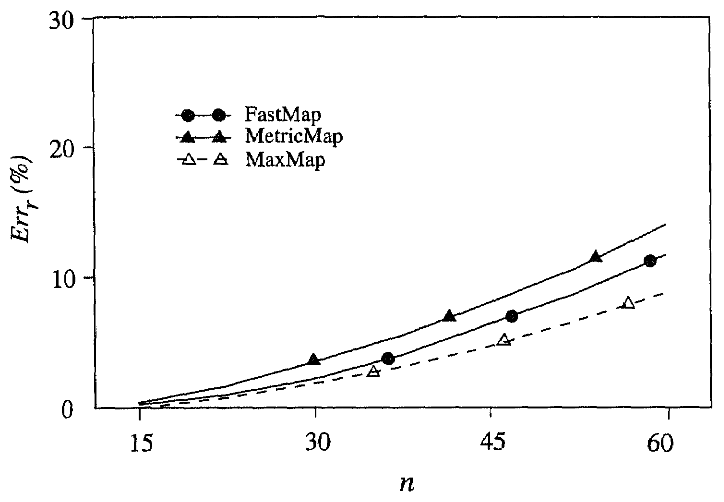

Figure 5.4 Average relative errors of the mappers as a function of the dimensionality of vectors for synthetic Euclidean data.

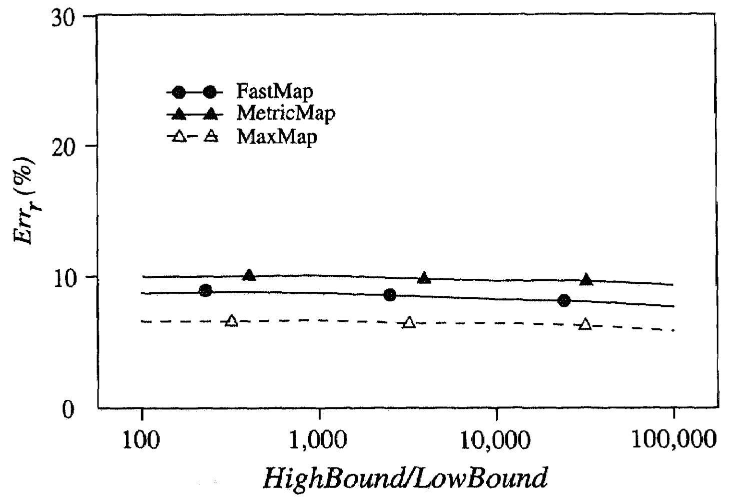

Figure 5.5 Effect of coordinate ranges for synthetic Euclidean data.

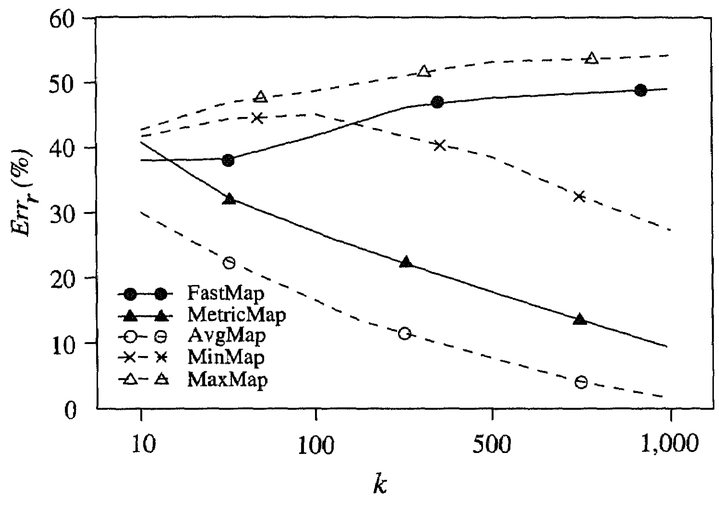

Figure 5.6 Average relative errors of the mappers as a function of the dimensionality of the target space for synthetic non-Euclidean data.

We then compared the relative performance of the mappers using the synthetic non-Euclidean data. Figure 5.6 graphs Err_r as a function of the dimensionality of the target space k. The parameters have the values shown in Table 5.1. The figure shows that *MetricMap* outperforms *FastMap* while *AvgMap* is superior to both of them. As k increases, the performance of *MetricMap* improves while the performance of *FastMap* degrades. The larger the k, the more negative dissimilarity values *FastMap* produces, cf. Equation (5.4). As a consequence, the more biased projections it creates. Note that *MetricMap* also produces negative dissimilarity values during the projection. It has a better performance probably because the images' coordinates are calculated by matrix multiplication through a single projection, rather than through a series of projections as done in *FastMap*, and hence the effect incurred by these negative dissimilarity values is reduced.

The next two figures show the scalability of the results. Figure 5.7 compares the relative performance of *FastMap*, *MetricMap* and *AvgMap* for varying N and Figure 5.8 plots Err_r as a function of $\ln(MaxDistance/MinDistance)$ for the three mappers. The k value in both figures is fixed at 1000 and the *MinDistance* in Figure

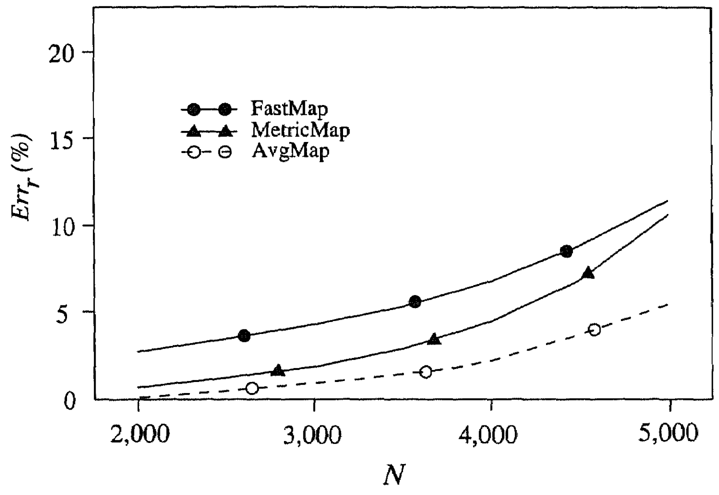

Figure 5.7 Effect of dataset size for synthetic non-Euclidean data.

5.8 is fixed at 10. The other parameters have the values shown in Table 5.1. It can be seen that Err_r depends on the dataset size N, but is independent of the distance ranges. Clearly, *AvgMap* is the best for all the non-Euclidean data. Both *FastMap* and *MetricMap* may overestimate or underestimate some inter-object distances. The fact that *AvgMap* outperforms either one individually is a good indication of the complementarity of the two index structures.

The trends observed from protein and RNA data are similar to those from the synthetic data. We omit the results for protein and only present those for RNA secondary structures (Figure 5.9). In sum, *MaxMap* is best for Euclidean data; its performance depends on the dimensionality of vectors n, but is independent of the size of datasets N. *AvgMap* is best for non-Euclidean data; its performance depends on the dataset size. Both mappers' performance improves as the dimensionality of the target space k increases. For Euclidean data, *MaxMap*'s Err_r drops to 0 as k approaches n. For non-Euclidean data, *AvgMap*'s Err_r approaches 0 when $k = N/2$, i.e. when all the $2k = N$ data objects are used in the sample to establish the target space.

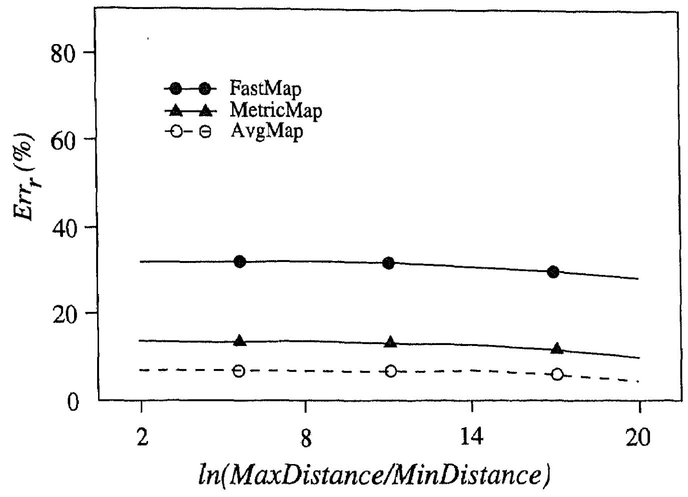

Figure 5.8 Effect of distance ranges for synthetic non-Euclidean data.

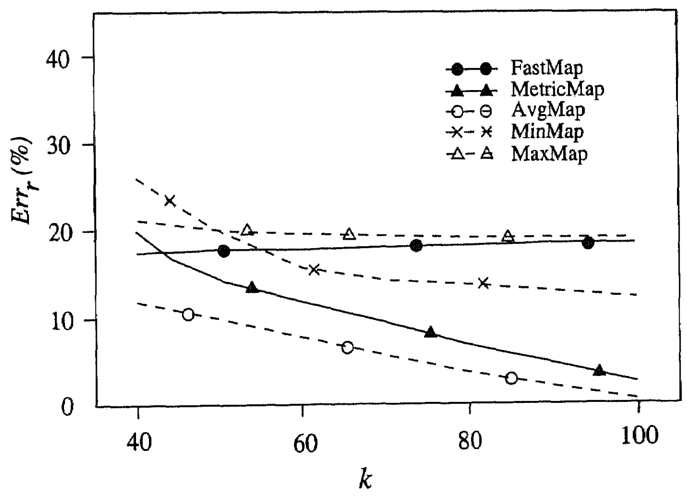

Figure 5.9 Average relative errors of the mappers as a function of the dimensionality of the target space for RNA secondary structures.

The last set of experiments examined the feasibility of retrieval with *MaxMap* and *AvgMap*. Let d_s, $s = a, x$, represent the dissimilarity measures for the two mappers, cf. Equations (22) and (24). We randomly picked an object O_c and considered the sphere G_1 with O_c as the centroid and a properly chosen ϵ as the radius, i.e. G_1 contained all the objects O where $d(O, O_c) \leq \epsilon$. Let P_c be the image of O_c. G_2 represented the sphere in the target space that contained all the images P where $|d_s(P, P_c)| \leq \epsilon$. Let O_i be an object and let P_i be its image. We say O_i is a *false positive* if $P_i \in G_2$ whereas $O_i \notin G_1$. O_i is a *false negative* if $P_i \notin G_2$ but $O_i \in G_1$. The performance measure used was the *accuracy* (*Accu*), defined as

$$Accu = \frac{|G_1| + |G_2| - (N_p + N_n)}{|G_1| + |G_2|} \times 100\% \qquad (5.26)$$

where $|G_i|$, $i = 1, 2$, was the size of G_i, N_p was the number of false positives, and N_n was the number of false negatives. One would like this percentage to be as high as possible. The higher *Accu* is, the fewer false positives and negatives are, and therefore the better performance a mapper has.

Figure 5.10 illustrates *MaxMap*'s performance for the synthetic Euclidean data and Figure 5.11 illustrates *AvgMap*'s performance for the synthetic non-Euclidean data. The four curves represent four different dataset sizes (N = 1,000, 10,000, 100,000, 1,000,000, respectively, in Figure 5.10, and N = 2,000, 3,000, 4,000, 5,000, respectively, in Figure 5.11). The four points on each curve correspond to four different k values. The *Accu* plotted in the figures is the average value over all the N spheres where each sphere uses a different object as the centroid. The radius of a sphere is fixed at 50, i.e. $\epsilon = 50$. The X-axis shows the CPU time spent in embedding the objects. From the figures we see that as the dimensionality of the target space, k, increases, both the time and accuracy increase. For the Euclidean data with 20-dimensional vectors, *Accu* approaches 100% when k = 18. For the non-Euclidean data, *Accu* approaches 100% when $k = 1,000$. These results indicate that with the two best mappers, one can conduct the range search [23, 24] on the k-dimensional

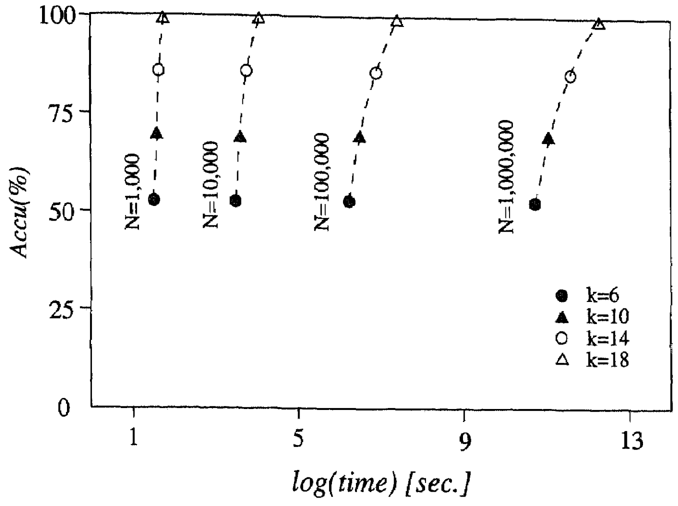

Figure 5.10 Accuracy of *MaxMap* for synthetic Euclidean data.

points by embedding the query object in the target space and then considering the sphere with the query object as the centroid in the target space. Embedding the data objects can be performed in the off-line stage, thus reducing the search time significantly.

5.5 Clustering

In this section we evaluate the accuracy of clustering in the presence of imprecise embedding. The purpose is twofold. First, this study shows the feasibility of clustering without performing expensive distance calculations. Second, through the study, one can understand how imprecision in the embedding may affect the accuracy of clustering.

5.5.1 Data

The data used in the experiments included the RNA secondary structures described in Section 5.4.1, because they roughly formed 2 clusters, each corresponding to an mRNA sequence. RNA distance is non-Euclidean. In addition, we generated Euclidean clusters as follows: we built $p = q^2$ clusters as in [105]. Specifically, we

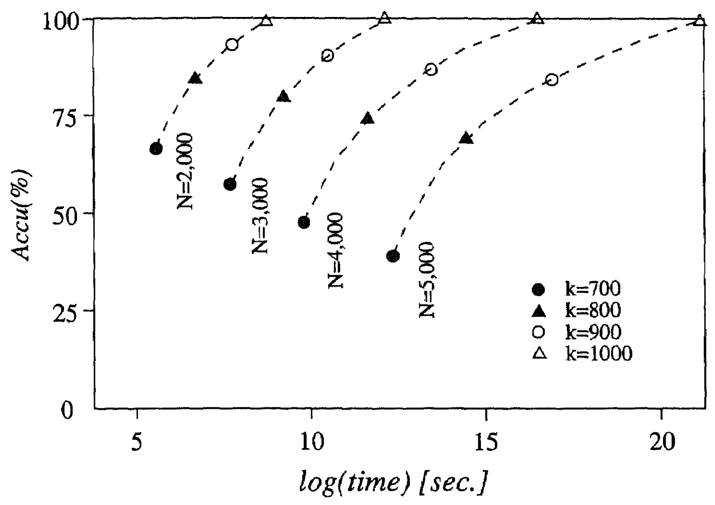

Figure 5.11 Accuracy of *AvgMap* for synthetic non-Euclidean data.

generated q groups of n-dimensional vectors from an n-dimensional hypercube. The vectors were generated as described in Section 5.4.1. Each group had C vectors.

Initially the groups (clusters) might overlap. We considered all the q groups as sitting on the same line and moved them apart along the line by adding a constant $(i \times c)$, $1 \leq i \leq q$, to the first coordinate of all the vectors in the ith group; c was a tunable parameter. We used CURE [36] to adjust the clusters so that they were not too far apart. Specifically, c was chosen to be the minimum value, by which CURE can just separate the q clusters. In our case, $c = 1.15$. Once the first q clusters were generated, we moved to the second line, which was parallel to the first line, and generated another q clusters along the second line. This step was repeated until all the q lines were generated, each line comprising q clusters. Again we used CURE to adjust the distance between the lines so that they were not too far apart. Table 5.2 summarizes the parameters and base values used in the experiments.

Table 5.2 Parameters and base values used in the experiments for evaluating the accuracy of clustering Euclidean vectors.

Parameter	Value	Description
k	10	Dimensionality of the target space
p	4	Number of clusters
n	20	Dimensionality of synthetic vectors
C	100	Number of vectors in a cluster

5.5.2 Experimental Results

The clustering algorithm used in our experiments was the well known average-group method [44], which works as follows. Initially, every object is a cluster. The algorithm merges two nearest clusters to form a new cluster, until there are only K clusters left where K is p for the Euclidean clusters and 2 for the RNA data. The distance between two clusters C_1 and C_2 is given as

$$\frac{1}{|C_1||C_2|} \sum_{O_p \in C_1, O_q \in C_2} |d(O_p, O_q)| \tag{5.27}$$

where $|C_i|$, $i = 1, 2$, is the size of cluster C_i. The algorithm requires $O(N^2)$ distance calculations where N is the total number of objects in the dataset.

An object O is said to be *mis-clustered* if O is in a cluster C created by the average-group method, but its image is not in C's corresponding cluster, which is also created by the average-group method, in the target space. The performance measure we used was the *mis-clustering rate* (Err_c), defined as

$$Err_c = \frac{N_c}{N} \times 100\% \tag{5.28}$$

where N_c was the number of mis-clustered objects.

Figure 5.12 graphs Err_c as a function the dimensionality of the target space, k, for the Euclidean clusters and Figure 5.13 shows the results for the RNA data. The parameters have the values shown in Table 5.2. For the Euclidean data, the average-group method successfully found the 4 clusters in the dataset. For the RNA

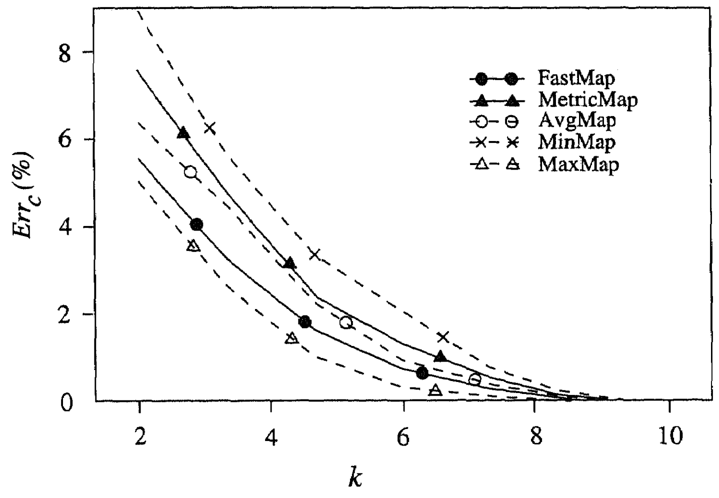

Figure 5.12 Mis-clustering rates of the mappers as a function of the dimensionality of the target space for synthetic Euclidean data.

data, the average-group method missed 5 objects in the dataset (i.e., the 5 RNA secondary structures were not detected to belong to their corresponding sequence's cluster). The images of these 5 objects were also missed in the target space; they were excluded when calculating Err_c.

As in Section 5.4.2, the clustering performance improves as the dimensionality of the target space increases, because the embedding becomes more precise. Figure 5.12 shows that the Err_cs of all the mappers approach 0 when $k = 9$. Figure 5.13 shows that *MetricMap* outperforms *FastMap*; its Err_c approaches 0 when $k = 80$. Overall, *MaxMap* is best for the Euclidean data and *AvgMap* is best for the non-Euclidean RNA data. The results indicate that with the two best mappers, one can perform clustering on the k-dimensional points. Embedding the data objects can be performed in the off-line stage, thus reducing the clustering time significantly.

It is worth pointing out that one may achieve an accurate clustering even with an imprecise embedding. For example, in Figure 5.12, the clustering accuracy is over 90% when $k = 2$, though the relative errors for the $k = 2$ case are over 50% (cf. Figure 5.2). This happens because after the embedding is performed, those objects

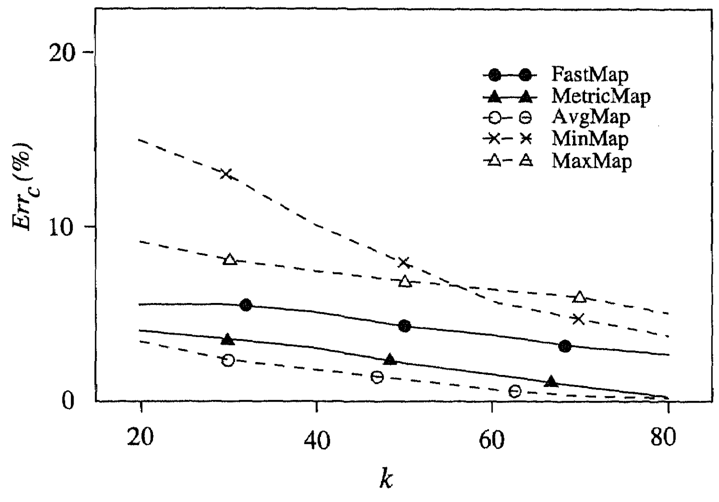

Figure 5.13 Mis-clustering rates of the mappers as a function of the dimensionality of the target space for RNA data.

that are close to each other in the original space remain close in the target space, though the distances are underestimated significantly.

We next examined the scalability of the results using Euclidean clusters. Figure 5.14 compares *FastMap*, *MetricMap* and *MaxMap* for varying numbers of clusters, Figure 5.15 compares them for varying sizes of clusters, and Figure 5.16 compares the mappers for varying dimensionalities of the vectors in each cluster. With higher dimensional vectors (e.g. 60-dimensions) and more clusters, the average-group method missed several objects in the dataset. However, *MaxMap* consistently gives the lowest mis-clustering rate in all the figures.

To see how different clustering techniques might affect the performance, we have also conducted experiments using some other clustering algorithms, e.g. the single-linkage and complete-linkage methods [44]. The two methods work in a similar way as the average-group method. The differences lie in the way they calculate the distance between two clusters. In the single-linkage algorithm, the distance between two clusters C_1 and C_2 is given as

$$\min_{O_p \in C_1, O_q \in C_2} |d(O_p, O_q)| \tag{5.29}$$

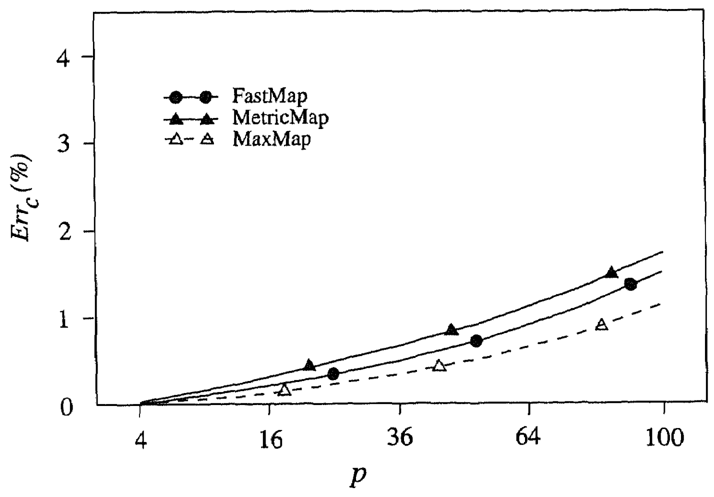

Figure 5.14 Impact of the number of clusters.

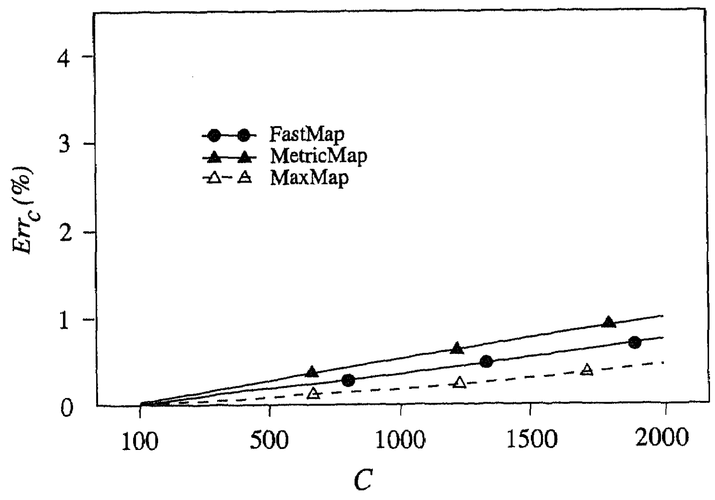

Figure 5.15 Impact of the size of clusters.

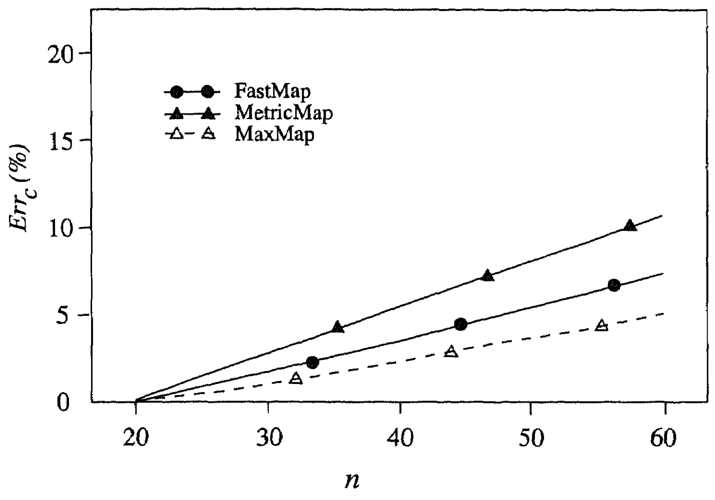

Figure 5.16 Effect of the dimensionality of vectors in a cluster.

In the complete-linkage algorithm, the distance is given as

$$\max_{O_p \in C_1, O_q \in C_2} |d(O_p, O_q)| \tag{5.30}$$

The results were slightly worse. The reason is that these two methods use the distance between a specific pair of objects, as opposed to the average distance between the objects in the two clusters. The errors incurred from measuring the distance between the specific pair of objects may affect the clustering accuracy seriously.

Finally we conducted experiments by replacing the random sampling objects used by *Metric- Map* with the $2k$ pivot objects found by *FastMap.* The performance of *MetricMap* improves for the Euclidean data, but degrades for the non-Euclidean data. *MaxMap* and *AvgMap* remain the best as in the random sampling case.

5.6 Discussion

Since *MaxMap* and *AvgMap* are educed from both *FastMap* and *MetricMap*, their cost is approximately the sum of the costs of *FastMap* and *MetricMap.* Figure 5.2 shows that when the dimensionality of the target space, k, increases, the relative errors of the mappers decrease. On the other hand, increasing k also increases the

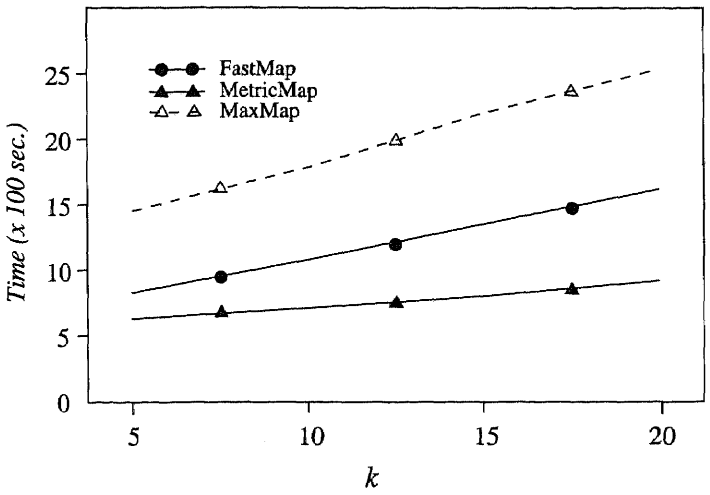

Figure 5.17 Running times of the mappers as a function of the dimensionality of the target space for synthetic Euclidean data.

embedding cost (cf. Figure 5.10). One may wonder whether using *MaxMap* and *AvgMap* with a smaller k is better than using *FastMap* and *MetricMap* with a bigger k when they all have approximately the same cost. We have conducted experiments to answer this question.

Figures 5.17 and 5.18 depict the running times of the mappers as a function of k for synthetic Euclidean and non-Euclidean data, respectively. The dataset size N was 5000 for the Euclidean data and 3000 for the non-Euclidean data. It can be seen from the figures that the costs of the mappers are proportional to the dimensionality of the target space k. The cost of *MaxMap* and *AvgMap* with a k-dimensional target space is approximately the same as the cost of *FastMap* with a $2k$-dimensional target space. Comparing with Figure 5.2, we see that using *FastMap* or *MetricMap* with a $2k$-dimensional target space yields a smaller relative error than using *MaxMap* with a k-dimensional target space for the synthetic Euclidean data. On the other hand, comparing with Figure 5.6, we see that using *AvgMap* with a k-dimensional target space achieves a more precise embedding than using *FastMap* or *MetricMap* with a $2k$-dimensional target space for the synthetic non-Euclidean data.

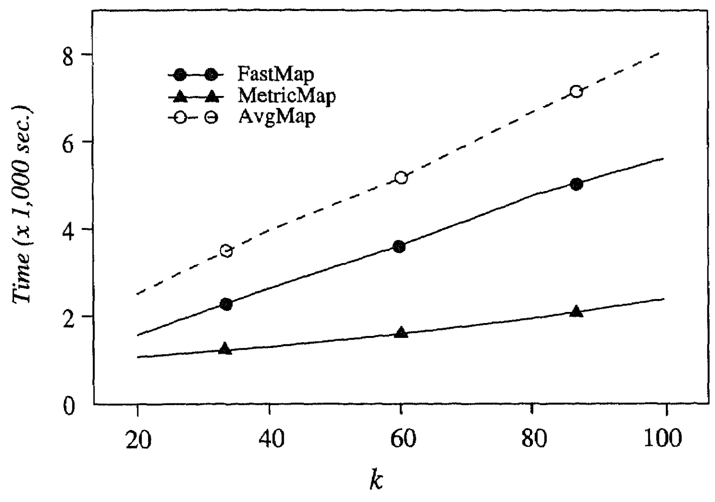

Figure 5.18 Running times of the mappers as a function of the dimensionality of the target space for synthetic non-Euclidean data.

In general, there is a tradeoff between the embedding cost and the embedding precision. Recall that the asymptotic cost of all the mappers is $O(Nk)$ where N is the size of the dataset. In the case of Euclidean data, k is independent of N. One can achieve a very precise embedding when k approaches the original dimensionality n of the vectors. Thus for a very large dataset of N Euclidean vectors, we can build a precise mapper (e.g. *MaxMap*) with a relatively low, asymptotically $O(N)$, cost. On the other hand, for the non-Euclidean data, the precision of the embedding depends on N. In order to build a precise mapper (e.g. *AvgMap*), k should be close to $N/2$, which leads to an $O(N^2)$ cost asymptotically.

We have experimented with different distance functions in the chapter. Our approach can also be applied to nominal values when a proper metric is defined for these values. Nominal values are identified by their names and do not have numeric values. The colors of eyes [44] are an example. Colors are represented by hexadecimal numbers in the SRGB (Standard Red Green Blue) model as used for Web pages. SRGB is a default color space for the Internet proposed by Hewlett-Packard and Microsoft, and accepted by the W3 organization as a standard. Each color corresponds to six hexadecimal digits, which are decomposed to three pairs. Each pair corresponds to a primary color. One can define the distance between two different colors as the sum of the differences between the corresponding components. Specifically, let $c_1 = x_{11}\ x_{12}\ x_{13}$ and $c_2 = x_{21}\ x_{22}\ x_{23}$ be two colors, where x_{ij}, $i = 1, 2$, $j = 1, 2, 3$, denotes two hexadecimal digits. We define the distance between c_1 and c_2, denoted $d(c_1, c_2)$, as

$$d(c_1, c_2) = \sum_{j=1}^{3} |x_{1j} - x_{2j}| \tag{5.31}$$

For example, suppose the color "blue" corresponds to 00 00 FF, the color "black" corresponds to 00 00 00, and the color "green" corresponds to 00 80 00. The distance between black eyes and blue eyes is $|00 - 00| + |00 - 00| + |FF - 00| = FF$ in hexadecimal number or 255 in decimal number. Similarly, the distance between green eyes and blue eyes is $|00 - 00| + |00 - 80| + |FF - 00| = 01\ 7F$ in hexadecimal number or 383 in decimal number. Clearly, for any three colors c_1, c_2 and c_3, we have $d(c_1, c_2) > 0$, $c_1 \neq c_2$ and $d(c_1, c_1) = 0$, $d(c_1, c_2) = d(c_2, c_1)$ and $d(c_1, c_2) \leq d(c_1, c_3) + d(c_3, c_2)$. Thus d is a metric and our approach is applicable.

5.7 Conclusion

In this chapter we have presented the performance evaluation of the *MetricMap* index structure and compared it with the previously published index structure *FastMap* [24]. The two index structures take a set of N objects, a distance metric d and embed those objects in a target space R^k, $k \leq N$, in such a way that the distances among objects are approximately preserved. *FastMap* considers R^k to be Euclidean; *MetricMap* considers R^k to be pseudo-Euclidean. Both index structures perform the embedding at an asymptotic cost $O(Nk)$.

We have conducted experiments to evaluate the accuracy of the embedding and the accuracy of clustering for the two index structures. The experiments were based on synthetic data as well as protein and virus datasets obtained from the Cold Spring Harbor Laboratory and National Cancer Institute. Our results showed that *MetricMap* complements *FastMap*. In every case, combining the two index structures performs better than using either one alone. Specifically, *FastMap* is more accurate than *MetricMap* for Euclidean distances, but taking the maximum of the distances (we use the term dissimilarities because some of these values can be negative) gives the best accuracy of all. *MetricMap* is more accurate than *FastMap* for non-Euclidean distances, but the average of the dissimilarities is best of all.

Besides the 4 datasets mentioned here, we have confirmed these results on 3 other datasets taken from dictionary words and other protein sequences. The practical significance of this work is that the proper use of these index structures can reduce the computation time substantially, thus achieving high efficiency for data mining and clustering applications.

CHAPTER 6

THE TOOLKIT

We have developed three tools based on the algorithms discussed in the dissertation.

6.1 Pdiscover

Our first tool *pdiscover* uses geometric hashing to discover frequently occur patterns in a database of 3D graphs.

There are 2 head files: Ghash.h and graph.h

There are 16 source files:

check.c,	evagroup.c,	extract.c,	getgroup.c,	graph.c,
hashdata.c,	identify.c,	loadXYZ.c,	loadnci.c,	mergeb.c,
merget.c,	pdiscover.c,	presort.c,	recover.c,	transf.c,
and transform.c.				

Executable file: pdiscover

Sample input data files: nci66, nci155, nci160, and nci161

To compile:

```
cc -o pdiscover pdiscover.c
```

To run:

```
pdiscover Size Mut Occur nci66 nci155 nci160 nci161
```

where Size is the minimum size of interesting patterns, Mut is the maximum number of mutations allowed, and Occur is the minimum occurrence number required.

Notes We use the term "motif" and "pattern" interchangably here.

Notes The number of input files can vary. If all input files start with nci, you can use nci* as input. Currently the maximum number of input data files is 500.

The input data file should be in the NCI format. However, it is very easy to adjust the loading program to read files in a different format.

If no qualified pattern is found, the program prints a message "No pattern is found" and exits. Otherwise, nothing is printed and the qualified patterns are written to a file called "motif". The patterns are numbered. Listed with each number is the identification number of the molecule from which the pattern is generated. (We assign an identification number to each molecule, where the number is consistent with the appearance order, from left to right, of the input data files.)

The program also generates two sets of files for each input data file (e.g. nci66):

*.molecule – which includes the coordinates of the molecule that have been transformed to be in the same coordinate system of the patterns that match the substructures in the molecule.

*.align – which includes the alignment between the patterns and the substructures.

We give an annotated example of a session of the pdiscover system. We assume that there are four 3D molecules, stored in the files nci66, nci155, nci160, and nci161, respectively. For example, the molecule in nci66 looks like the following:

```
$$$$

...

23 25
 -0.0187   1.5258   0.0104 C  0  0  0  0  0
  0.0021  -0.0041   0.0020 C  0  0  0  0  0
  1.3951   2.0474  -0.0003 C  0  0  0  0  0
 -0.7475   2.0250  -1.2105 C  0  0  0  0  0
 -0.7240   2.0118   1.2503 C  0  0  0  0  0

...

  2  1  1  0  0  0
  3  1  1  0  0  0
  4  1  1  0  0  0
  5  1  1  0  0  0
  6  2  1  0  0  0

...

...
```

The number 23 means that there are 23 atoms in this molecule. The number 25 means that there are 25 bonds. The row "-0.0187 1.5258 0.0104 C 0 0 0 0 0" means that there is an atom C whose coordinate is (-0.0187, 1.5258, 0.0104). These atoms are numbered, consistent with their appearance order (from top to bottom).

The row "2 1 1 0 0 0" means that there is a single bond between atom 2 and atom 1. The row "8 3 2 0 0 0" means that there is a double bond between atom 8 and atom 3.

Now to start, type in the following command at the operating system level:

```
pdiscover 6 1 3 nci66 nci155 nci160 nci161
```

You will obtain the following files in the same directory:

```
motif,
nci66.molecule,   nci66.align,   nci155.molecule,  nci155.align,
nci160.molecule,  nci160.align,  nci161.molecule,  nci161.align.
```

The file "motif" contains all the qualified patterns (motifs) found, and it looks like the following:

```
5

Motif 1

#From nci66 molecule id: 1; 6; 3

6 6
 -1.3310  3.4758  0.0273  C  1  2
 -1.3090  2.0812  0.0196  C  3  1
 -2.5383  4.1439  0.0361  C  4  3
 -3.7256  3.4331  0.0374  C  5  4
 -3.7100  2.0489  0.0245  C  5  6
 -2.5092  1.3701  0.0156  C  6  2

Motif 2

...

...
```

The number 5 in the beginning of the file indicates the number of motifs found. The motifs are numbered and listed in the order they are found. In the above example, “Motif 1” means that this is the first motif. The next row “#From nci66 molecule id: 1; 6; 3” indicates that this motif is generated from the molecule numbered one. The size of the motif is 6 and it (approximately) occurs in 3 input molecules.

In the row “6 6”, the first number 6 means that there are 6 atoms in the motif; the second number 6 means that there are 6 bonds in the motif. The row “-1.3310 3.4758 0.0273 C” means that there is an atom C whose coordinate is (-1.3310, 3.4758, 0.0273). The atoms in the motif are numbered, consistent with their appearance order (from top to bottom). The row “1 2” means that there is a bond between atom 1 and atom 2.

The file “nci66.align” lists the alignment between each found pattern and a substructure in the molecule. If there are more than one substructure of the molecule that can match the pattern, all of these substructures are listed. The data in the file looks like the following:

```
Motif 1
 1  -   7
 2  -   3
 3  -  11
 4  -  15
 5  -  12
DELETE 6


Motif 1
 1  -   4
 2  -   6
 3  -  19
 4  -  20
 5  -  22
RELABEL 6(Br) - > 16(O)
```

```
Motif 2
NULL


Motif 3
 1  -   5
 2  -  13
 3  -   1
 4  -   2
 5  -  10
 6  -   9
INSERT 7


...

...
```

The motif numbers are consistent with those in the file "motif". "Motif 1" followed by a list of integer pairs indicates that the first motif is found in the molecule nci66 and the integer pairs show an alignment between the motif and the molecule. For example, "1 – 7" means that atom 1 in Motif 1 must be aligned with atom 7 in the molecule nci66 in order for the match to occur. "DELETE 6" means that atom 6 in Motif 1 must be deleted for the match to occur. "RELABEL 6(Br) – > 16(O)" means that atom 6 in Motif 1 must be relabeled from "Br" to "O" to match atom 16 in the data molecule. "INSERT 7" means that one more atom must be inserted to Motif 1 for the match to occur.

In this example, Motif 1 appears twice. This means that Motif 1 can be matched with two different substructures in the molecule nci66, and therefore we list the alignment between the motif and each of the substructures.

"Motif 2" followed by "NULL" means that motif 2 does not occur in the molecule nci66.

For each found motif, the file "nci66.molecule" lists the coordinates of the molecule nci66 that have been transformed to be in the same coordinate system in which the motif is defined. This information is used to best visualize the alignment. The data in the file nci66.molecule looks like the following:

```
Motif 1

#The transformed coordinates

23 25
 -0.0164   1.3582   0.0095  C
  0.0021  -0.0041   0.0020  C
  1.2453   2.1098   0.0015  C
 -1.3090   2.0812   0.0196  C
  1.2822  -0.7201  -0.0141  C

...

 2  1
 3  1
 4  1
 5  1
 6  2

...

...

Motif 2

NULL

...

...
```

Again, "Motif 2" followed by "NULL" means that motif 2 does not occur in the molecule nci66.

6.2 Gsearch

The second tool *gsearch* deals with similarity search in a database of 3D graphs.

There are 2 head files: Ghash.h and graph.h

There are 21 source files:

check.c,	extract.c,	getgroup.c,	ghash.c,	graph.c,
hashdata.c,	identify.c,	loadXYZ.c,	loadcotable.c,	loadhtable.c,
loadnci.c,	mergeb.c,	merget.c,	presort.c,	recognize.c,
recover.c,	gsearch.c,	savecotable.c,	savehtable.c,	transf.c,
and transform.c.				

Executable files: ghash and gsearch

Sample input data files: nci66, nci155, nci160, and nci161

To compile:

```
cc -o ghash ghash.c
```

```
cc -o gsearch gsearch.c
```

To run:

```
ghash nci66 nci160 nci161
```

then

```
gsearch -b nci155
```

or

```
gsearch -s nci155
```

"ghash" hashes the molecules in the database and saves them in two files called "hl.nci" and "ht.nci". The program also creates a file called "flist.nci", which records the file names of the molecules in the order they are hashed. In our example, the database has three molecules, stored in three files nci66, nci160, nci161, respectively. Given a target molecule (e.g. nci155), "gsearch" performs best match retrieval with the "-b" option, or substructure search with the "-s" option.

For the best match retrieval, the tool finds the molecule in the database that is closest to the target.

For the substructure search, the tool finds the molecule in the database that contains a subgraph such that the subgraph is closest to the target molecule.

Notes The number of input files of "ghash" can vary. If all input files start with nci, you can use nci* as input. Currently the maximum number of input data files is 500. "gsearch" takes only one input file, which is the target molecule.

The input data file should be in the NCI format. However, it is very easy to adjust the loading program to read files in a different format.

We give an annotated example of a session of the gsearch system. We assume that there are four 3D molecules, stored in the files nci66, nci155, nci160, and nci161, respectively. For example, the data in nci66 looks like the following:

```
$$$$

...

...

23 25
 -0.0187    1.5258    0.0104 C  0  0  0  0  0
  0.0021   -0.0041    0.0020 C  0  0  0  0  0
  1.3951    2.0474   -0.0003 C  0  0  0  0  0
 -0.7475    2.0250   -1.2105 C  0  0  0  0  0
 -0.7240    2.0118    1.2503 C  0  0  0  0  0

...

  2  1  1  0  0  0
  3  1  1  0  0  0
  4  1  1  0  0  0
  5  1  1  0  0  0
  6  2  1  0  0  0

...

...
```

The number 23 means there are 23 atoms in this molecule. The number 25 means there are 25 bonds. The row "-0.0187 1.5258 0.0104 C 0 0 0 0 0" means that there is an atom C whose coordinate is (-0.0187, 1.5258, 0.0104). These atoms are numbered, consistent with their appearance order (from top to bottom).

The row "2 1 1 0 0 0" means that there is a single bond between atom 2 and atom 1. The row "8 3 2 0 0 0" means that there is a double bond between atom 8 and atom 3.

Now to start, type in the following command at the operating system level:

```
ghash nci66 nci160 nci161
```

You will obtain the following files in the same directory:

hl.nci and ht.nci.

"ht.nci" contains the hash table entries. "hl.nci" records the starting file offset of each hash bin and the number of entries stored in this hash bin in "ht.nci".

After the hash table has been generated, you can type in the following command at the operating system level:

```
gsearch -b nci155
```

or

```
gsearch -s nci155
```

The first command (with option "-b") returns the result of best match search, i.e., it returns the molecule that is closest to the target molecule. If there are more than one best match, the system returns all of them.

The output looks like the following:

```
nci155 matches nci160 with distance 5.

 20  -  19
 18  -  18
 17  -  17
 16  -  16
 15  -  15
```

```
14  -  14
13  -  13
11  -  11
10  -  10
 9  -   9
 8  -   8
 7  -   7
 6  -   6
 5  -   5
 4  -   4
 3  -   3
 2  -   2
 1  -   1
DELETE 19

DELETE 12

RELABEL 21(C) - > 21(Br)

INSERT 23

INSERT 22
```

This means the molecule in the database closest to the target molecule nci155 is nci160 and the distance between them is 5.

The pairs of integers indicate the alignment between the atoms in nci155 and those in molecule nci160. "DELETE 19" means that atom 19 in nci155 must be deleted for the match to occur. "RELABEL 21(C) – > 21(Br)" means that atom 21 in nci155 must be relabeled from "C" to "Br" to match atom 21 in molecule nci160. "INSERT 23" means that atom 22 was inserted to nci155 when matching nci155 with nci160.

The second command (with option "-s") returns the result of substructure search, i.e., it returns the molecule containing a subgraph that is closest to the target molecule. If there are more than one molecule satisfying the condition, the system returns all of them.

The output looks like the following:

nci161 contains nci155 with distance 2.

```
19 - 19
18 - 18
17 - 17
16 - 16
15 - 15
14 - 14
13 - 13
12 - 12
11 - 11
10 - 10
 9 -  9
 8 -  8
 7 -  7
 6 -  6
 5 -  5
 4 -  4
 3 -  3
 2 -  2
 1 -  1
DELETE 20
RELABEL 21(C) - > 21(Br)
```

"DELETE 20" means that atom 20 in nci155 must be deleted for the match to occur. "RELABEL 21(C) − > 21(Br)" means that atom 21 in nci155 must be relabeled from "C" to "Br" to match atom 21 in molecule nci161.

Notes: In this example, the distance between nci155 and nci160 is 5, while the distance between nci155 and nci161 is 6. The best match is nci160. However, for substructure search, nci160 contains a subgraph that has a distance 3 to nci155, while nci161 contains a subgraph that has a distance 2 to nci155. So nci161 is returned as the answer.

6.3 MetricMap

There are 4 tools in this package:

6.3.1 The MetricMap System

Given a set of objects and a distance metric, the tool *MetricMap* first establishes a pseudo-Euclidean space based on a sampling data set, and then projects the data objects to the pseudo-Euclidean space.

There are 2 head files: nrl.h and main.h

There are 14 source files:

angle1.c,	ind1.c,	lud1.c,	ortho1.c,	qli1.c,
tri1.c,	util.c,	eigw.c,	fbilinw.c,	fchow.c,
fheadw.c,	prow.c,	repeatw.c,	project.c	

Executable files: femb and proj

Sample input data files: d400.20 and coxrhi.dist

"d400.20" contains the pairwise distances of 400 randomly generated 20 dimensional vectors, which form 4 clusters. "coxrhi.dist" contains the pairwise distances of 200 RNA secondary structures, where 100 RNA secondary structures are pertaining to the human rhinovirus and the other 100 RNA secondary structures are pertaining to the coxsackievirus. Thus, these RNA secondary structures roughly form 2 clusters, one corresponding to the human rhinovirus and the other corresponding to the coxsackievirus. These sample data files may be used to replace the parameter Distance_in_file in the commands listed below.

To compile:

```
make -f Makelib

make femb

cc -o proj project.c -lm
```

To run:

```
femb Sample_Size Dimen < Distance_in_file

proj Distance_in_file Nobj Dimen Vect_out_file Dist_out_file
```

"femb" establishes a Dimen dimensional pseudo-Euclidean space based on the sampling data set. It generates 3 files: b.ind, b.val, and gram.mat. b.ind contains the indices of the objects that are chosen to be the base of the pseudo-Euclidean space. b.val contains the eigenvalues of the bilinear form that correspond to the chosen objects. gram.mat is the gram matrix that is used to project objects to the pseudo-Euclidean space.

"proj" projects the data objects to the pseudo-Euclidean space. Distance_in_file contains the pairwise distances of data objects, Sample_Size is the size of the sample set, Dimen is the dimensionality of the pseudo-Euclidean space, Nobj is the total number of data objects, Vect_out_file contains the image vectors of the objects in the pseudo-Euclidean space, and Dist_out_file contains the pairwise distances of the image vectors.

We give an annotated example of a session of the MetricMap system. We assume there is a file d400.20 which contains the pairwise distances of 4 clusters of randomly generated vectors in 20 dimensional Euclidean space. There are 100 vectors in each cluster. The file looks like the following:

```
3.5331
3.3376 2.8868
3.3015 3.3660 3.5378
4.0033 3.8468 3.6920 4.3646
3.2924 3.2653 3.8241 3.5259 4.2307
3.9440 3.3932 4.3023 3.9482 4.0962 3.5242
3.8446 3.5387 4.4129 3.7491 3.3720 3.1809 3.1663
3.7694 4.0969 3.2754 3.7708 4.4286 3.3644 4.7370 4.0737
3.6367 3.6421 3.6069 2.8791 4.0440 4.4357 4.0226 3.7571 4.2270
```

...

...

We index the objects, starting from 0. Strictly speaking, the pairwise distances of N objects is an $N \times N$ matrix. Since the matrix is symmetric, i.e. $d(i,j) = d(j,i)$, and $d(i,i) = 0$ for all i, we store only that part which is below the diagonal line of the metrix, i.e. $j < i$. In the above table, an entry at the ith row and jth column represents the distance between object i and object $j-1$. So, "3.5331" represents the distance between object 1 and object 0. "3.3660" represents the distance between object 3 and object 1. We list objects based on clusters. Thus cluster 1 contains objects with indexes ranging from 0 to 99; cluster 2 contains objects with indexes ranging from 100 to 199, etc.

To map these vectors to a 10 dimensional pseudo-Euclidean space, assume a sampling set of 20 vectors (here we assume a random sampling).

We first run:

```
femb 40 10 < d400.20
```

The file b.ind looks like the following:

```
9 25 36 28 10 37 14 31 39 32
```

This means that object 9, object 25, ..., object 32 are chosen as the reference objects. These reference objects are used to build the pseudo-Euclidean space.

The file b.val looks like the following:

```
 244.295985815851878  30.840193003299831  27.331134046091876
  22.693324721447667  21.848601030670395  19.968715757559004
  17.760763670010231  15.492304704396824  13.657936946677481
  11.905276204308640
```

Here b.val contains the eigenvalues corresponding to the reference objects. For example, "244.295985815851878" is the eigenvalue corresponding to object 9; "30.840193003299831" is the eigenvalue corresponding to object 25, and so on.

The file gram.mat looks like the following:

```
 0.115574453235548  -0.051501465876904  -0.045854384778602
-0.073070673365977  -0.009605172001804
-0.112828982820657   0.088720024289652  -0.099648201210417
-0.083911615757602  -0.119962106364417
 0.130328716802373  -0.342840761030932   0.303066694308480
 0.339452617555608  -0.381437909747193
-0.405149430555989   0.207206955370795   0.007917643375473
 0.073360446342078  -0.272648797992660
 0.161125014894303  -0.081818856765714  -0.090949331640256
-0.382668529714077   0.362174216869933
```

Here, gram.mat is the Gram matrix used in the transformation when embedding the objects in the pseudo-Euclidean space.

We then run:

```
proj d400.20 400 10 d400.vect d400.dist
```

Here we want to project 400 objects, whose pairwise distances are stored in file d400.20, to a 10 dimensional pseudo-Euclidean space. The output includes the vectors (d400.vect), which are the images of those objects in the pseudo-Euclidean space, and the pairwise distances (d400.dist) of those vectors.

The output in the file d400.vect looks like the following:

```
400 10
 0.0000   0.0000   0.0000   0.0000   0.0000
 0.0000   0.0000   0.0000   0.0000   0.0000
-2.5781  -2.1680   0.5737   2.0081  -0.7672
-0.0987   0.2544  -0.3053   0.3483   0.0392
-2.3080   0.8428   0.4520   0.8193  -0.8753
 0.0016   0.4910  -0.0696  -0.2953  -0.2928
-1.6848  -0.4318   1.1193   2.0989   0.6211
 0.3638   0.1002   0.5503   0.7714   0.5975
-3.1964  -0.4338   0.3476  -1.4289  -1.5407
 0.6868   1.0198   0.1987   0.1276  -0.3175

...

...
```

The number 400 indicates that there are 400 vectors. The number 10 indicates that these are 10 dimensional vectors. Each line of this file represents the coordinates of an image vector in the pseudo-Euclidean space. The first line represents image vector 0, the second line represents image vector 1, and so on.

The output in the file d400.dist looks like the following:

```
4.0728
2.8456 3.3502
3.2352 2.7398 2.9889
4.0755 4.1815 2.9879 4.7249
2.8299 3.9779 3.1020 3.5049 4.1980
3.5606 4.5433 3.7960 4.1910 3.8231 3.1871
3.8953 3.9691 3.6289 4.4674 3.3331 3.1036 2.7665
4.1445 5.3213 3.4076 4.2380 4.8977 3.1386 4.5469 4.7804
4.3856 3.2260 3.7689 2.2141 4.9199 4.9404 4.8649 4.6019 5.5956
3.8667 3.9858 2.8405 3.7353 2.1089 3.7809 3.1858 3.0554 4.7936 3.8987

...
...
```

This file contains the pairwise distances of the images. As in d400.20, the entry at the ith row and jth column represents the distance between image vector i (i.e. the image of object i) and image vector j-1 (i.e. the image of object j-1). Again, the vectors are indexed starting from 0, consistent with the object indexing.

So, “4.0728” represents the distance between the image of object 1 and the image of object 0. “2.7398” represents the distance between the image of object 3 and the image of object 1.

6.3.2 The Clustering Program Average Group Method

Average Group Method (AGM) is a clustering algorithm described in many text books, e.g. in [44]. Its implementation is as follows.

There is one head file: agm.h

There are three source files: agm.c, agmuti.c, and distance.c

Executable file: agm

To compile:

```
cc -o agm agm.c
```

To run:

```
agm Distance_in_file N_obj N_cluster
```

Distance_in_file contains the pairwise distances between the objects, N_obj is the total number of the objects, and N_cluster is the number of clusters to be generated.

For example, if we want to cluster 400 objects, whose pairwise distances are stored in d400.20, to 4 clusters, we run:

```
agm d400.20 400 4
```

The output looks like the following:

```
Everything is ready.
Initialize heap complete...
Clustering complete...
Cluster 0:
17 63 45 44 71 83 90 58 69 19 86 95 97 93 80 20 87 47 46 25 10 60 15 79 68 59 64 14
82 92 96 55 33 75 11 91 70 66 37 31 99 21 65 5 34 74 29 73 12 26 51 0 72 57 36 28 9
56 16 4 89 38 50 7 40 23 41 3 67 8 98 39 22 54 43 53 24 2 30 49 52 81 42 76 94 78
32 1 85 6 84 61 77 35 88 13 48 27 18 62
Total: 100 objects.
Cluster 1:
```

286 267 278 244 258 237 251 249 261 266 247 252 257 250 210 227 287 220 289 211
282 285 299 213 268 225 214 294 206 216 224 212 231 245 273 219 238 246 276 232
242 201 270 236 275 204 202 290 207 240 291 215 239 274 203 283 218 281 298 228
205 229 272 292 253 262 241 293 254 264 295 265 284 280 260 223 243 222 248 234
256 200 259 297 230 208 233 217 209 235 255 288 263 279 226 296 269 271 277 221
Total: 100 objects.

Cluster 2:

194 196 154 164 173 174 119 159 108 198 121 175 134 120 163 141 191 179 115 195
116 104 185 144 127 131 107 186 189 106 172 155 183 113 101 103 187 123 133 184
128 130 124 111 180 136 150 142 129 138 132 197 158 166 188 117 190 199 167 153
161 140 160 126 114 145 102 125 151 139 182 157 135 137 181 193 118 165 192 156
110 147 146 176 178 112 122 168 149 169 148 152 162 170 177 143 100 109 171 105
Total: 100 objects.

Cluster 3:

310 366 378 372 312 346 368 356 380 342 333 348 381 377 302 303 397 391 338 349
341 327 384 313 326 357 371 392 329 367 389 300 374 330 361 385 344 395 322 364
321 324 353 360 396 339 387 332 369 373 307 315 376 323 386 309 388 347 317 336
345 328 383 306 314 399 340 352 375 354 308 394 318 370 390 304 301 359 393 334
351 365 358 320 325 362 379 305 335 316 350 343 355 382 331 319 337 363 311 398
Total: 100 objects.

In each cluster we list object indexes. The data are generated in such a way that the first cluster includes objects with indexes ranging from 0 to 99, the second cluster includes objects with indexes ranging from 100 to 199, the third cluster includes objects with indexes ranging from 200 to 299, and the fourth cluster includes objects with indexes ranging from 300 to 399. We can see from the outputs that AGM achieves perfect clustering.

Average Group Method has the complexity of $O(N \times N)$. Assuming the calculation of distances between the objects is expensive, applying Average Group Method directly to the data set is not feasible. Thus we can take a small sample set of m objects and use MetricMap to map the objects to vectors in the pseudo-Euclidean space in time $O(N \times m)$. Once the data objects are embedded in the target space, the calculation of distances between the vectors is much cheaper. We then apply Average Group Method to the pairwise distances of the vectors in the pseudo-Euclidean space and cluster them.

For example, to apply Average Group Method directly to the RNA input data file coxrhi.dist, we execute the following command at the operating system level:

```
agm coxrhi.dist 200 2
```

The output on the screen looks like the following:

```
Everything is ready.
Initialize heap complete...
Clustering complete...
Cluster 0:
180 116 196 146 155 156 170 183 181 163 108 144 141 167 186 122 145 195 138 177
134 149 123 199 179 190 128 178 119 113 118 131 160 191 162 135 100 150 130 126
173 154 102 104 151 153 148 182 111 109 169 143 172 176 114 107 165 106 194 133
193 136 166 101 192 157 142 137 159 132 103 139 124 129 188 105 171 112 115 174
175 127 187 120 185 189 168 198 110 121 117 184 147 152 164
Total: 95 objects.
Cluster 1:
17 18 70 68 26 86 20 22 9 43 29 62 58 64 33 65 76 75 60 27 72 30 32 28 87 97 93 5 4
46 92 99 50 91 90 42 81 3 7 16 55 80 88 45 37 71 73 39 66 23 13 14 56 89 10 52 19
12 69 54 25 47 40 67 53 36 41 35 84 78 49 95 21 15 77 82 1 83 51 8 6 0 48 98 94 96
```

```
11 2 57 79 63 61 31 24 59 161 197 140 158 125 44 85 38 74 34
Total: 105 objects.
```

Suppose we want to take a sample set of 120 RNA secondary structures, some coming from the human rhinovirus family and the other coming from the coxsackievirus family. Map the RNA secondary structures to a 80 dimensional space, and then use Average Group Method to cluster their image vectors in the pseudo-Euclidean space.

We can do this by typing the following commands at the operating system level:

```
femb 120 80 < coxrhi.dist
proj coxrhi.dist 200 80 cr.vect cr.dist
agm cr.dist 200 2
```

The output on the screen looks like the following:

```
Everything is ready.
Initialize heap complete...
Clustering complete...
Cluster 0:
115 112 139 188 171 124 129 105 103 168 186 162 116 167 130 169 156 182 101 106
178 111 114 128 109 113 104 108 107 149 123 100 199 135 177 193 134 102 163 131
194 183 184 190 148 144 192 151 180 179 143 146 126 133 150 166 191 138 160 136
189 195 125 187 127 120 145 165 175 140 196 164 137 159 158 161 142 172 157 197
181 173 185 118 119 154 153 132 176 170 155 141 122 174 147 152 110 198 117 121
Total: 100 objects.
Cluster 1:
36 41 35 67 53 47 40 77 15 21 59 31 6 48 57 82 2 8 51 83 96 79 63 61 95 1 11 49 0
24 78 84 98 94 44 74 38 85 34 27 76 75 65 60 30 26 68 70 18 17 20 22 86 32 28 87 9
29 72 43 33 62 37 71 73 66 23 39 45 88 42 3 80 7 16 81 55 90 69 54 12 4 50 92 99 91
```

97 93 46 5 56 13 14 64 58 52 19 89 10 25

Total: 100 objects.

6.3.3 The Clustering Program CURE

CURE is published in ACM SIGMOD'98 by S. Guha, R. Rastogi, and K. Shim [36]. It is a vector based clustering algorithm. Its implementation is as follows.

There is one head file: cure.h

There are there source files: cure.c, cureuti.c, and distance.c

Executable file: cure

To compile:

```
cc -o cure cure.c
```

To run:

```
cure Vector_file N_vect N_cluster
```

Vector_file contains the vectors to be clustered, N_vect is the number of vectors to be clustered, and N_cluster is the number of clusters to be generated.

For example, the file "v400.20" contains 400 randomly generated 20 dimensional vectors. The file looks like the following:

```
400 20
 -0.1620   0.7580  -0.8870   0.5150   0.0510
  0.6270   0.0100   0.4190  -0.7880  -0.9140
 -0.2510  -0.2330   0.0840  -0.9400  -0.7750
  0.5430   0.0890   0.1830   0.1370   0.5660
 -0.0340  -0.0220  -0.5050  -0.6890   0.3670
 -0.9460   0.0310   0.1450   0.8820   0.7360
 -0.4760  -0.4950  -0.6060  -0.8980  -0.1490
  0.0670  -0.2460   0.6530  -0.4390   0.0960
  0.6280   0.1880  -0.9150  -0.8570  -0.0330
  0.4060  -0.8350   0.4030   0.5620  -0.1660
  0.3530  -0.0800  -0.5560  -0.1970   0.9620
  0.3180   0.4220   0.3270  -0.5430   0.9450

...

...
```

The number 20 indicates that these are 20 dimensional vectors. To apply CURE to v400.20 we run:

```
cure v400.20 400 4
```

The output on the screen looks like the following:

```
Everything is ready.
Initialize heap complete...
Clustering complete...
Cluster 0:
263 286 267 251 249 222 202 289 299 294 219 274 203 230 262 258 254 253 233 293
237 250 232 226 287 220 255 207 291 223 239 271 206 259 296 269 245 231 240 236
276 290 213 297 208 209 217 270 205 229 200 201 242 234 256 248 225 268 292 235
288 278 244 252 261 238 246 212 224 277 221 285 210 243 275 216 265 295 228 215
218 281 257 204 298 211 227 282 279 264 272 241 266 284 280 247 214 260 283 273
Total: 100 objects.
Cluster 1:
196 150 147 198 166 185 108 161 102 151 174 194 125 103 176 130 162 128 126 120
178 146 139 135 157 160 177 199 190 148 152 170 107 186 119 189 106 172 155 113
173 101 100 149 121 175 115 191 129 138 114 134 136 180 158 197 111 124 143 118
193 183 104 127 144 179 171 105 109 112 122 165 156 110 192 154 164 184 159 133
131 168 141 181 153 167 163 132 169 195 116 182 137 117 142 188 140 187 123 145
Total: 100 objects.
Cluster 2:
27 85 30 66 31 54 58 10 9 3 11 24 53 36 21 76 94 17 37 71 0 56 47 22 15 95 20 87 73
68 59 78 32 1 91 7 70 74 34 5 65 33 75 79 18 42 81 52 45 98 40 50 44 62 93 84 61 41
25 46 48 77 72 57 38 4 16 29 12 26 2 99 97 83 64 14 82 92 28 96 55 86 89 19 69 39
23 60 90 35 6 63 80 49 88 13 67 8 43 51
Total: 100 objects.
```

Cluster 3:

302 318 326 352 397 300 346 395 341 391 303 337 363 379 366 310 329 362 325 374 305 353 385 321 367 347 335 323 317 376 307 332 373 312 351 365 349 334 399 340 336 306 350 370 328 393 304 343 301 359 342 390 375 345 316 330 364 354 394 378 348 333 320 339 396 387 388 386 309 356 322 389 398 308 371 313 319 382 355 361 377 381 392 357 372 324 315 369 383 368 327 384 380 314 358 338 331 360 311 344

Total: 100 objects.

Like AGM, CURE achieves a perfect clustering on these data.

We may map these 20 dimensional vectors to a 5 dimensional pseudo-Euclidean space using MetricMap using the following commands:

```
femb 100 5 < d400.20
```

```
proj d400.20 400 5 d400.vect d400.dist
```

Notice that d400.20 contains the pairwise distances of the vectors in v400.20. The data in d400.vect now looks like the follwoing:

```
400 5
  0.0000   0.0000   0.0000   0.0000   0.0000
 -2.9230  -0.1298   1.3652  -0.7308   0.9252
 -2.6179  -0.3876   1.0235  -0.1215  -0.4779
 -1.9882   0.5153   0.2969   0.0072  -0.4473
 -2.5031  -1.5796  -0.5920  -1.5827   0.5528
 -2.0708   1.2086   0.6483  -1.1900  -0.4187
 -2.7634   0.2079   1.0544   0.8281   0.9377
 -2.9396   0.4679  -0.1456  -0.2773   0.1866
 -2.5543   1.1021  -0.5163  -0.5840  -0.2894
 -2.7844  -0.1489  -0.1641   2.1055   0.0639

...

...
```

We may then apply CURE to the 5-dimensional vectors in d400.vect by executing the following command at the operating system level:

```
cure d400.vect 400 4
```

The output on the screen looks like the following:

```
Everything is ready.

Initialize heap complete...

Clustering complete...

Cluster 0:

220 285 224 211 286 287 204 202 290 299 27 203 282 267 244 270 229 263 276 248

246 228 298 279 232 231 219 200 225 259 241 206 294 222 218 288 271 245 262 281

235 280 215 264 250 239 269 247 293 261 255 252 266 205 240 236 230 212 207 292

242 257 295 291 265 213 217 209 201 278 233 223 260 216 254 289 284 214 238 275

296 283 268 253 256 234 208 297 258 249 221 277 237 272 210 226 243 251 274 227

273

Total: 101 objects.

Cluster 1:

51 57 58 74 5 65 11 10 28 52 29 12 56 41 25 68 6 46 87 60 88 9 92 38 76 81 42 82 44

79 62 71 77 35 84 34 61 98 40 50 8 85 3 7 15 66 99 90 86 69 72 24 33 70 20 64 39 16

53 32 1 47 26 37 73 55 2 22 91 36 13 95 14 75 48 59 83 67 96 54 43 30 49 17 97 21

19 80 45 18 93 4 89 0 31 23 94 63

Total: 98 objects.

Cluster 2:

353 324 385 362 355 382 309 386 351 305 389 301 343 354 341 333 342 381 307 379

364 374 390 388 316 350 373 370 347 329 387 318 345 339 304 360 356 393 321 327

320 348 359 394 378 335 332 310 367 375 380 371 369 361 322 315 308 396 398 323

399 336 358 372 352 303 376 317 344 311 312 330 326 313 338 397 383 328 392 391

306 366 331 395 325 300 340 384 314 334 319 349 365 377 363 346 368 357 302 337

78

Total: 101 objects.

Cluster 3:
```

158 187 122 163 103 154 181 166 108 101 196 175 182 113 106 188 168 185 178 109

105 184 190 130 140 128 161 174 162 170 120 156 189 191 110 132 167 172 124 133

116 138 127 195 123 157 171 126 121 100 135 115 102 177 104 143 160 129 150 119

192 179 139 176 107 148 180 149 151 142 183 144 125 117 169 173 155 199 114 194

111 136 186 197 141 134 152 153 118 193 159 131 112 137 145 147 165 146 198 164

Total: 100 objects.

Notice that two objects, object 27 and 78, are mis-clustered. The mis-clustering rate is 0.5CURE is a vector based clustering algorithm, which can not be applied to a general distance metric directly. We used MetricMap to map objects to vectors so that CURE can be used to cluster those objects.

6.3.4 The Best Match Search and Range Search Program Using MetricMap

Our last tool *msearch* performs best match retrieval and ϵ-range search using MetricMap.

There are no head files.

There are 3 source files: distance.c, vector.c, and msearch.c.

Executable file: msearch

To compile:

```
cc -o msearch msearch.c -lm
```

To run:

```
msearch -b Target-object
```

or

```
msearch -r Target-object Epsilon-value
```

Given a target object and a database of objects, "msearch" performs best match retrieval with the "-b" option, or ϵ-range search with the "-r" option. For the best match retrieval, the msearch tool finds the object in the database that is closest to the target. If there are more than one best match, the tool returns all the best-matching objects. For the ϵ-range search, the msearch tool finds the objects in the database whose distances to the target are within the given ϵ value.

Here we assume all the database objects have been embedded in a pseudo-Euclidean space using MetricMap. The indexes of the reference objects are stored in a file called "b.ind" (cf. the MetricMap tool). The image vectors of the objects are stored in a file called "v.base".

We give two annotated examples of sessions of the msearch system, one for best match retrieval and the other for ϵ-range search.

Refer to the MetricMap system. Suppose we have a database of 400 20-dimensional vectors, indexed from 0 to 399. These vectors (objects) are stored in file v400.20 (cf. the CURE program). The pairwise distances of the objects are stored in file d400.20. We can embed those objects in a 10-dimensional pseudo-Eucliden space by executing the following commands:

```
femb 40 10 < d400.20

proj d400.20 400 10 v.base v.dist
```

Recall that the "femb" program and the "proj" program generate two files, "b.ind" and "v.base". The file "b.ind" contains the indexes of the reference objects, which looks like the following:

```
9 25 36 28 10 37 14 31 39 32
```

This means that object 9, object 25, ... object 32 are used as reference objects to build the target space.

The file "v.base" contains the image vectors of the objects, which looks like the follwoing:

```
400 10
```

```
 0.0000   0.0000   0.0000   0.0000   0.0000
 0.0000   0.0000   0.0000   0.0000   0.0000
-2.5781  -2.1680   0.5737   2.0081  -0.7672
-0.0987   0.2544  -0.3053   0.3483   0.0392
-2.3080   0.8428   0.4520   0.8193  -0.8753
 0.0016   0.4910  -0.0696  -0.2953  -0.2928
-1.6848  -0.4318   1.1193   2.0989   0.6211
 0.3638   0.1002   0.5503   0.7714   0.5975
-3.1964  -0.4338   0.3476  -1.4289  -1.5407
 0.6868   1.0198   0.1987   0.1276  -0.3175

...

...
```

The number 400 indicates that there are 400 vectors. The number 10 indicates that these are 10-dimensional vectors. Each line of this file represents the coordinates of an image vector in the pseudo-Euclidean space.

Now suppose we are given a target object in a file called "target". For example, the data in the target file looks like the following:

```
-2.9375  -1.8045  -2.4635  -2.8335  -1.5975
-1.9245  -1.6905  -2.5165  -2.7335  -1.4645
 0.9480  -0.0230   0.5400  -0.3580  -0.0180
 0.0440   0.7980  -0.7720   0.0490  -0.8840
```

To find the best match of the target, type the command:

```
msearch -b target
```

The output on the screen looks like the following:

```
The nearest neighbor of the target is object with the index 111.
```

Basically, the msearch tool first computes the distances from the target to the reference objects stored in the file b.ind. Based on these distances, the tool is able to embed the target in the pseudo-Euclidean space. The tool then finds best matches in the pseudo-Euclidean space.

For ϵ-range search, suppose we want to find objects that are within distance 2 of the target object stored in the file "target". One may type in the following command:

```
msearch -r target 2
```

The output looks like the following:

```
The data objects that are within distance 2 of the target have indexes 111, 124, 158,
180.
```

To speed up search in the target space, we have implemented the VA-file technique introduced by R. Webber et. al. in a paper entitled "A quantitative Analysis and Performance Study for Similarity-Search Methods in High-Dimensional Spaces" which appeared in the Proc. of VLDB'98.

CHAPTER 7

SUMMARY OF THE THESIS AND FUTURE WORK

7.1 Summary

We introduced an approach to finding active patterns in 3D graphs. Our approach is an extension of the geometric hashing technique originally proposed by Lamden and Wolfson [48, 49] for tackling computer vision problems. Major differences between our technique and the previously published geometric hashing technique are listed below.

- The existing geometric hashing technique considers every triplet of points in the data object as a reference system, and therefore the records in the hash table are highly redundant. For an object with n nodes, it will produce $(n-3) \times \begin{pmatrix} n \\ 3 \end{pmatrix}$ entries in the hash table. In contrast, our approach produces only $\begin{pmatrix} n \\ 3 \end{pmatrix}$ entries. In the on-line phase, the geometric hashing technique runs in time $\mathcal{O}(n^4)$, while our approach runs in time $\mathcal{O}(n^3)$.

- Our approach divides an object into substructures. Thus it is capable of dealing with substructure matches in which two substructures are rotatable with respect to each other via a common edge. This phenomenon occurs frequently in scientific data such as chemical compounds.

- The geometric hashing technique is sensitive to errors [34, 70]. Intuitively, this is because the hash table addresses are calculated based on linear transformation. In contrast, our approach simply uses lengths of line segments to calculate the hash table addresses. Thus our approach can tolerate certain errors caused by the inaccuracy of measurement.

We also presented a new data structure for data clustering and data mining. Our contributions include:

- the development of a framework that utilizes sampling and the global knowledge of the data set to optimize the vector representation;
- the development of a general projection formula for both an embeddable new object and an unembeddable new object;
- estimating precisely the errors incurred by dimensionality reduction in pseudo-Euclidean space.

7.2 Future Work

Our future work includes:

- the application of the three dimensional discovery algorithm to protein data and developing new algorithms for protein clustering;
- the development of efficient algorithms based on the proposed index structure to facilitate fast similarity search in metric spaces.

REFERENCES

1. E. E. Abola, F. C. Bernstein, S. H. Bryant, T. F. Koetzle, and J. Weng, "Protein data bank," in *Crystallographic Databases – Information Contents, Software Systems, Scientific Applications* (F. H. Allen, G. Bergerhoff, and R. Sievers, eds.), Data Commission of the International Union of Crystallography, pp. 107–132, 1987.

2. R. Agrawal, J. Gehrke, D. Gunopulos, and P. Raghavan, "Automatic subspace clustering of high dimensional data for datamining applications," in *Proceedings of the 1998 ACM SIGMOD International Conference on Management of Data*, Seattle, Washington, pp. 237–248, June 1998.

3. R. Agrawal, S. Ghosh, T. Imielinski, B. Iyer, and A. Swami, "An interval classifier for database mining applications," in *Proceedings of the 18th International Conference on Very Large Data Bases*, Vancouver, Canada, pp. 560–573, Aug. 1992.

4. R. Agrawal, C. Faloutsos, and A. Swami, "Efficient similarity search in sequence databases," *Lecture Notes in Computer Science*, vol. 730, pp. 69–84, 1993.

5. R. Baeza-Yates, W. Cunto, U. Manber, and S. Wu, "proximity matching using fixed-queries trees," in *Combinatorial Pattern Matching, Lecture Notes in Computer Science*, pp. 198–212, June 1994.

6. D. H. Ballard, "Generalizing the hough transform to detect arbitrary shapes," *Pattern Recognition*, vol. 13, no. 2, pp. 111–122, 1981.

7. S. Berchtold, C. Bohm, B. Braunmuller, D. A. Keim, and H.-P. Kriegel, "Fast parallel similarity search in multimedia databases," in *Proceedings of the ACM SIGMOD International Conference on Management of Data*, pp. 1–12, May 1997.

8. F. C. Bernstein, T. F. Koetzle, G. J. B. Williams, E. F. Meyer, M. D. Brice, J. R. Rodgers, O. Kennard, T. Shimanouchi, and M. Tasumi, "The protein data bank: A computer-based archival file for macromolecular structures," *Journal of Molecular Biology*, vol. 112, pp. 535–542, 1977.

9. O. Bourdon and G. Medioni, "Object Recognition Using Geometric Hashing on the Connection Machine," in *10th International Conference on Pattern Recognition: 16–21 June 1990, Atlantic City, New Jersey, USA: Proceedings* (H. Freeman, ed.), 1109 Spring Street, Suite 300, Silver Spring, MD 20910, USA, pp. 596–600, IEEE Computer Society Press, 1990.

10. G. Burel, H. Henocq, and J. Y. Catros, "Registration of 3D objects using linear algebra," in *Computer Vision, Virtual Reality and Robotics in Medicine* (N. Ayache, ed.), Lecture Notes in Computer Science, Springer-Verlag, April 1995. ISBN 3-540-59120-6.

11. C. Burks, M. Cassidy, M. J. Cinkosky, K. E. Cumella, P. Gilna, J. E.-D. Hayden, G. M. Keen, T. A. Kelley, M. Kelly, D. Kristofferson, and J. Ryals, "GenBank," *Nucleic Acids Research*, vol. 19, pp. 2221–2225, 1991.

12. G. J. S. Chang, J. T. L. Wang, G. W. Chirn, and C. Y. Chang, "A visualization tool for pattern matching and discovery in scientific databases," in *Proceedings of the Eighth International Conference on Software Engineering and Knowledge Engineering*, Lake Tahoe, Nevada, June 1996.

13. J. Chao, K. Minowa, and S. Tsujii, "Unsupervised learning of 3D objects conserving global topological order," *IEICE Transactions on Fundamentals of Electronics, Communications and Computer Sciences*, vol. E76-A, no. 5, pp. 749–53, May 1993.

14. J. Chao and J. Nakayama, "Cubical singular simplex model for 3D objects and fast computation of homology groups," in *Proceedings of the 13th International Conference on Pattern Recognition*, vol. 4, IEEE Comput. Soc. Press, Los Alamitos, California, USA, pp. 190–4, 1996.

15. D. Conklin, *Knowledge Discovery in Molecular Structure Databases*, Ph.D. dissertation, Department of Computing and Information Science, Queen's University, Canada, 1995.

16. D. Conklin, "Machine discovery of protein motifs," *Machine Learning*, vol. 21, pp. 125–150, 1995.

17. D. Conklin, S. Fortier, and J. Glasgow, "Knowledge discovery in molecular databases," *IEEE Transactions on Knowledge and Data Engineering*, vol. 5, no. 6, pp. 985–987, 1993.

18. L. S. Davis and N. Roussopoulos, "Approximate pattern matching in a pattern database system," *Information Systems*, vol. 5, pp. 107–119, 1980.

19. L. Dehaspe, H. Toivonen, and R. D. King, "Finding frequent substructures in chemical compounds," in *Proceedings of the 4nd International Conference on Knowledge Discovery and Data Mining*, New York, New York, pp. 30–36, Aug. 1998.

20. S. Djoko, D. J. Cook, and L. B. Holder, "An empirical study of domain knowledge and its benefits to substructure discovery," *IEEE Transactions on Knowledge and Data Engineering*, vol. 9, no. 4, pp. 575–586, 1997.

21. R. O. Duda and P. E. Hart, *Pattern Classification and Scene Analysis*, John Wiley & Sons, Inc., New York, New York, 1973.

22. M. Ester, H.-P. Kriegel, J. Sander, and X. Xu, "A density-based algorithm for discovering clusters in large spatial databases with noise," in *Proceedings of the 2nd International Conference on Knowledge Discovery and Data Mining*, Portland, Oregon, pp. 226–231, Aug. 1996.

23. C. Faloutsos, *Searching Multimedia Databases by Content*, Kluwer Academic Publishers, Norwell, Massachusetts, 1996.

24. C. Faloutsos and K.-I. Lin, "*fastmap*: A fast algorithm for indexing, data-mining and visualization of traditional and multimedia datasets," in *Proceedings of the 1995 ACM SIGMOD International Conference on Management of Data*, pp. 163–174, May 1995.

25. C. Faloutsos, M. Ranganathan, and Y. Manolopoulos, "Fast subsequence matching in time-series databases," in *Proceedings of the 1994 ACM SIGMOD International Conference on Management of Data*, Minneapolis, Minnesota, pp. 419–429, May 1994.

26. P. Finn, L. Kavraki, J.-C. Latombe, R. Motwani, C. Shelton, S. Venkatasubramanian, and A. Yao, "RAPID: Randomized pharmacophore identification for drug design," in *Proceedings of the 13th International Annual Symposium on Computational Geometry (SCG-97)*, New York, pp. 324–333, ACM Press, June 4–6, 1997.

27. D. Fischer, O. Bachar, R. Nussinov, and H. J. Wolfson, "An efficient automated computer vision based technique for detection of three dimensional structural motifs in proteins," *J. Biomolec. Struct. Dynam.*, vol. 9, no. 4, pp. 769–789, 1992.

28. K. Fukunaga, *Introduction to Statistical Pattern Recognition*, Academic Press, Inc., San Diego, California, 1990.

29. H. N. Gabow, Z. Galil, and T. H. Spencer, "Efficient implementation of graph algorithms using contraction," in *Proceedings of the 25th Annual IEEE Symposium on Foundations of Computer Science*, pp. 347–357, 1984.

30. K. Gardels, "Open gis and on-line environmental libraries," *ACM SIGMOD Record*, vol. 26, no. 1, pp. 32–38, March 1997.

31. L. Godfarb, "A new approach to pattern recognition," in *Progress in Pattern Recognition* (L. Kanal and A. Rosenfeld, eds.), vol. 2, North-Holland, Amsterdam, pp. 241–402, 1985.

32. G. H. Golub and C. F. V. Loan, *Matrix Computations*, The Johns Hopkins University Press, Baltimore, Maryland, 1996.

33. W. Greub, *Linear Algebra*, Springer-Verlag, Inc., New York, New York, 1975.

34. W. E. L. Grimson, D. P. Huttenlocher, and D. W. Jacobs, "Affine matching with bounded sensor error: Study of geometric hashing and alignment," Technical Memo AIM-1250, Massachusetts Institute of Technology, Artificial Intelligence Laboratory, August 1991.

35. P. Grossmann, "From 3D line segments to objects and spaces," in *CVPR'89 (IEEE Computer Society Conference on Computer Vision and Pattern Recognition, San Diego, CA, June 4–8, 1989)*, Washington, DC., pp. 216–221, Computer Society Press, June 1989.

36. S. Guha, R. Rastogi, and K. Shim, "CURE: An efficient clustering algorithm for large databases," in *Proceedings of the 1998 ACM SIGMOD International Conference on Management of Data*, Seattle, Washington, pp. 73–84, June 1998.

37. R. W. Hamming, "Error detecting and error correcting codes," *The Bell System Technical Journal*, vol. 29, no. 2, pp. 147–160, 1950.

38. J. C. Hart, W. O. Cochran, and P. J. Flynn, "Similarity hashing: A computer vision solution to the inverse problem of linear fractals," Presented at the NATO Advanced Study Institute on Fractal Image Encoding and Analysis, Trondheim, Norway, July 1995, September 1995.

39. Y. C. Hecker and R. M. Bolle, "On geometric hashing and the generalized Hough transform," *IEEE Trans. Systems, Man, and Cybernetics*, vol. 24, no. 9, pp. 1328–1338, September 1994.

40. L. Hunter, ed., *Artificial Intelligence and Molecular Biology*, AAAI Press/The MIT Press, Menlo Park, California, 1993.

41. R. W. Irving and C. B. Fraser, "Two algorithms for the longest common subsequence of three (or more) strings," in *Combinatorial Pattern Matching, Lecture Notes in Computer Science, 644* (A. Apostolico, M. Crochemore, Z. Galil, and U. Manber, eds.), Springer-Verlag, pp. 211–226, 1992.

42. A. K. Jain and R. C. Dubes, *Algorithms for Clustering Data*, Prentice Hall, Englewood Cliffs, New Jersey, 1988.

43. K. Kanatani, "3d euclidean versus 2D non-euclidean: Two approaches to 3D recovery from images," *IEEE Transactions on Pattern Analysis and Machine Intelligence*, vol. 11, pp. 329–332, 1989.

44. L. Kaufman and P. J. Rousseeuw, *Finding Groups in Data: An Introduction to Cluster Analysis*, John Wiley & Sons, Inc., New York, New York, 1990.

45. J. L. Kelley, *General Topology*, D. Van Nostrand Company, Inc., Princeton, New Jersey, 1955.

46. D. Keren, J. Subrahmonia, and D. B. Cooper, "Integrating algebraic curves and surfaces, algebraic invariants and Bayesian methods for 2D and 3D object recognition," *Lecture Notes in Computer Science*, vol. 825, pp. 493–498, 1994.

47. A. Krotopoulou, P. Spirakis, D. Terpou, and A. Tsakalidis, "A conceptual database approach for modelling 3D objects of irregular geometry," *Lecture Notes in Computer Science*, vol. 856, pp. 290–299, 1994.

48. Y. Lamdan, J. T. Schwartz, and H. J. Wolfson, "Object recognition by affine invariant matching," in *CVPR'88 (IEEE Computer Society Conference on Computer Vision and Pattern Recognition, Ann Arbor, MI, June 5–9, 1988)*, Washington, DC., pp. 335–344, Computer Society Press, June 1988.

49. Y. Lamdan and H. J. Wolfson, "Geometric hashing: A general and efficient model-based recognition scheme," in *Second International Conference on Computer Vision*, Innesbrook Resort, Tampa, Florida, pp. 238–249, IEEE Computer Society Press, December 1988.

50. P. D. Lax, *Linear Algebra*, John Wiley & Sons, Inc., New York, New York, 1997.

51. H. Mannila and H. Toivonen, "Levelwise search and borders of theories in knowledge discovery," *Data Mining and Knowledge Discovery*, vol. 1, no. 3, pp. 241–258, 1997.

52. J. E. W. Mayhew and J. P. Frisby, *3d Model Recognition From Stereoscopic Cues*, MIT Press, Cambridge, Massachusetts, 1989.

53. J. A. McHugh, *Algorithmic Graph Theory*, Prentice Hall, Englewood Cliffs, New Jersey, 1990.

54. R. S. Michalski and R. E. Stepp, "Learning from observation: Conceptual clustering," in *Machine Learning: An Artificial Intelligence Approach, volume I* (R. S. Michalski, J. G. Carbonell, and T. M. Mitchell, eds.), Morgan Kaufmann, pp. 331–363, 1983.

55. M. Minsky and S. Papert, *Perceptrons: An Introduction to Computational Geometry*, M.I.T. Press, Cambridge, Massachusetts, 1969.

56. D. W. Murray and D. B. Cook, "Using the orientation of fragmentary 3D edge segments for polyhedral object recognition," *International Journal of Computer Vision*, vol. 2, no. 2, pp. 153–169, September 1988.

57. R. T. Ng and J. Han, "Efficient and effective clustering methods for spatial data mining," in *Proceedings of the 20th International Conference on Very Large Data Bases*, Santiago, Chile, pp. 144–155, Sep. 1994.

58. R. Nussinov and H. J. Wolfson, "Efficient detection of three-dimensional structural motifs in biological macromolecules by computer vision techniques.," in *Proceedings of National Academy of Science of USA*, vol. 88, pp. 10495–10499, December 1991.

59. I. Nystroem and G. Borgefors, "Synthesising objects and scenes using the reverse distance transformation in 2D and 3D," *Lecture Notes in Computer Science*, vol. 974, pp. 441–446, 1995.

60. J. M. Ortega, *Matrix Theory*, Plenum Press, New York, New York, 1987.

61. X. Pennec and N. Ayache, "An O(n2) algorithm for 3D substructure matching of proteins," in *First International Workshop on Shape and Pattern Matching in Computational Biology* (A. Califano, I. Rigoutsos and H. J. Wolson, eds.), pp. 25–40, June 1994.

62. J. Ponce and D. J. Kriegman, "On recognizing and positioning curved 3D objects from image contours," in *Image Understanding Workshop (Palo Alto, CA, May 23-26, 1989)*, San Mateo, CA, pp. 461–470, Defense Advanced Research Projects Agency, Morgan Kaufmann, 1989.

63. I. Rgoutsos and R. Hummel, "On a parallel implementation of geometric hashing on the connection machine," Tech. Rep. TR-554, Department of Computer Science, New York University, April 1991.

64. W.-F. Riekert, R. Mayer-Foll, and G. Wiest, "Management of data and services in the environmental information system (uis) of baden-wurttemberg," *ACM SIGMOD Record*, vol. 26, no. 1, pp. 22–26, March 1997.

65. I. Rigoutsos and R. Hummel, "Scalable parallel geometric hashing for hypercube SIMD architechtures," Technical Report TR-553, New York University, Jan. 1991.

66. I. Rigoutsos, D. Platt, and A. Califano, "Flexible substructure matching in very large databases of 3D-molecular information," research report, IBM T. J. Watson Research Center, 1996.

67. J. Sadowski and J. Gasteiger, "From atoms and bonds to three-dimensional atomic coordinates: Automatic model builders," *Chemical Reviews*, vol. 93, pp. 2567–2581, 1993.

68. F. Sandakly and G. Giraudon, "Reasoning strategies for 3D object detection," in *IEEE International Symposium on Computer Vision*, November 1995.

69. D. Sankoff and J. B. Kruskal, eds., *Time Warps, String Edits, and Macromolecules: The Theory and Practice of Sequence Comparison*, Addison-Wesley, Reading, Massachusetts, 1983.

70. K. B. Sarachik, "Limitations of geometric hashing in the presence of gaussian noise," Technical Memo AIM-1395, Massachusetts Institute of Technology, Artificial Intelligence Laboratory, October 1992.

71. J. Serra, ed., *Image Analysis and Mathematical Morphology*, Academic Press, New York, New York, 1982.

72. B. A. Shapiro and J. Navetta, "A massively parallel genetic algorithm for RNA secondary structure prediction," *Journal of Supercomputing*, vol. 8, pp. 195–207, 1994.

73. D. Shasha, J. T. L. Wang, K. Zhang, and F. Y. Shih, "Exact and approximate algorithms for unordered tree matching," *IEEE Transactions on Systems, Man and Cybernetics*, vol. 24, no. 4, pp. 668–678, April 1994.

74. D. Shasha and T. L. Wang, "New techniques for best-match retrieval," *ACM Transactions on Information Systems*, vol. 8, no. 2, pp. 140–158, April 1990.

75. D. Shasha and K. Zhang, "Fast algorithms for the unit cost editing distance between trees," *Journal of Algorithms*, vol. 11, no. 4, pp. 581–621, 1990.

76. A. Shashua, "On geometric and algebraic aspects of 3D affine and projective structures from perspective 2D views," *Lecture Notes in Computer Science*, vol. 825, pp. 127–132, 1994.

77. G. Sheikholeslami, S. Chatterjee, and A. Zhang, "WaveCluster: A multi-resolution clustering approach for very large spatial databases," in *Proceedings of the 24th International Conference on Very Large Data Bases*, New York, New York, pp. 428–439, Aug. 1998.

78. A. F. Smeaton and C. J. V. Rijsbergen, "The nearest neighbor problem in information retrieval: an algorithm using upperbounds," *ACM SIGIR Forum*, vol. 16, pp. 83–87, 1981.

79. R. Steinmetz and K. Nahrstedt, eds., *Multimedia: Computing, Communications and Applications*, Prentice Hall, Englewood Cliffs, New Jersey, 1995.

80. R. R. Stoll, *Linear Algebra and Matrix Theory*, McGraw-Hill, Inc., New York, 1952.

81. R. L. Tatusov, S. F. Altschul, and E. V. Koonin, "Detection of conserved segments in proteins: iterative scanning of sequence databases with alignment blocks," *Proceedings of National Academy of Science of USA*, vol. 91, pp. 12091–12095, 1994.

82. I. I. Vaisman, A. Tropsha, and W. Zheng, "Compositional preferences in quadruplets of nearest neighbor residues in protein structures: Statistical geometry analysis," in *Proceedings of IEEE International Join Symposia on Intelligence and Systems*, Rockville, Maryland, pp. 163–168, Aug. 1998.

83. R. A. Wagner and M. J. Fischer, "The string-to-string correction problem," *Journal of the ACM*, vol. 21, no. 1, pp. 168–173, Jan. 1974.

84. J. T. L. Wang, G. W. Chirn, T. G. Marr, B. A. Shapiro, D. Shasha, and K. Zhang, "Combinatorial pattern discovery for scientific data: Some preliminary results," in *Proceedings of the 1994 ACM SIGMOD International Conference on Management of Data*, Minneapolis, Minnesota, pp. 115–125, May 1994.

85. J. T. L. Wang, T. G. Marr, D. Shasha, B. Shapiro, and G. W. Chirn, "Discovering active motifs in sets of related protein sequences and using them for classification," *Nucleic Acids Research*, vol. 22, no. 14, pp. 2769–2775, 1994.

86. J. T. L. Wang, T. G. Marr, D. Shasha, B. Shapiro, G. W. Chirn, and T. Y. Lee, "Complementary classification approaches for protein sequences," *Protein Engineering*, vol. 9, no. 5, pp. 381–386, 1996.

87. J. T. L. Wang, B. A. Shapiro, and D. Shasha, eds., *Pattern Discovery in Biomolecular Data: Tools, Techniques and Applications*, Oxford University Press, New York, New York, Mar. 1999.

88. J. T. L. Wang, B. A. Shapiro, D. Shasha, K. Zhang, and C.-Y. Chang, "Automated Discovery of Active Motifs in Multiple RNA Secondary Structures," in *Proceedings of the 2nd International Conference on Knowledge Discovery and Data Mining*, Portland, Oregon, pp. 70–75, Aug. 1996.

89. J. T. L. Wang, D. Shasha, G. Chang, L. Relihan, K. Zhang, and G. Patel, "Structural matching and discovery in document databases," in *Proceedings of the 1997 ACM SIGMOD International Conference on Management of Data*, Tucson, Arizona, pp. 560–563, May 1997.

90. J. T. L. Wang, K. Zhang, and G. W. Chirn, "Algorithms for approximate graph matching," *Information Sciences*, vol. 82, pp. 45–74, 1995.

91. J. T. L. Wang, K. Zhang, K. Jeong, and D. Shasha, "A system for approximate tree matching," *IEEE Transactions on Knowledge and Data Engineering*, vol. 6, no. 4, pp. 559–571, August 1994.

92. J. T. L. Wang, X. Wang, K.-I. Lin, D. Shasha, B. A. Shapiro, and K. Zhang, "Evaluating a class of distance-mapping algorithms for data mining

and clustering," in *Proceedings of the ACM SIGKDD International Conference on Knowledge Discovery and Data Mining*, San Diego, California, pp. 307–311, August 1999.

93. T. L. Wang and D. Shasha, "Query processing for distance metrics," in *Proceedings of the 16th International Conference on Very Large Data Bases*, Brisbane, Australia, pp. 602–613, Aug. 1990.

94. W. Wang, J. Yang, and R. Muntz, "STING: A statistical information grid approach to spatial data mining," in *Proceedings of the 23rd International Conference on Very Large Data Bases*, Athens, Greece, pp. 186–195, Aug. 1997.

95. X. Wang and J. T. L. Wang, "Fast similarity search in databases of 3d objects," in *Proceedings of the 10th IEEE International Conference on Tools with Artifical Intelligence*, Taipei, Taiwan, pp. 16–23, November 1998.

96. X. Wang, J. T. L. Wang, D. Shasha, B. A. Shapiro, S. Dikshitulu, I. Rigoutsos, and K. Zhang, "Automated discovery of active motifs in three dimensional molecules," in *Proceedings of the 3rd International Conference on Knowledge Discovery and Data Mining*, Newport Beach, California, pp. 89–95, August 1997.

97. X. Wang, J. T. L. Wang, K.-I. Lin, D. Shasha, B. A. Shapiro, and K. Zhang, "Implementation and evaluation of an index structure for data clustering," *Knowledge and Information Systems: An International Journal*, To appear, 2000.

98. X. Wang, J. T. L. Wang, D. Shasha, B. Shapiro, I. Rigoutsos, and K. Zhang, "Finding patterns in three dimensional graphs: Algorithms and applications to scientific data mining," Research Report CIS-99-04, Computer and Information Science Department, New Jersey Institute of Technology, 1999.

99. H. J. Wolfson, "Model-based object recognition by geometric hashing," in *Proceedings of the 1st European Conference on Computer Vision* (O. Faugeras, ed.), vol. 427 of *LNCS*, Berlin, pp. 526–536, Springer, April 1990.

100. M. C. Yang and W. H. Tsai, "Recognition of single 3D curved objects using 2D cross-sectional slice shapes," *Image and Vision Computing*, vol. 7, pp. 210–216, 1989.

101. Y. Yang, K. Zhang, X. Wang, J. T. L. Wang, and D. Shasha, "An approximate oracle for distance in metric spaces," in *Combinatorial Pattern Matching* (M. Farach-Colton, ed.), Lecture Notes in Computer Science, 1448, Springer-Verlag, pp. 104–117, 1998.

102. B.-K. Yi, H. V. Jagadish, and C. Faloutsos, "Efficient retrieval of similar time sequences under time warping," in *Proceedings of 14th IEEE International Conference on Data Engineering*, Orlando, Florida, pp. 201–208, Feb. 1998.

103. K. Zhang, D. Shasha, and J. T. L. Wang, "Fast serial and parallel algorithms for approximate tree matching with VLDC's," in *Proc. of the 3rd Annual Symposium on Combinatorial Pattern Matching* (A. Apostolico, M. Crochemore, Z. Galil, and U. Manber, eds.), Lecture Notes in Computer Science, 644, Springer-Verlag, pp. 151–161, 1992.

104. K. Zhang, J. T. L. Wang, and D. Shasha, "On the editing distance between undirected acyclic graphs," *International Journal of Foundations of Computer Science, Special Issue on Computational Biology*, vol. 7, no. 1, pp. 43–57, 1996.

105. T. Zhang, R. Ramakrishnan, and M. Livny, "BIRCH: An efficient data clustering method for very large databases," in *Proceedings of the 1996 ACM SIGMOD International Conference on Management of Data*, Montreal, Quebec, Canada, pp. 103–114, June 1996.